Energy Storage Materials 45 (2022) 332–369

Contents lists available at ScienceDirect

Energy Storage Materials

journal homepage: www.elsevier.com/locate/ensm

Halogen-enabled rechargeable batteries: Current advances and future perspectives

Kaiqiang Zhang[a,b], Zhong Jin[a,b,*]

[a] MOE Key Laboratory of Mesoscopic Chemistry, MOE Key Laboratory of High Performance Polymer Materials and Technology, Jiangsu Key Laboratory of Advanced Organic Materials, School of Chemistry and Chemical Engineering, Nanjing University, Nanjing 210023, China
[b] Shenzhen Research Institute of Nanjing University, Shenzhen 518063, China

ARTICLE INFO

Keywords:
Halogen and halogen compounds
Rechargeable batteries
Stable solid electrolyte interfaces
Improved kinetics
Various battery integrities

ABSTRACT

The state-of-the-art battery technologies appear in various fields ranging from stationary electric stations to mobile electronics and vehicles. The subsequent development of batteries mainly relies on the following aspects: high-performance electrode/electrolyte materials and innovative battery designs. Studies on halogen species for battery applications have been conducted in recent decades due to their attractive advantages, such as the high redox potentials, low cost, and source abundance for massive applications. Halogen species utilized in battery chemistries mainly obey two different concepts: (i) participating redox reactions for charging/discharging and (ii) serving as a crucial redox-free component for other specific functions, such as promoting charge transfer and composing electrode or electrolyte compounds. In this review article, we extensively outlined the utilization of halogen and halogen compounds in various rechargeable batteries from the two perspectives above, with the focus on how the halogen species function during battery operation. The remaining challenges and potential opportunities for the adoption of halogen and halogen compounds in secondary batteries have been highlighted. The widely covered review article aims to provide a comprehensive understanding for the halogen chemistry in batteries, which differs from the enormous articles with deep study on a branch. We hope to stimulate more future research efforts on halogen-enabled batteries

1. Introduction

Electrochemical batteries have played an increasingly important role in energy supply systems, which are closely related to daily life [1,2]. The ever-growing dependence on electric energy has created a dramatic demand for the corresponding storage devices [3–6]. Electrochemical secondary batteries with advanced and powerful performances, such as high energy and power densities and long durability, are promising candidates to fill this demand [7,8]. The research on lithium-ion batteries was the pioneering research on metal-ion batteries; afterward, many studies beyond lithium-ion battery chemistry, such as sodium-, potassium-, and zinc-ion batteries together with redox flow batteries, received intensive focus given the disadvantages of lithium-ion batteries, such as the limited and uneven distribution of lithium resources and flammable electrolytes. Recent research efforts have mainly focused on the development of high-performance electrode and/or electrolyte materials and on innovative battery designs to push the boundary of rechargeable battery technologies.

Halogen elements are widely adopted in battery chemistries, ranging from metal-ion batteries to halogen-ion batteries and redox flow batteries, in which the halogen species serve in two different ways: (i) participating in redox reactions for charging/discharging and (ii) simply existing in battery systems for other specific functions without redox reactions, such as promoting charge transfer, composing electrode and/or electrolyte compounds, and stabilizing electrode/electrolyte interfaces.

In this review article, we present a comprehensive and in-depth overview of the halogen-enabled battery chemistries, including metal-ion, halogen-ion, molten-salt, metal-halogen, and redox flow batteries, with a focus on their functions during battery operation and how they improve the electrochemical performances. The functions of halogen species are summarized as follows: first, halogen-containing compounds, including metal halides and metal-oxy-halides, for composing electrodes; second, halogen for doping electrodes; third, halogen compounds in electrolytes, including liquid-phase and solid-state electrolytes as well as solid electrolyte interfaces; fourth, halogen conversion-based battery chemistries, ranging from chlorine to iodine in nonflowing and redox flow batteries (Fig. 1). In this review article, we summarize the current different types of mainstream battery families with a focus on the relationship between halogen and the corresponding critical electrochemical performances and special functions, as well as the remaining challenges and possible opportunities.

* Corresponding author.
E-mail address: zhongjin@nju.edu.cn (Z. Jin).

https://doi.org/10.1016/j.ensm.2021.11.048
Received 13 July 2021; Received in revised form 10 November 2021; Accepted 28 November 2021
Available online 4 December 2021

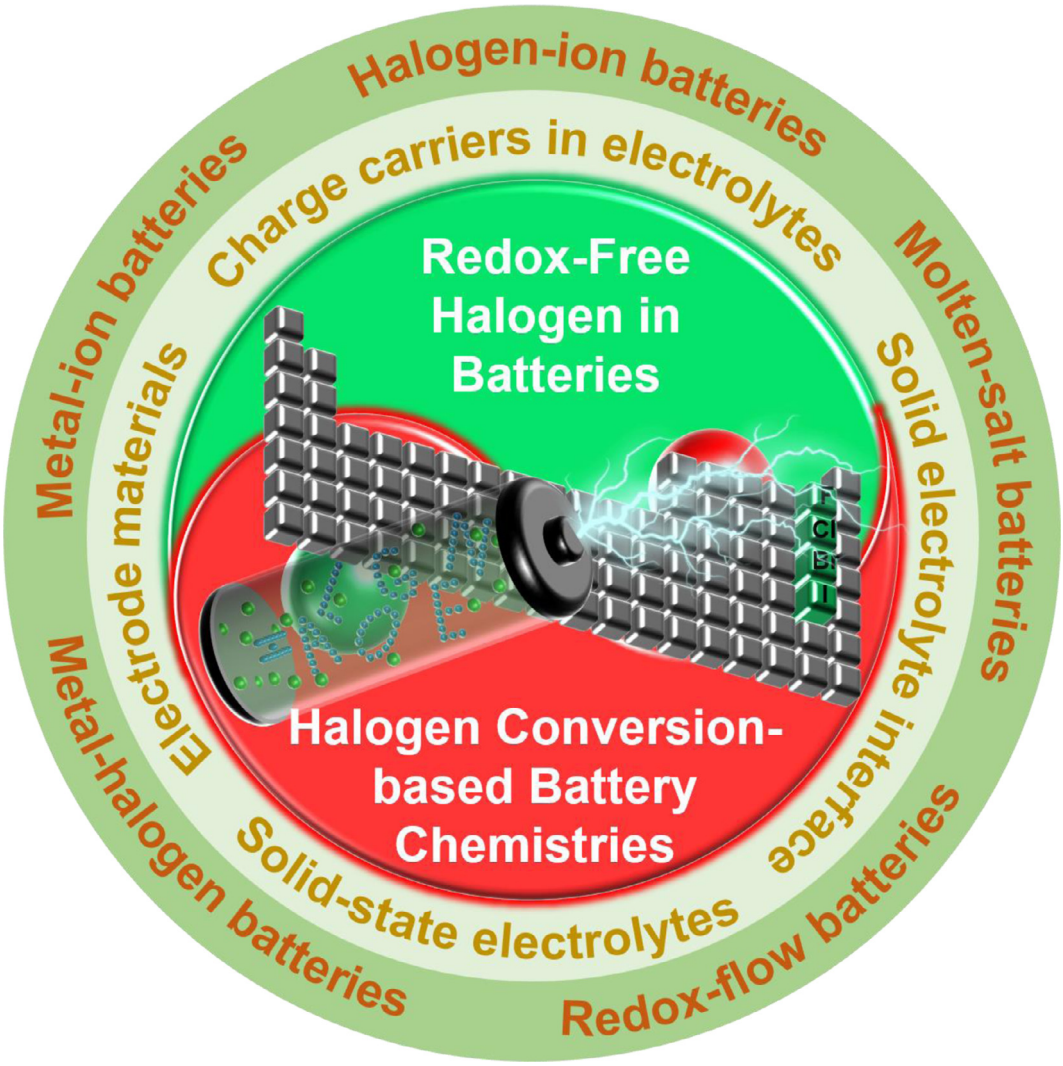

Fig. 1. Schematic outline of the halogen-enabled rechargeable battery chemistries.

2. Redox-free halogen in batteries

Halogen has been widely utilized in electrode and electrolyte designs and constructions for customized performances due to their unique traits, such as large electronegativity. In this chapter, we will mainly talk about the unique functions of redox-free halogen that used in electrode and electrolyte fabrications. The redox-free definition refers to the halogen that shows no redox process or valence conversion during the whole charging/discharging process of batteries, namely, the absence of redox reactions from halogen during the charging/discharging operations. Other unique functions by halogen were discussed and overviewed instead. In this chapter, the studies on redox-free halogen in batteries were summarized and emphasized according to their applications in either electrode portion or electrolyte portion. This chapter was organized based on the structure of battery construction, which is distinct from other review articles, in which the discussion was elaborated based on different types of battery chemistries.

2.1. Halogen study in electrodes

In this chapter, we mainly reviewed the reports on electrodes that were designed and fabricated based on or involving halogen chemistry. This chapter was organized and arranged from the perspective of different types of halogen-containing compounds, including metal halides, metal-oxy-halides, fluoride-containing polyanions, and halogen-containing composites. Each segment was unfolded with the discussion of different battery chemistries.

2.1.1. Metal halide compounds

Metal halides have thus far been extensively studied in rechargeable battery chemistries from various aspects for different objectives [9–11]. In this section, we outline the recent studies on metal halides used in rechargeable batteries. The effects of the introduction of metal halides are discussed and emphasized by correlation with the improved electrochemical performances. Finally, the related shortcomings and disadvantages when using metal halides in rechargeable batteries and the possible solutions and directions toward future research efforts are provided.

The research on electrode technologies includes exploring advanced electrochemical performances, affordable costs and facile manufacturing, good environmental friendliness, and renewability and sustainability [12–15]. Apart from the significant use of metal oxides and sulfides, metal halides are another extremely promising candidate for rechargeable battery chemistries; the electronegativity of halogen ions is similar to that of chalcogen ions, and halogen ions stably coordinate with enormous cations, which makes applications of metal halides in rechargeable battery chemistries possible [16]. With appropriate material manufacturing and engineering techniques, high-performance electrodes based

on metal halides can be obtained. In this chapter, we will comprehensively discuss the metal halide electrodes in rechargeable battery chemistries.

2.1.1.1. Alkali metal-ion batteries. Metal fluorides for lithium-ion batteries promise dramatically higher energy density relative to state-of-the-art electrodes for lithium-ion and the lithium-sulfur batteries [17–19]. In recent years, metal fluorides have gained increasing attention for use as electrode materials in metal-ion batteries, particularly lithium-ion batteries [20–23]. Metal fluoride electrodes theoretically deliver higher capacities relative to intercalation-type oxide cathodes, thus enabling the development of next-generation high-performance batteries [24]. However, their high performance is restricted by their low-capacity utilization, which is attributed to the sluggish reaction kinetics, poor conductivity, unstable metal fluoride/electrolyte interfaces, side reactions with electrolytes, and dissolution of active species, the challenges faced by current metal fluoride electrodes, causing limited rate capability and rapid capacity decay upon charging/discharging [25,26].

To overcome above issues related to the metal halide electrodes, numerous methods and strategies have been attempted. Iron fluorides with hydration water tunnels are the favorable structure for utilization as cathodes in lithium-ion batteries [27]. A study on iron fluoride electrodes with hydration water tunnels inside the crystal lattice as a cathode of lithium-ion batteries was conducted by Bai et al. [28]. The designed and synthesized iron fluoride product with a flower-like morphology, as shown in Fig. 2a, delivered a reversable capacity of 172.3 mAh g^{-1} at 23.7 mA g^{-1} with a 97.33% capacity retention after 50 cycles (Fig. 2b) due to the hydration water molecules that promoted lithium-ion diffusion capability (Fig. 2c).

To address the sluggish reaction kinetics of metal fluoride electrodes, a composite honeycomb-like FeF_3@C electrode was designed and synthesized by Wu et al. [29]. The highly porous matrices facilitated the infiltration of electrolytes and the diffusion of lithium ions and transport of electrons, which helped the FeF_3@C composite electrode with high areal loading amounts of 2.2 and 5.3 mg cm^{-2} deliver a high-rate capability of 100 C and remarkable cycle stability for 1000 cycles. However, metal fluorides might undergo side reactions, such as the irreversible formation of elemental metals and fluorides. Such an unfavorable side reaction was studied by Bensalah et al. by using MnF_2 as a cathode in lithium-ion batteries, exhibiting the irreversible formation of Mn and lithium fluoride from MnF_2 during the initial cycles, even though a high capacity of 480 mAh g^{-1} at 0.1 C with a high coulombic efficiency of close to 100% was achieved [30]. The side reactions originating from the interface between metal fluorides and electrolytes result in severe capacity decay over electrochemical cycles. Zhang et al. demonstrated that modification by graphene quantum dots could be used to suppress the notorious side reactions during redox chemistry [31]. A self-supported FeF_3 electrode decorated with graphene quantum dots (GQDs) delivered a capacity of 161.5 mAh g^{-1} at 200 mA g^{-1} and a high-rate capability of 117 mAh g^{-1} at 4 A g^{-1} (Fig. 3a). Benefitting from the suppressing effect on side reactions, a long lifespan of over 1,000 cycles at 400 mA g^{-1} was attained with a low fade rate of 0.03% per cycle.

The poor stability of metal fluorides during charge/discharge imposes barriers for their use in practical applications and commercialization. The adoption of protective layers to prevent metal fluorides from dissolution and, thus, maintain capacities is an efficient methodology [32]. A stable FeF_2 electrode attained by electrolyte engineering has been studied by Huang et al. [33]. After replacing the conventional liquid electrolyte with a solid-state polymer-type electrolyte, the FeF_2 electrode delivered a high capacity of more than 450 mAh g^{-1} with a long lifespan of 300 cycles at 50°C, benefitting from the improved preservation of FeF_2 due to the formation of a robust, homogeneous, and elastic cathode electrolyte interface, which was generated under a mechanical-robust solid-state polymer-type electrolyte. Furthermore, Wu et al. demonstrated the similar concept of forming a protective layer on the metal fluoride surfaces to restrain the dissolution of active materials by adopting metal-organic framework-derived CoF_2, as shown in Fig. 3b [34]. The cross-linked carbon walls generated to confine the CoF_2 nanoparticles and improve the conductivity of the whole cathode enabled the cathode to have a high capacity of approximate 500 mAh g^{-1} at 110 mA g^{-1} for 200 cycles, as shown in Fig. 3b.

In addition to the one-step wrapping concept retarding the dissolution of the active species, a dual-step protecting strategy was proposed by Zhao et al. by ex-situ forming an aluminum oxide protective layer and an in-situ formed cathode electrolyte interface on an FeF_3 cathode in lithium-ion batteries [35]. The dual-layer protected FeF_3 cathode efficiently prevented the discharge products from dissolving into electrolytes, and the cathode thus delivered a long lifespan of 300 cycles at 100 mA g^{-1} with 90% capacity retention.

The metal fluorides phase was also demonstrated to impact the electrochemical performance, as reported by Cheng et al. [36]. In particular, octahedral- and spinel-type FeF_3 was synthesized through use of a co-pyrolysis method; sequentially, octahedral FeF_3 delivered a higher capacity of 142 mAh g^{-1} than its spinel-type counterpart (128 mAh g^{-1}), as well as a long lifespan of 1,000 cycles at 474 mA g^{-1} (Fig. 4a). Modification of the material phase is, thus, an efficient method for improving the ionic conductivity and decreasing the impedance of grain boundaries [37].

In addition to metal fluorides, metal chlorides are also favorable as potential electrodes. A bi-intercalation compound composed of a $CoCl_2$-$FeCl_3$-graphite anode material, studied by Qi et al., demonstrated extremely high capacities of 1,033 mAh g^{-1} at 200 mA g^{-1} and 536 mA h g^{-1} at 1,000 mA g^{-1} when serving as the anode of lithium-ion batteries [38], which was attributed to the extra active sites for the lithiation reaction benefitting from the intercalated $CoCl_2$ and $FeCl_3$ components. A nickel chloride anode for lithium-ion batteries was reported by Lim et al. [39]. The layered nickel chloride was electrochemically prepared from a nickel hydroxy chloride, Ni(OH)Cl, precursor. In particular, the Ni(OH)Cl transformed into a coexistence state of $Ni(OH)_2$ and $NiCl_2$ after the first charging/discharging cycle; subsequently, the lithium ions were reversibly stored through a heterointerface reaction, as shown in Fig. 4b. The unique lithium-ion storage method thus delivered a high capacity of 1,236 mAh g^{-1} at the 150th cycle at 200 mA g^{-1}, as shown in Fig. 4b.

Another type of metal halide electrode-based battery, which is molten salt batteries, is a typical type of high-temperature battery, which have working temperatures generally higher than 100 °C. A common ceramic electrolyte with good ionic conductivity is necessary for isolating liquid-state electrodes to guarantee safety during battery operation. Molten salt batteries are more like a combination of redox-flow batteries, as we discuss in the following context, and conventional metal-ion batteries, having both a liquid state of the former and construction of the latter. Advantages such as lack of metal dendrites and degradation of active materials are potentially obtained. The notorious lithium dendrite issue is thoroughly solved by the liquidation of lithium metal and robust solid-state electrolytes. However, there are still various key challenges that need to be overcome, such as rapid self-discharge at elevated operating temperatures [40]. In this segment, we mainly provide an overview and discuss over recent advances in molten salt batteries by using metal halides as electrodes and provide our own perspectives and insights into the following research efforts.

Bromine and iodine are widely adopted for sodium molten salt batteries by dissolving them in aqueous solvents and isolating them with a sodium-ion conductive NaSICON solid-state electrolyte [41]. Owing to the excellent solubility of bromine/bromide and iodine/iodide, both static and flow batteries are possible. Regarding this type of molten-salt battery, the vapor pressure of bromine and polybromide is a considerable issue. Metal halide compounds in molten-salt batteries, such as sodium-metal chloride molten battery chemistry, ZEBRA batteries, typically known as sodium-nickel-chloride batteries, have, thus, demonstrated superior safety and efficient protection from overcharging/discharging [42–44].

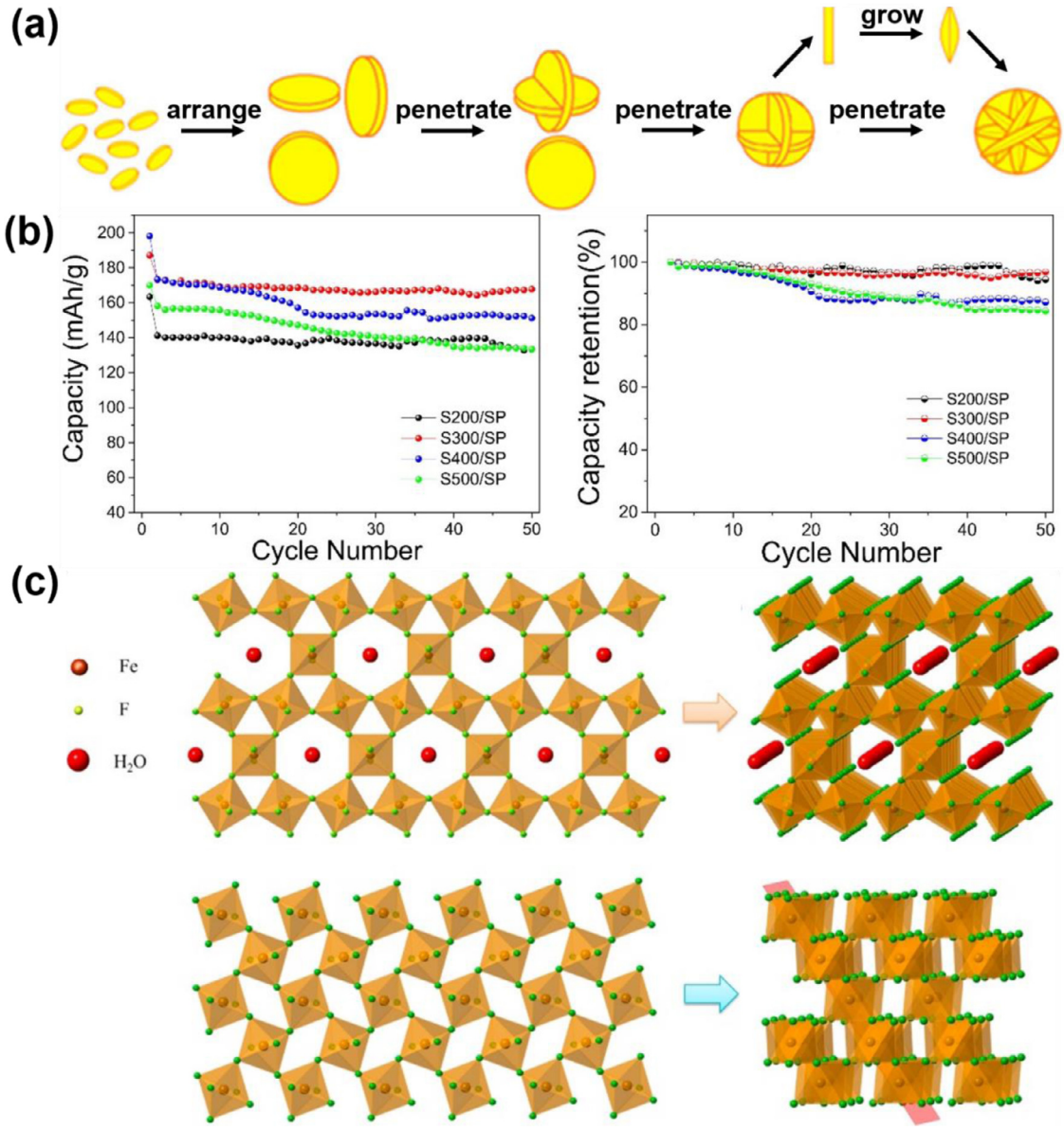

Fig. 2. (a) Schematic illustration of the growth mechanism for flower-like particles. (b) The corresponding capacity retentions of different iron fluoride samples. (c) Chemical bonding between iron and fluoride, schematic drawings of the structures of $FeF_{3.0}$•$33H_2O$ and FeF_3 [28] Copyright 2017 Elsevier.

Another issue in the molten salt battery community is the limited capacity utilization, which is caused by the bulky metals generated by the aggregation of small metal particles upon discharge. Once the metal particles aggregated, redox reactions are only limited to at the surficial region, leading to the fast capacity loss. Regarding such an issue, Xu et al. demonstrated an alloying/dealloying concept by introducing molybdenum into the $FeCl_2$ cathode in lithium-$FeCl_2$ molten salt battery; the modified charging/discharging process was accompanied by spontaneous dealloying/alloying of the Fe_3Mo alloy. The conductive molybdenum framework restricted the generation of pure and large iron particles and maintained a high performance of 472 mAh g_{LiCl}^{-1} at the 300th cycle [45]. In addition to the molybdenum frameworks, Liu et al. demonstrated a copper framework for restricting nickel particle growth by using cost-efficient brass, as shown in Fig. 5a [46]. The specially designed and constructed molten salt battery delivered a high energy density of 750 Wh kg^{-1} and 2,250 Wh L^{-1}.

A dual-metal concept was developed by Ahn et al. utilizing a Na-(Fe,Ni)Cl_2 molten salt battery, which demonstrated that the microstructure of nickel-iron highly affects the electrochemical performance, as shown in Fig. 5b. Benefiting from the dual electrochemical reactions of nickel and iron, the capacity was highly increased [47].

Transition metal halides are theoretically promising for use as electrode materials in alkaline metal-ion batteries, particularly lithium-ion battery, due to their high gravimetrical and volumetric energy densities and rational redox potentials. A systematic comparison of the electrochemical performances was provided in Table 1. However, the remaining challenges and issues faced by metal halide electrodes, including poor ionic and electronic conductivities, dissolution of metal species into electrolytes, structural decomposition, undesirable side reactions, and unstable electrode/electrolyte interfaces, need to be addressed. Inspired by the development of metal oxide and sulfide electrodes, as well as current studies on metal halides, morphology control and lattice modulation as well as designs of composites are effective strategies for improving conductivity, thus modifying electrochemical kinetics. In-situ and ex-situ formation of protective layers on the metal halides to prevent them from dissolution and structural collapse upon consecutive charging/discharging is beneficial for stabilizing the capacity utilization and inhibiting lifetime fade. The current studies on metal halides are mainly

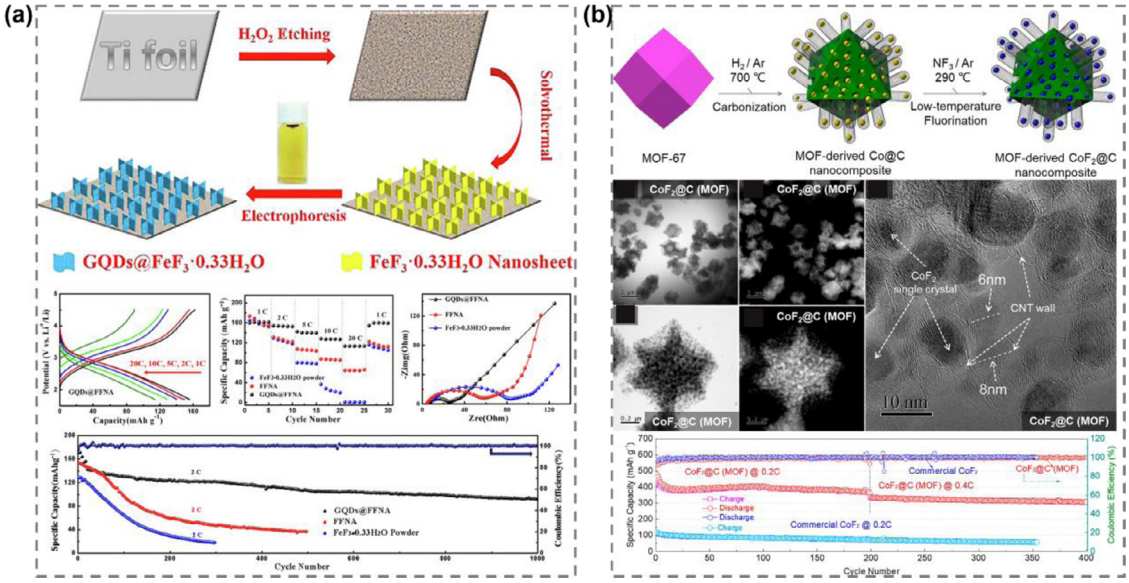

Fig. 3. (a) Schematic illustration of the synthesis of GQDs@FeF_3•0.33H_2O nanosheet arrays. Charge and discharge profiles at different current rates for the GQDs@FeF_3•0.33H_2O nanosheet array electrode; rate performance of the FeF_3•0.33H_2O powder, FeF_3•0.33H_2O nanosheet array, and GQDs@FeF_3•0.33H_2O nanosheet array electrodes; Nyquist plots and cycle performances of the three electrodes [31] Copyright 2019 Elsevier. (b) Schematic synthesis of CoF_2@C. Scanning transmission electron microscopy and high-resolution transmission electron microscopy characterizations of the CoF_2@C nanocomposite: bright field scanning transmission electron microscopy, high angle annular dark field-scanning transmission electron microscopy, and high-resolution transmission electron microscopy images of the CoF_2@C nanocomposite. Long-term cycle stability of the CoF_2@C cathode [34] Copyright 2021 American Chemical Society.

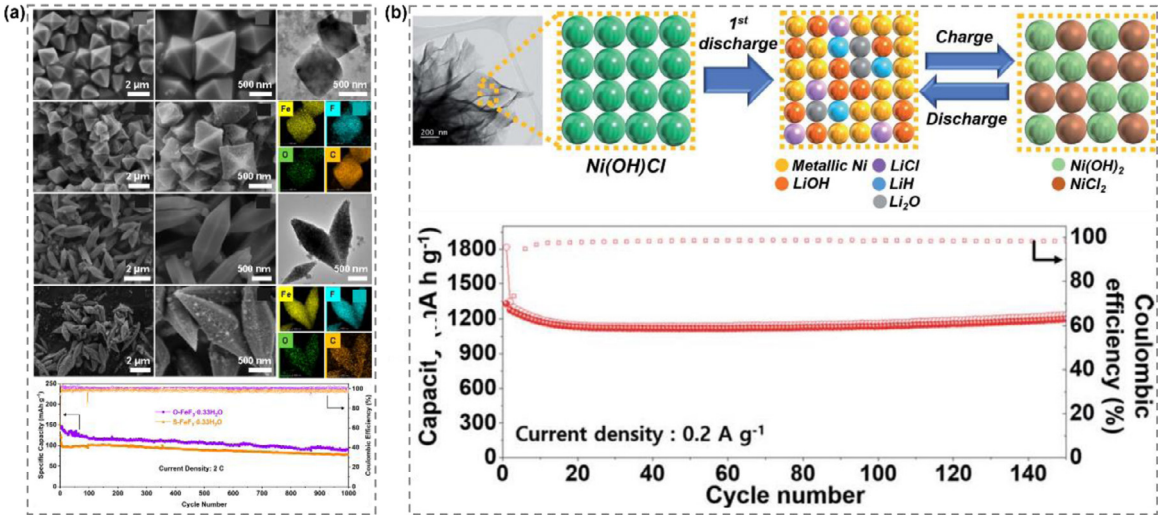

Fig. 4. (a) Scanning electron microscopy and transmission electron microscopy images and energy disperse spectroscopy mapping of octahedral-iron-metal organic framework, octahedral-FeF_3•0.33H_2O, and octahedral-FeF_3•0.33H_2O; spinel-iron-metal organic framework, spinel-FeF_3•0.33H_2O, and spinel-FeF_3•0.33H_2O. Long cycling properties of FeF_3•0.33H_2O [36] Copyright 2020 American Chemical Society. (b) Reaction mechanism of Ni(OH)Cl for lithium ion storage and electrochemical cycling properties of Ni(OH)Cl [39] Copyright 2020 The Royal Society of Chemistry.

Table 1
Systematic comparison of the electrochemical performances.

Material	Lifetime (cycles)	Capacity (mAh g^{-1})	Current density (mA g^{-1})	Ref.
Flower-like FeF_3	50	172.3	23.7	[28]
honeycomb-like FeF_3@C	1,000	~200	1,200	[29]
Multiwall carbon nanotube-MnF_2	100	480	0.1C	[30]
FeF_3/graphene quantum dots	1,000	162	200	[31]
FeF_2	300	450	50	[33]
CoF_2@C	200	~500	110	[34]
FeF_3/C nanotubes	300	~150	100	[35]
Octahedral FeF_3	1000	142	474	[36]
$CoCl_2$-$FeCl_3$-graphite	300	1,033	200	[38]
$CoCl_2$-$FeCl_3$-graphite	300	536	1,000	[38]
Layered Ni(OH)Cl	150	1,236	200	[39]
Mo-$FeCl_2$	300	472	300	[45]

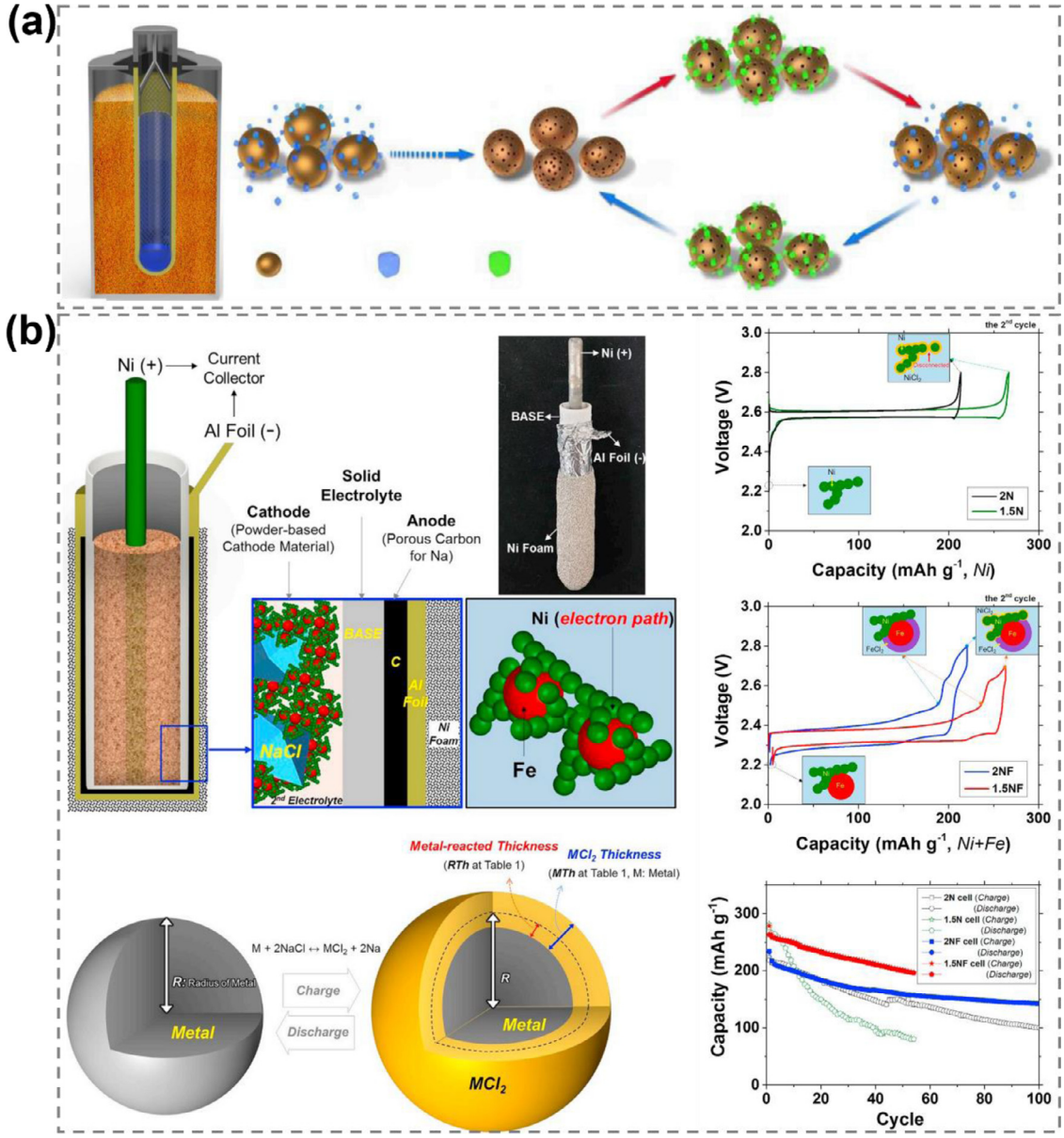

Fig. 5. (a) Schematic of the battery. Illustration of the evolution of the lithium chloride and brass particles during cycling [46] Copyright 2020 Elsevier. (b) Schematic cell diagram and microstructure variation; charge and discharge profiles and cycle performances [47] Copyright 2019 Elsevier.

focused on the morphologies, compositions, and lattice modulation, and further in-depth disclose of structural evolution during operation may be helpful for advanced electrode designs. Molten salt batteries could efficiently resolve most the involved issues, but whereas still face the challenge of limited practical usage due to its high operating temperatures. Other issues, such as rapid capacity decay and safety concerns, need more research attention as well. Employing modeling technology to pre-simulate the battery designs is a cost-efficient pathway for the fabrication of advanced energy storage devices [48].

2.1.1.2. Halogen-ion batteries. Metal-ion batteries are named after the charge carriers, *e.g.*, lithium ions are the charge carriers and shuttle between the anode and cathode upon charge (lithium ions move toward the anode from the cathode side) and discharge (lithium ions migrate oppositely) in lithium-ion batteries [49]. In contrast, shuttling inside batteries can also be achieved by using certain anions, such as chloride ions, as charge carriers, leading to the following halogen-ion batteries featuring anion-type charge carriers. These batteries are based on the use of halogen ions, such as fluoride, and chloride ions, as charge carriers and shuttling between the anode and cathode to achieve the charge and discharge of batteries, which differ from conventional metal-ion batteries that use metal ions to shuttle charges. In this chapter, we mainly discuss halogen-ion batteries containing fluoride and chloride ions; a focus is placed on both the advantages and disadvantages of each type of halogen-ion batteries. Finally, the remaining issues and challenges were discussed. Some possible solutions and strategies to were suggested to guide the following research efforts.

Fluoride-ion batteries featuring fluoride ion shuttling between the anode and cathode, as well as fluorination/defluorination of electrodes upon charging/discharging are potential candidates for post-lithium-ion battery technology due to their high energy density, which is comparable to that of lithium-ion batteries, and wide availability of resources [50,51]. However, the lack of a suitable electrolyte with satisfactory electrode/electrolyte interface stability and ionic conductivity imposes a barrier to the progress of fluoride-ion batteries. Enormous research efforts have been made to improve the electrochemical per-

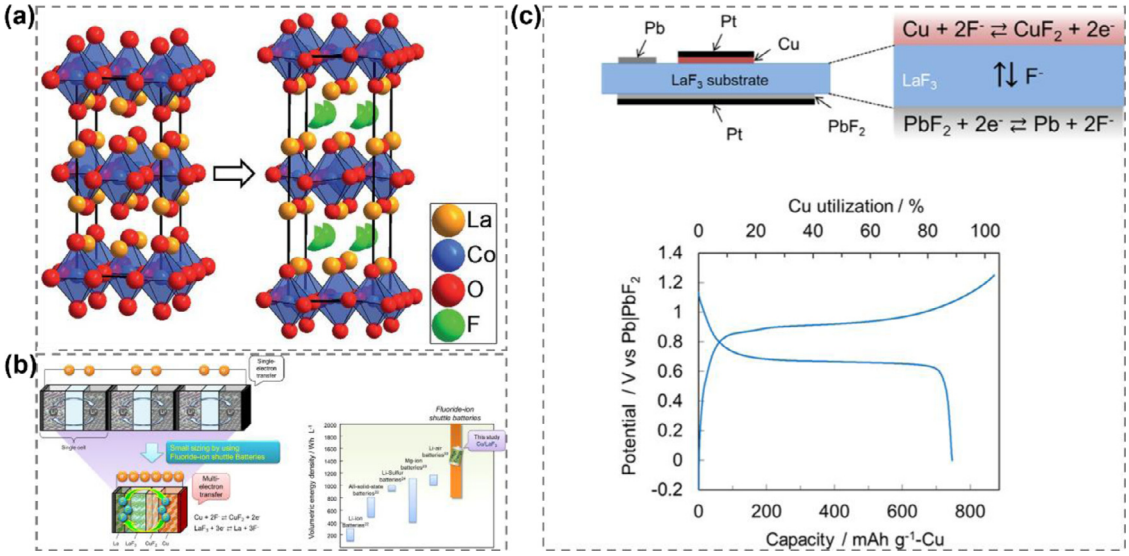

Fig. 6. (a) Schematic illustration of the charge intercalation process: La_2CoO_4 (left) and $La_2CoO_4F_y$ (right) [58] Copyright 2018 The Royal Society of Chemistry. (b) Charge-discharge mechanisms of the proposed multielectron chemistry, comparison of the energy density. (c) Schematic of the cell for studying the copper electrochemical reaction, charging/discharging curves under constant current conditions at 150°C [62] Copyright 2021 American Chemical Society.

formances of fluoride-ion batteries. Good chemical compatibility was demonstrated by Grenier et al. by studying a solid fluoride/carbon composite for solid-state fluoride-ion batteries [52]. Simultaneous percolation between $La_{0.95}Ba_{0.05}F_{2.95}$ and carbon in the composite ensured good electronic and ionic conductivities. The carbon materials were extensively adopted in electrodes to form composites to overcome or improve the poor conductivity of metal fluorides and to eventually improve the electrochemical performance of the batteries. Carbon nanotubes are good electronic conductor. Zhang et al. demonstrated the efficiency of introducing carbon nanotubes into a metal halide anode as a conductive additive, which delivered good electrochemical performance, with a capacity of 67 mAh g^{-1} at the 30th discharge [53]. A similar work by Konishi et al. demonstrated that adding carbon into the lead fluoride electrode helped to improve their capacities relative to those without carbon additives [54].

Regarding the dissolution of metal fluoride electrodes into electrolytes when utilized in fluoride-ion batteries [55], Konishi et al. demonstrated an electrolyte modification solution by dissolving a certain amount of cesium fluoride into the fluorobis(2,4,6-trimethylphenyl)borane electrolyte; subsequently, the dissolution issue of bismuth during charge operation was efficiently suppressed [56]. In addition, methods based on material structural design for addressing the electrode dissolution are extensively demonstrated, too. Intercalation, as one of the typical charge storage mechanisms, is an effective approach to storage charged ions without largely distorting the original electrode structure. The intercalation amount of charged ions into the hosting material is controllable by adjusting the cutoff voltage to avoid possible side reactions. Nowroozi et al. unprecedently demonstrated the selective fluoride-ion extraction from an oxyfluoride matrix, highlighting the feasibility of the materials with such lattice structures as electrodes of fluoride-ion batteries [57]. In particular, the storage amount of fluoride ions in the $LaSrMnO_4$ electrode was regulated by adjusting the cutoff voltage, which enabled a precise control over the insertion amount of fluoride. In combination with the density functional theory, a two-step fluoride-ion storage process, *i.e.*, $LaSrMnO_4 \rightarrow LaSrMnO_4F$ at approximately 1 V and $LaSrMnO_4F \rightarrow LaSrMnO_4F_{2-x}$ at approximate 2 V, was confirmed. Notably, the intercalated fluoride ions were completely extracted upon discharging with a capacity of approximate 100 mAh g^{-1}. Another example by Nowroozi et al. reported a new interaction-based cathode, *i.e.*, La_2CoO_4, which enables 1.2 fluoride ions storage per formula accompanied by a large volume expansion (Fig. 6a) [58]. Furthermore, side reactions were efficiently avoided by adjusting the cutoff capacity. Therefore, the (de)intercalation capability and during which the structural evolution is highly crucial factors [59]. Yamanaka et al. studied the microevolution of electrode materials during fluorination and defluorination process by adopting BiF_3 as the research subject [60]. The defluorination of BiF_3 always started from the protruded positions with a small curvature radius, *i.e.*, positions far from the current collector, which thus suggested that small size of active materials are beneficial. The favored pathways within metal fluoride electrodes were studied by Haruyama et al. through the first-principal theory [61]. As a result, fluorination and defluorination of metal fluoride electrodes occurred, obeying a two-phase process based on the calculation of formation enthalpies, fluoride-vacancy enthalpies, and interstitial fluorine defect enthalpies.

To enable multielectron redox chemistry for higher capacity values, Nakano et al. introduced multielectron redox chemistry by using the concept of combining multicells in a signal unit, as shown in Fig. 6b [62]. The assembled cell delivered a high capacity of 870 mAh g^{-1} (Fig. 6c), benefiting from the multielectron transfer chemistry.

Chloride-ion batteries, as a typical type of anion shuttling-based battery chemistry, have recently obtained extensive research efforts due to the abundant reserves of chlorine-containing composites and the advantages of chloride-shuttling electrolytes at room temperature [63–65]. However, a lack of favorable and superior cathode candidates significantly hampers the further development of chloride-ion batteries. The conventional metal chloride compounds featuring a perovskite-like microstructure are well known for their dissolution in electrolytes after the discharge operation in rechargeable chloride-ion batteries, due to the formation of lower-charged products. Recently, a multiple metal-containing electrode with a layered structure was studied by Yin et al. The layered double hydroxide ($Ni_2V_{0.9}Al_{0.1}$-Cl) as a cathode material of chloride-ion batteries exhibited good electrochemical performances of 312 mAh g^{-1} at 200 mA g^{-1} and a long lifespan of 1,000 cycles with a capacity retention of 114 mAh g^{-1} [66]. The good performance was attributed to a synergetic effect among the V^{m+} (for higher redox activity), Ni^{2+} (for favorable electronic conductivity), and Al^{3+} (for a robust physical structure) cations inside the cathode matrix. One unsatisfactory factor of the reported layered double metal hydroxide is the absence of distinct charging/discharging plateaus, which is extraordinarily dif-

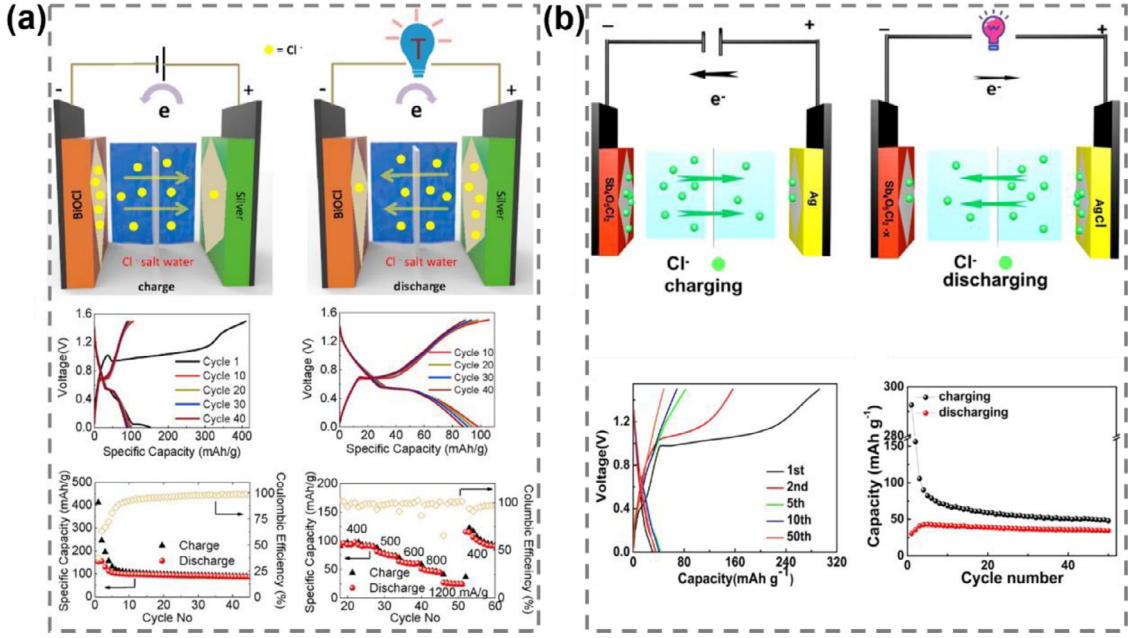

Fig. 7. (a) Schematic illustration of the rechargeable chloride-ion batteries during the charging/discharging process. Electrochemical performance of the chloride-ion batteries: charge and discharge curves, cycling performance, and rate capabilities [72] Copyright 2017 Elsevier. (b) Schematic representation of the aqueous chloride-ion battery. Electrochemical performance: charging/discharging curves and cycling tests [75] Copyright 2019 American Chemical Society.

ferent from the conventional intercalation/deintercalation-based charge storage mechanism for layered electrodes with mono- or multiple charging/discharging plateaus [67–69].

2.1.2. *Metal-oxy-halogen electrodes*

Metal-oxy-halogen is a typical type of layered material that is similar to metal dichalcogenides, such as molybdenum sulfide and tungsten sulfide, with an alternative arrangement of metal and halogen/oxygen species to form a sandwich structure [70]. Van der Waals forces bond each sandwich layer, which allows charge carriers intercalation and deintercalation upon discharging and charging. Such layered materials, thus, received intensive attention for being employed as cathode materials of chloride-ion batteries, enabling an intercalation/deintercalation-based chloride ions storage mechanism [71]. Among the metal-oxy-halogen compounds, metal-oxychlorides have been the focus of intensive research efforts as cathode materials in chloride-ion batteries. A typical aqueous chloride-ion battery designed by Chen et al. using BiOCl as an anode and silver as a cathode, together with an aqueous sodium chloride electrolyte, delivered a capacity of 92.1 mAh g^{-1} at 400 mA g^{-1} (Fig. 7a). Such chloride-ion battery operation rely on both conversion (silver electrode) and intercalation (BiOCl electrode) reactions, suggesting a good balance between these two charge-storage mechanisms [72].

Composite cathodes are extensively designed and studied to overcome the shortcomings of pure metal oxy-halogen compounds [73]. Lakshmi et al. designed and fabricated a composite cathode, $Sb_4O_5Cl_2$/graphene aerogel, using layered $Sb_4O_5Cl_2$ for chloride-ion batteries; it delivered a capacity of approximate 100 mAh g^{-1} and a lifespan of 80 cycles with a capacity retention of approximate 65 mAh g^{-1} [74]. Hu et al. designed and fabricated a metal-oxy-chloride, $Sb_4O_5Cl_2$, and demonstrated its potential for use as an anode of chloride-ion batteries (Fig. 7b) [75]. When pairing such an anode with a silver cathode, a discharge capacity of 34.6 mAh g^{-1} at 600 mA g^{-1} with a lifespan of 50 cycles was attained (Fig. 7b). Gao et al. demonstrated a superior high-rate capability of 113 mAh g^{-1} after 100 cycles at 522 mA g^{-1} [76]. Further research efforts focusing on VOCl electrodes are needed to obtain an in-depth understanding of the underlying reasons for the high-rate performance.

Structural modification is an efficient pathway for promoting the structural stability of materials. An interstitial space expended metal-oxy-halides, FeOCl, studied by Yu et al. exemplified the use of polyaniline-inserted for chloride-ion batteries [77]. The interlayer space was greatly expanded from 0.79 to 1.4 nm by the intercalation of polyaniline; such an expanded interspace improved the lifespan, delivering a higher capacity retention of 82% relative to normal FeOCl, which is only 42%, by mitigating structural collapse. A vacuum impregnation and thermal treatment-enabled FeOCl/CMK-3 was designed and fabricated by Yu et al. (Fig. 8) [78]. The layered cathode demonstrated good electrochemical performance, delivering a capacity of 202 mAh g^{-1}. The electrolyte demonstrated a good affinity toward the chloride layer within the FeOCl, which resulted in favorable expansion along the *b*-axis (Fig. 8).

Double metal hydroxides with layered microstructures demonstrated high potential as cathode materials for chloride-ion batteries, too. A dual metal hydroxide, CoFe-Cl, was designed and fabricated by Yin et al. for use as the cathode of chloride-ion batteries; such a cathode delivered an unprecedented high capacity of 239 mAh g^{-1} and a lifespan of 100 cycles, with a capacity retention of approximate 160 mAh g^{-1} [79]. Later, Yin et al. fabricated a layered double hydroxide, NiFe-Cl, and demonstrated its superior capacity of 351 mAh g^{-1} and a long lifespan of 800 cycles with a capacity retention of 101 mAh g^{-1} at 100 mA g^{-1}, which is among the highest capacity values obtained (Fig. 9a) [80]. Various in-situ and ex-situ characterizations were used to demonstrate the redox pairs of $Fe^{2+/3+}$ and $Ni^{2+/3+}$, which are responsible for the charge storage process.

To mitigate the structural distortion and prolong the lifetime of metal-oxy-halogen electrodes, composite electrodes have been widely studied. Luo et al. demonstrated a composite cathode comprising NiMn-Cl active materials and highly conductive carbon nanotubes for chloride-ion batteries (Fig. 9b) [81]. Benefitting from the robust host, the composite cathode delivered a decent lifespan of 150 cycles with a capacity of approximate 130 mAh g^{-1}. The migration coefficient of chloride ions in the NiMn-Cl/carbon nanotubes was found to be 10^{-10}-10^{-12} cm^2 s^{-1} (Fig. 9b). Coating of protective polymer is also efficient to prevent the active material from decomposition [82]. In addition, we provided a systematic comparison of the electrochemical performances in Table 2.

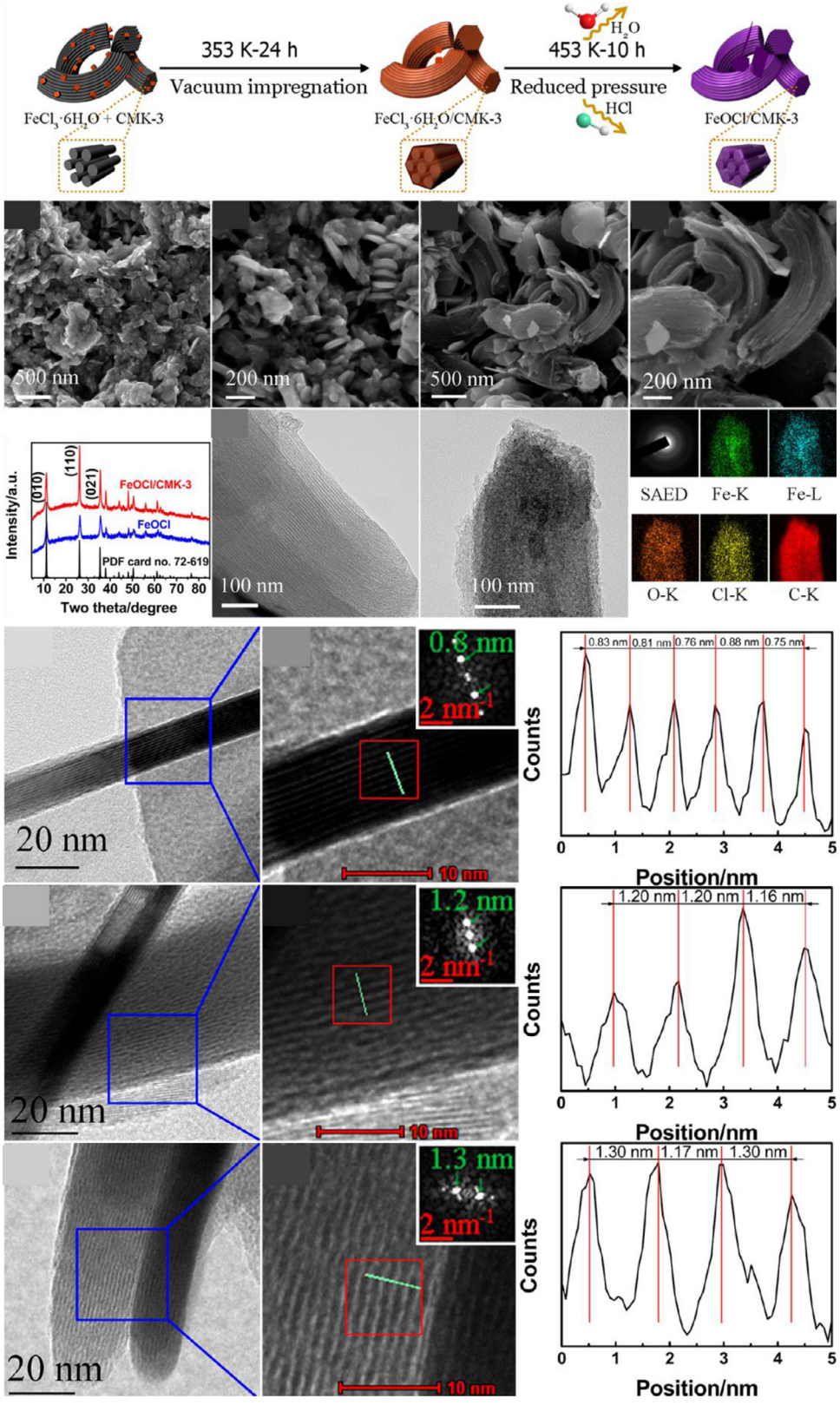

Fig. 8. Fabrication process of FeOCl/CMK-3: scanning electron microscope images, X-ray diffraction patterns, transition electron microscope image, the corresponding selected area electron diffraction, and elemental mapping. High resolution transition electron microscope images of the FeOCl nanosheet [78] Copyright 2017 American Chemical Society.

2.1.2.1. Metal ion batteries. Metal oxyfluorides have been extensively studied in metal ion batteries. A fluorine-doped $Na_{0.44}MnO_2$ electrode proposed by Shi et al. demonstrated an extraordinary capacity of 149 (0.5 C) and 138 (1 C) mA h g^{-1}, as well as impressive cyclic capability of 400 cycles at 5 C with a 79% capacity retention, benefitting from the modified structure through the substitution of structural oxygen by fluoride ions [83]. An in-depth review summarized the reported use of transition metal oxyfluoride materials for lithium- and sodium-ion batteries [84]. In addition, a recent review by Zhao and co-workers summarized the typical application of metal-oxy-halogen

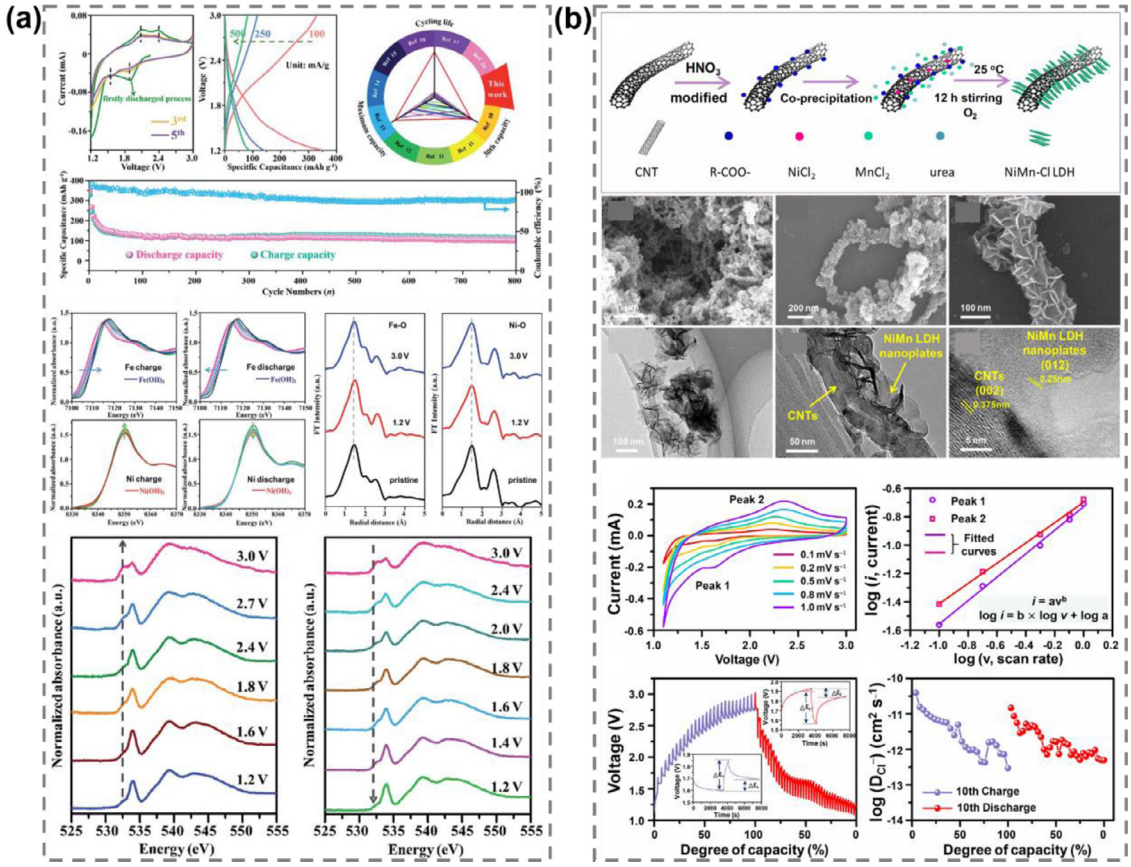

Fig. 9. (a) Electrochemical performance of the chloride-ion battery assembled with the NiFe-Cl cathode: cyclic voltammetry curves, galvanostatic charging/discharging curves, cycle performances and corresponding coulombic efficiency, discharge capacity and cycling life. In-situ X-ray absorption near-edge structure spectra of iron and nickel K-edges. Normalized oxygen K-edge soft X-ray absorption spectra [80] Copyright 2020 The Royal Society of Chemistry. (b) Schematic preparation of NiMn-Cl/carbon nanotubes and characterizations, scanning electron microscopy and transition electron microscopy. Electrochemical performances: cyclic voltammetry curves, log *i* vs. log *v* plots, galvanostatic intermittent titration technique profiles, and the chloride ion diffusion coefficient [81] Copyright 2020 American Chemical Society.

Table 2
Systematic comparison of the electrochemical performances.

Material	Lifetime (cycles)	Capacity (mAh g^{-1})	Current density (mA g^{-1})	Ref.
BiOCl	40	92	400	[72]
$Sb_4O_5Cl_2$/graphene aerogel	80	100	10	[74]
$Sb_4O_5Cl_2$	50	35	600	[75]
VOCl/C	100	113	522	[76]
FeOCl/CMK-3	30	202	10	[78]
CoFe-Cl layered double hydroxide	100	160	100	[79]
NiFe-Cl layered double hydroxide	800	101	100	[80]
NiMn-Cl layered double hydroxide/C nanotubes	150	130	50	[81]

compounds in many common battery chemistries, such lithium and magnesium ion batteries [12]. Besides the studies on elemental substitution to form dual-metal-oxy-halogen compounds as summarized in those review articles, some composite designs suggest another approach for the structural construction [85,86]. Sun and co-workers developed a graphene anchored few-layer BiOCl for sodium ion storage application [87]. The introduction of such graphene significantly enforces the charge transfer and structural integrity. Transition metal oxyhalides have seen great progress so far with highly improved electrochemical performances, such as cycling durability and charge storage capacity, which highly promote the commercialization of such materials. But whereas more spotlight should be put on the further study of structural integrity by introducing other assisted functional materials such as two-dimensional and layered wrapping materials [88,89].

2.1.3. Fluoride-containing metal-based polyanions

The metal-based polyanions, such as $NaVPO_4F$, are a type of critical materials which have been extensively exploited as cathodes of sodium-ion batteries. Numerous reports have demonstrated that the substitution of fluorides is beneficial for a higher voltage plateau due to the inductive effect, by which it promotes a higher energy density. In addition, such a high voltage is helpful for the (de)insertion of more charge carriers for an even larger capacity. To date, many research efforts on the fluoride-containing transition metal-based, such as iron, vanadium, and cobalt, polyanions have been conducted as cathodes of sodium-ion batteries. Regarding this field, some pioneering review articles have systematically summarized these materials with a focus on the metal-based polyanions, such as phosphates and fluorophosphates. In those efforts, the fluoride-containing meal-based polyanions are well organized in individual chapters with the discussion from structural traits to

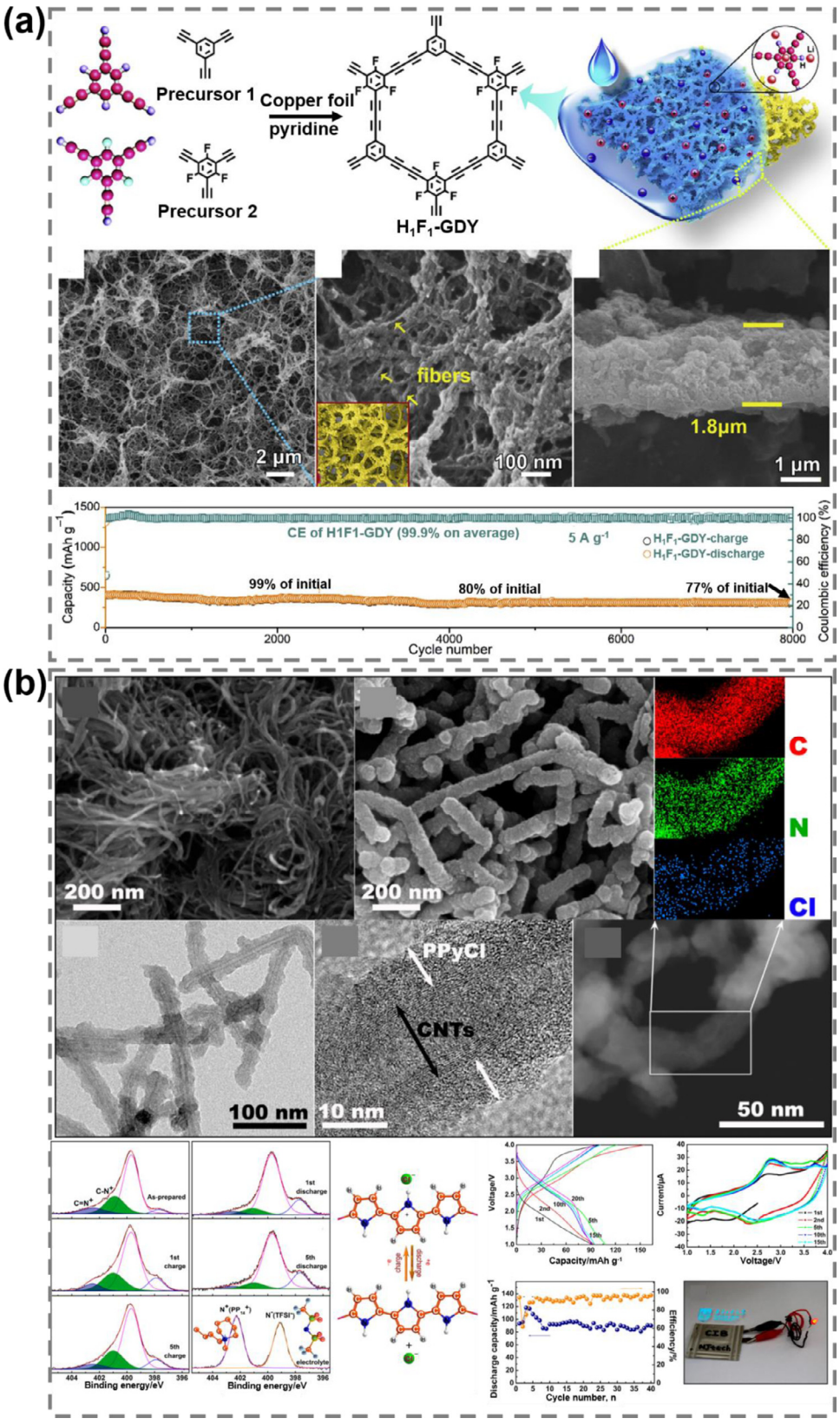

Fig. 10. (a) Structure and morphology characterizations of H1F1-GDY. Cycling performance of H1F1-GDY [91] Copyright 2020 Elsevier. (b) Material characterizations of nanostructured polymer electrode. X-ray photoelectron spectra of N 1s region and a schematic illustration of the charge and discharge reactions. Electrochemical performance: discharge and charge curves, cyclic voltammetry patterns, cycling performance, and optical image [95] Copyright 2017 American Chemical Society.

electrochemical performances. Herein, a repeated summarization of the fluoride-containing metal-based polyanions is avoided. But a brief summarization and particular focus on the remaining issues and scientific challenges, however, are necessary to emphasize. Regarding the synthesis of fluoride-containing metal-based polyanions, there still lacks a highly efficient technology with low cost and non-rigorous experimental conditions for precise control over the stoichiometric of products. More studies on the phase design of electrode materials as well as the phase evolution during battery operation will be beneficial for the fundamental understanding of the interrelationship between crystal phases

and electrochemical behaviors, given the current controversial opinions about whether the charge-storage process in fluoride-containing metal-based polyanions is insertion or solid-solution. In addition, limited lifetime is another shortage for this kind of materials. Given these remaining issues, more future research efforts need to focus on the exploration of the fundamental relationship between constitutions and structures, structures and electrochemical performances. Furthermore, product-controllable synthesis process by adjusting the precursors plays a basic role for the research of material science. Finally, more composite structures, such as carbon coating, conductive polymer wrapping, and layered materials supporting, need to be extensively studied for prolonging the efficient lifetime.

2.1.4. Halogen-doped composite electrodes

Halogen and halogen-containing compounds can also be employed as dopants for electrodes to improve the electrochemical performance of basal materials, which is capable of having beneficial synergetic effects on the electrochemical cycles. Wang et al. studied the doping effect of iodine on carbon by synthesizing iodide- and nitrogen-co-doped carbon spheres for use as an anode material in lithium-ion batteries [90]. The assembled cell exhibits a tremendously high volumetric capacity of 1,418 mAh g^{-1} at 0.05 mA cm^{-2} and good lifetimes of 100 cycles at 0.1 mA cm^{-2} with 1,335 mAh cm^{-3} capacity retention and 500 cycles at 1 mA cm^{-2} with 1,090 mAh cm^{-3} capacity retention, benefitting from the synergistic effect. A study on the fluoride-doping effect on graphdiyne (GDY) by Lu et al. demonstrated a high capacity of 2,050 mAh g^{-1} at 50 mA g^{-1} and a long lifetime of 8,000 cycles with only a 23% capacity reduction, benefitting from the co-doping of hydrogen (for large capacity) and fluoride (for high stability), as shown in Fig. 10a. Fluoride doping adjusted the pore structure of GDY, and formed a more stable interfacial structure [91].

Furthermore, chlorine-doped GDY was further studied by Wang et al. [92]. The introduction of chloride atoms into the GDY matrix synergistically assisted to stabilize the intercalated lithium ions by their large atomic size and electronegativity, which thus generated more lithium-ion storage sites. In addition, halogen has been demonstrated to be a good dopant for organic electrodes, such as poly-pyrrole and polyaniline [93,94], to functionalize the basal materials. Zhao et al. designed and fabricated a chloride-doped poly-pyrrole for use as a cathode of chloride-ion batteries; such an organic electrode demonstrated that the redox process was modified by nitrogen species and chloride ions within the matrices [95]. The chloride-ion batteries assembled with the chloride-doped organic cathode delivered a capacity of 118 mAh g^{-1} and superior cycling stability (Fig. 10b).

2.2. Halogen-containing compounds in electrolytes

Halogen-containing compounds are intensively studied as a critical portion of electrolytes in rechargeable batteries. The ionic conductive capability of metal halides is a key parameter for the realization of all solid-state batteries. Furthermore, unique ionic sizes of halogen species promote the ionic conductivity of solid-state electrolytes when used as dopants in solid-state electrolytes. Unique chemical activity and electrochemical performances of halogen ions enable uniform and smooth electrolyte/electrode interfaces by stabilizing metal ion deposition during charging operations. For the halogen ion batteries, halogen ions serve as the shuttling species to storage electric energy. In this chapter, we summarized the utilization of active halogen-containing compounds in electrolytes, and the summarization and discussion were organized from the perspective of their utilization objectives, including transport of charge carriers, improvement of ionic conductivity, and stabling solid electrolyte interfaces. We focus on the effects of halogen species in those compounds on the electrochemical performances, such as rate performances and cycling capability. Halogen-containing salts only were under consideration for the applications of halogen-containing compounds in liquid-state electrolyte systems, and the halogen-containing solvents were not under consideration.

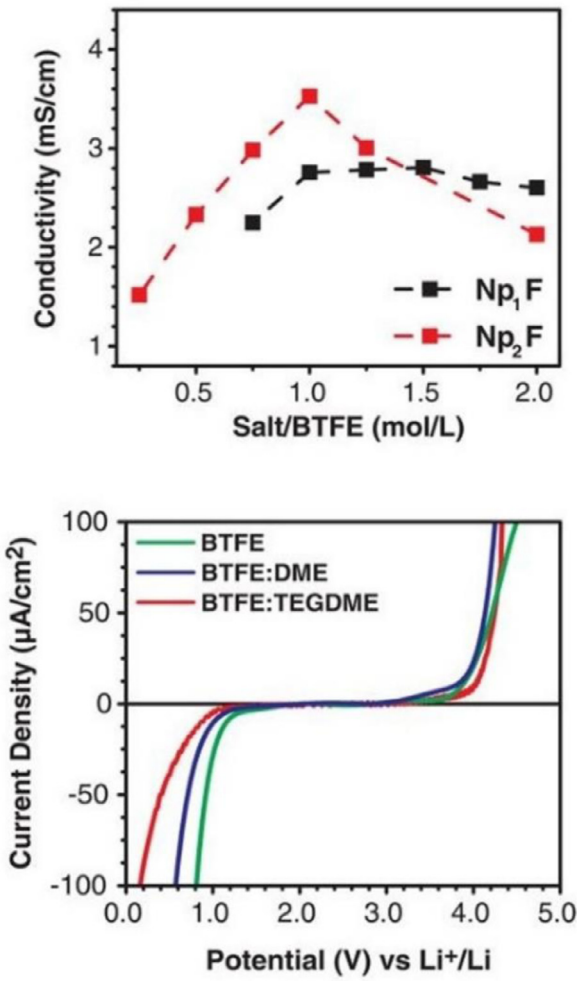

Fig. 11. Ionic conductivity of N,N,Ntrimethyl-N-neopentylammonium fluoride (Np1F, black) or N,N,N-dimethyl-N,N-dineopentylammonium fluoride (Np_2F) in liquid bis(2,2,2-trifluoroethyl)ether (BTFE) electrolyte solutions as a function of concentration. Linear sweep voltammograms for the as-prepared electrolytes. 1,2-Dimethoxyethane (DME); bis[2-(2-methoxyethoxy)ethyl]ether (TEGDME) [97] Copyright 2018 Science.

2.2.1. As charge carriers for shuttling

2.2.1.1. Organic electrolytes in fluoride-ion batteries. Dissolving fluoride-containing salts into organic solvents has been extensively studied thus far [96]. Due to the poor solubility of metal fluoride salts, studies on fluoride-containing organic salts were widely reported. Davis et al. developed an organic electrolyte by dissolving tetraalkylammonium fluoride salts into ether solvents for high ionic conductivity [97]. Organic fluoride salts (N,N,Ntrimethyl-N-neopentylammonium fluoride (Np1F) and N,N,N-dimethyl-N,N-dineopentylammonium fluoride) are synthesized given the insolubility of metal fluorides. The authors screened three broad classes of organic solvents, which are, above synthesized, salt insoluble, soluble but fluoride reactive (higher electrolyte concentrations, over 0.5 M), and soluble and fluoride stable (limited electrolyte concentrations). As a consequence, a high fluoride ionic conductivity of approximately 3.5 mS cm^{-1} (Fig. 11) was attained for a 1 M N,N,N-dimethyl-N,N-dineopentylammonium fluoride solution using a bis(2,2,2-trifluoroethyl)ether solvent, which is comparable to ionic liquid-based electrolytes. Moreover, the linear sweep voltammograms suggest a 3 V wide potential window (Fig. 11), enabling the operation

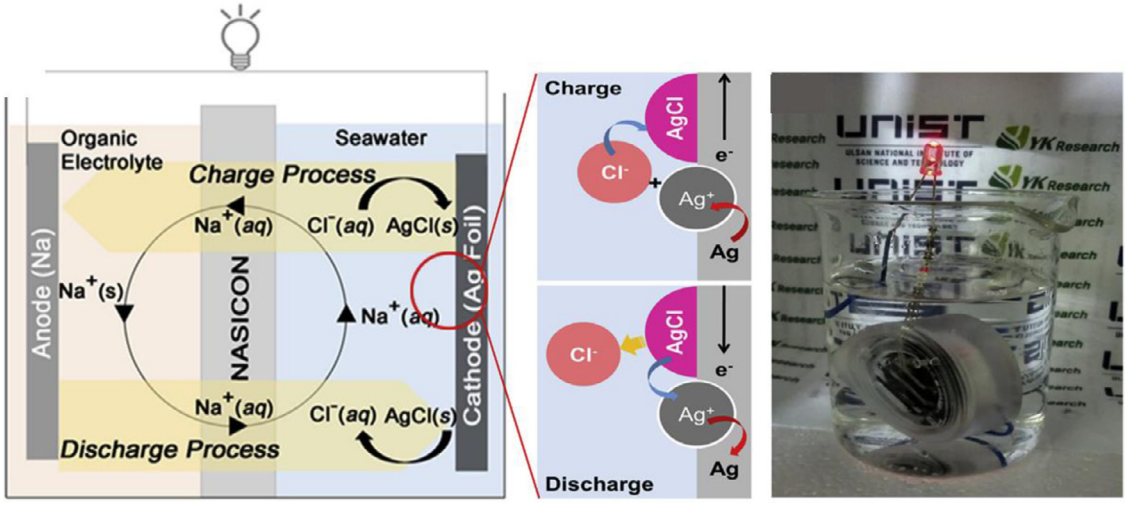

Fig. 12. Schematic illustration of the seawater battery [100] Copyright 2016 Elsevier.

of more electrode material. More studies on organic liquid-phase electrolytes are suggested to widen the understanding of this field given the currently limited reports.

2.2.1.2. Aqueous electrolytes in fluoride-ion batteries. Aqueous electrolytes are promising for forming batteries with reliable safety and affordable cost efficiency. Hou et al. reported an aqueous fluoride-ion battery using sodium fluoride salt solution as the electrolyte [98]. Reversible charging/discharging was realized by the redox couples of Bi^{3+}/Bi and 4-hydroxy-TEMPO/4-hydroxy-TEMPO^{+} with an appropriate capacity of 89.5 mAh g^{-1} after 85 cycles at a specific current of 1,000 mA g^{-1}.

2.2.1.3. Aqueous electrolytes in chloride-ion batteries. Given the large abondance of resources, seawater comprises enormous chlorides, thus inspiring researchers to study seawater electrolyte-based rechargeable batteries [99]. A study by Kim et al. using Ag foil as the cathode reversibly formed silver chloride with chloride ions from the seawater electrolyte (Fig. 12) [100]. Furthermore, a concentration flow battery designed and constructed by Tan et al. demonstrated that metal chlorides, such as $BiCl_3$, $CoCl_2$, and VCl_3, have high potential as cathodes for such batteries due to their chloride-ion insertion and extraction capabilities [101]. Improved electrochemical kinetics were attained when the metal chlorides were replaced with metal oxychlorides [102].

2.2.1.4. Ionic liquid electrolytes in fluoride-ion batteries. Along with the development of solid-state electrolytes for fluoride-ion batteries, attention has been focused on seeking desirable liquid-state electrolytes to improve the ion concentration and the diffusion kinetics [103]. Okazaki et al. developed an ionic liquid-based liquid-state electrolyte by dissolving an organic fluoride into an ionic liquid, forming an electrolyte with a rational fluoride ion conductivity of 2.5 mS cm^{-1} at room temperature [104]. The feasibility of the room temperature fluoride-ion batteries was further demonstrated with favorable electrochemical revisability when assembled with bismuth (cathode) and lead (anode). The surficial change in bismuth before and after oxidation was clearly confirmed through scanning electron microscopy; a rough and crack-rich surface was formed, suggesting the bismuth oxidation (Fig. 13).

2.2.1.5. Ionic liquid electrolytes in aluminum-ion batteries. In addition, chloride-containing ionic liquid was extensively studied in aluminum-ion batteries and dual-ion batteries. The ionic liquid based electrolyte made by anhydrous aluminum chloride and 1-ethyl-3-methylimidazolium chloride mixture was reported by Lin et al., which thereafter was widely adopted as the common electrolyte in aluminum-ion batteries and dual-ion batteries. [105–108]. The stripped aluminum ions from anode side associated with aluminum chloride anions ($AlCl_4^-$) to form a dual-aluminum chloride anions ($Al_2Cl_7^-$), and the aluminum chlorides inserted in the cathode could be deintercalated into the ionic liquid electrolyte to complete the discharging process. The charging process goes the other way around. Currently, the studies on aluminum-ion batteries mainly focus on the exploration of novel cathode materials, thus, more efforts are encouraged on the exploration of high-performance electrolytes given that the feasibility of other electrolyte systems has been demonstrated in some pioneering reports [109,110].

2.2.1.6. Molten electrolytes in alkali metal-ion batteries. In addition, molten alkali metal halide salts have favorable electrochemical/thermal stability and conductivity, which make them promising electrolyte candidates. Sodium iodide-lithium iodide-potassium iodide has the lowest melting temperature among the alkali metal halide electrolytes for liquid metal batteries, which helps to reduce the self-discharge and operating temperatures of batteries. The good ionic conductivity promises lower voltage hysteresis, improving the capacity utilization. A concept of a liquid-state pseudo-binary electrolyte was proposed by Gong et al. [111]. Sodium iodide was dissolved into a binary lithium iodide-potassium iodide solvent at a relatively low temperature of approximate 290°C, with a solubility of approximate 7 mol%. Based on the phase diagram (Fig. 14) validated by the experimental results, the lithium iodide-potassium iodide mixture exhibited a lower melting point relative to the chloride counterpart. The low melting point and sufficient sodium-ion conductivity, thus, enable the use of a low-temperature electrolyte for liquid sodium-ion batteries.

2.2.1.7. Solid-state electrolyte in fluoride-ion batteries. Two classes of solid-state electrolytes, *i.e.*, alkali-metal fluorides and alkaline-earth metal fluorides, are widely employed in solid-state fluoride ion batteries, where the former has a fluorite-type structure and the latter has a tysonite-type structure. Bhatia et al. [112] optimized the conductivity of tysonite-type $La_{1-x}Ba_xF_{3-x}$ solid electrolytes by reducing the grain boundary resistance upon sintering. The obtained product exhibits an ionic conductivity of 1.26×10^{-4} at 60°C, which is one order of magnitude higher than that of the as-prepared pellet and ball-milled batches. To further enhance the ionic conductivity of the tysonite-type solid-state electrolyte, Zhang et al. synthesized a fluoride-containing solid-state thin film ($La_{0.9}Ba_{0.1}F_{2.9}$) [113]. The authors found that a higher conductivity of 1.6×10^{-4} S cm^{-1} was attained at 170 °C through sintering at 450 °C for 4 h. Similarly, Rongeat et al. studied the ionic conductivity using alternating current and direct current analyses, emphasizing

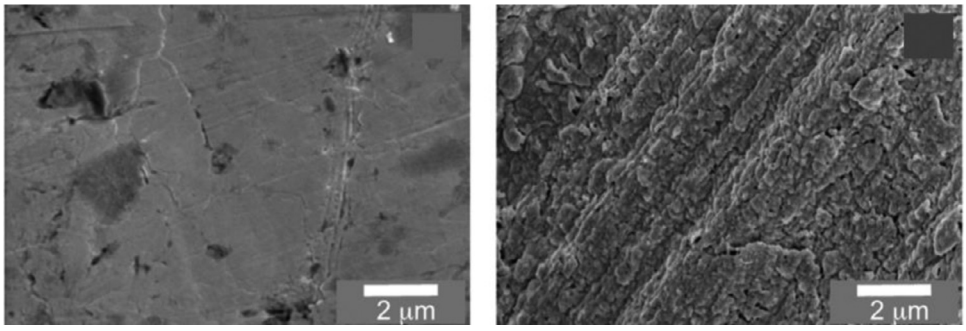

Fig. 13. Scanning electron microscopy images of the bismuth electrode before and after oxidation [104] Copyright 2017 American Chemical Society.

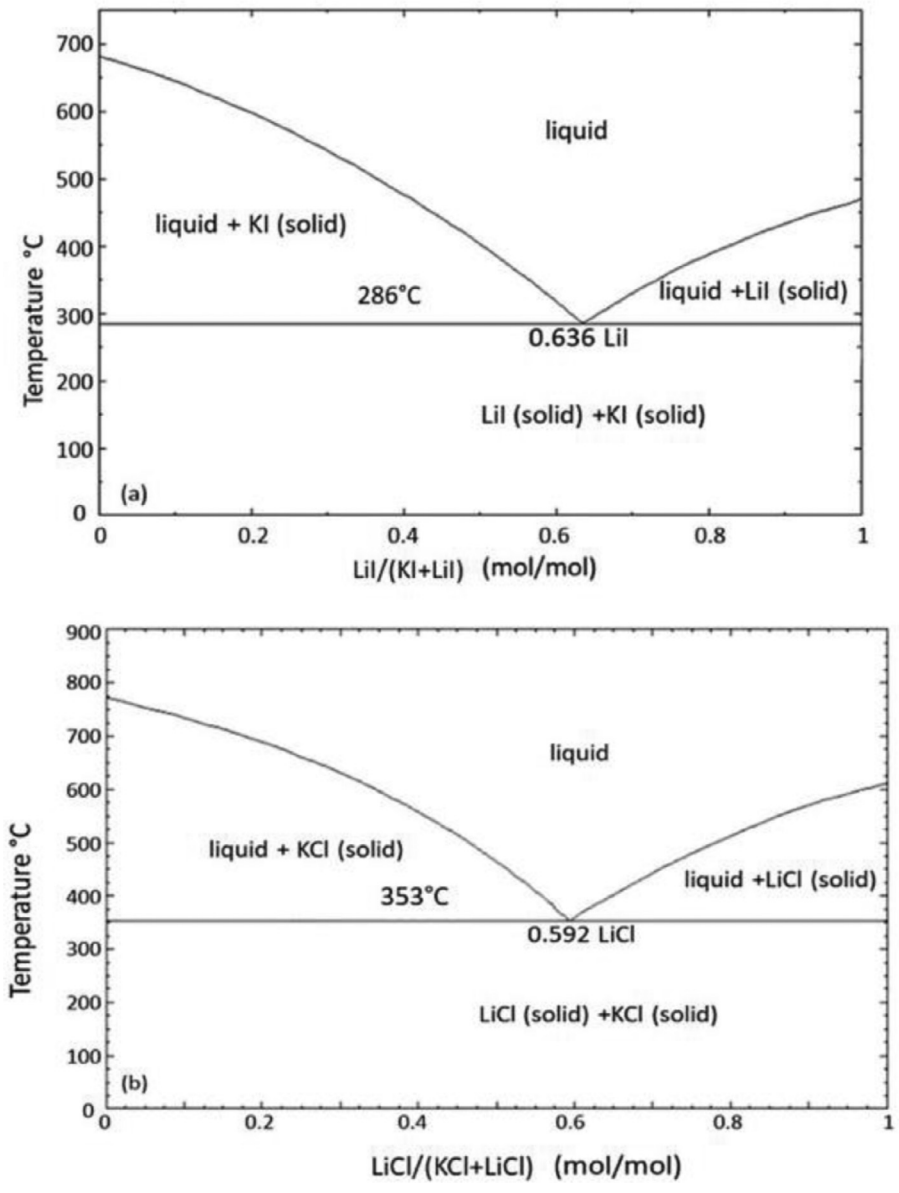

Fig. 14. Phase diagrams of the binary system: lithium iodide-potassium iodide (top) and lithium chloride-potassium chloride (bottom) [111] Copyright 2020 Elsevier.

the blocking effect of grain boundaries on ionic transports [114]. Sintering to have fewer grain boundaries and a larger grain size is thus pursued for higher ionic conductivity. Pan et al. presented halogen interdiffusion behavior in the halogen-containing perovskite cesium-lead-bromide [115]. Chloride-bromide couples diffuse within the perovskite with an activation energy of 0.44 ± 0.02 eV. In contrast, iodide-bromide couples are not allowed to migrate owing to the possible complex phase behaviors. This study provides more insights into halogen transfer in the development of solid-state electrolytes for halogen-ion batteries [116].

Lattice engineering is another solution to enhance the ionic conductivity of solid-state electrolytes for fluoride-ion shuttling. The use of a solid-state electrolyte with fluoride-ion hoping sites and migrating pathways is beneficial to decrease the energy barrier for long-range ionic transport. Breuer et al. studied the doping effect of strontium on LaF_3; a

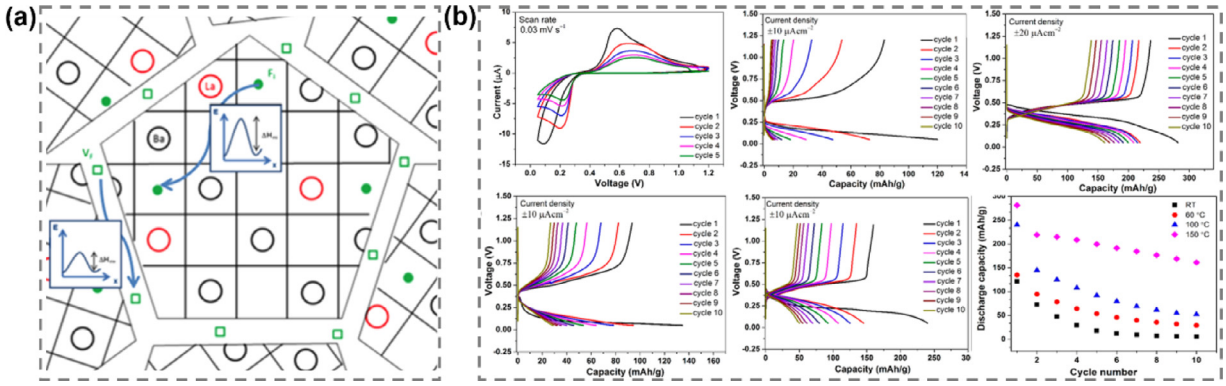

Fig. 15. (a) Schematic diagram of fluoride ion migration pathways [118] Copyright 2013 American Chemical Society. (b) Electrochemical studies on a Sn/$BaSnF_4$/BiF_3 cell: cyclic voltammogram, charging/discharging profiles, and repeated cycling performance [121] Copyright 2018 American Chemical Society.

several orders of magnitude increase in ionic conductivity was attained relative to strontium-free conductivity, benefiting from the lattice strain and fluoride defect sites generated by introducing strontium ions [117]. Furthermore, the activation energy of ionic transfer is decreased by 0.26 eV, *i.e.*, from 0.75 eV for LaF_3 to 0.49 eV for $La_{0.9}Sr_{0.1}F_{2.9}$. Introducing larger strontium ions resulted in increased strain, as confirmed by the X-ray diffraction patterns with a small shift of the characterized peak upon introducing strontium ions. The beneficial effect of a certain amount of point defects inside the solid-state electrolyte, which participate in and facilitate the ionic transport, was further proved by Rongeat et al. [118]. Moreover, the generation of grain boundaries by nanotechnology provides additional pathways for fluoride ion conduction (Fig. 15a).

Apart from the introduction of dopant species, modifying the crystalline sizes and morphologies also plays a significant role in improving the ionic conductivity. Regarding this factor, Patro et al. demonstrated the synthesized method dependence of the ionic conductivity [119]. Samples synthesized by the mechanochemical method exhibited higher ionic conductivity than those synthesized by the normal solid-state reaction technique [120]. Mohammad et al. demonstrated a full-cell fluoride ion battery with $BaSnF_4$ as the solid-state electrolyte at room temperature, tin or zinc as the anode, and BiF_3 as the cathode, confirming the feasibility of $BaSnF_4$ for fluoride ion batteries [121]. However, poor revisability and quick decay are the remaining issues. Favorable charging/discharging operation was only attained at a very small current density of 10 μA cm^{-2} (Fig. 15b), which suggests the need of a study on large current densities. Vergentev et al. demonstrated that the ionic conductivity of LaF_3 can be increased by SrF_2, due to the redistribution of charge carriers at diverse chemical potentials [122], and the ion transport may proceed via lattice mismatch or the formation of a new solid phase. A $PbSnF_4$ synthesized by Fujisaki et al. through mechanical milling exhibited two phases, *i.e.*, γ and β, strikingly, the fluoride interstitial sites increase upon the γ to β phase transition [123].

Special battery designs are also attained wide attention. Mohammad et al. developed a dual-electrolyte concept for the solid-state fluoride ion batteries by adopting $BaSnF_4$ for high ionic conductivity and $La_{0.9}Ba_{0.1}F_{2.9}$ for a wide potential window (Fig. 16) [124]. Through optimizing the thickness of each layer, a one order of magnitude higher ionic conductivity (0.89×10^{-5} S cm^{-1}) relevant to bare $La_{0.9}Ba_{0.1}F_{2.9}$ was thus attained with 45-μm thick $La_{0.9}Ba_{0.1}F_{2.9}$ at room temperature. This report presents an efficient but facile design mechanism for solid-state electrolytes with high ionic conductivity, highlighting the feasible concept of combining electrolytes with different features. Furthermore, the development of solid-state electrolytes might also be an efficient method for addressing the dissolution and loss of cathode active species, which has been demonstrated in principle pioneered by Chen et al. [125]. Regarding solid-state electrolytes for fluoride ion batteries, more detailed information refers to the excellent review article by Nowroozi et al. [126].

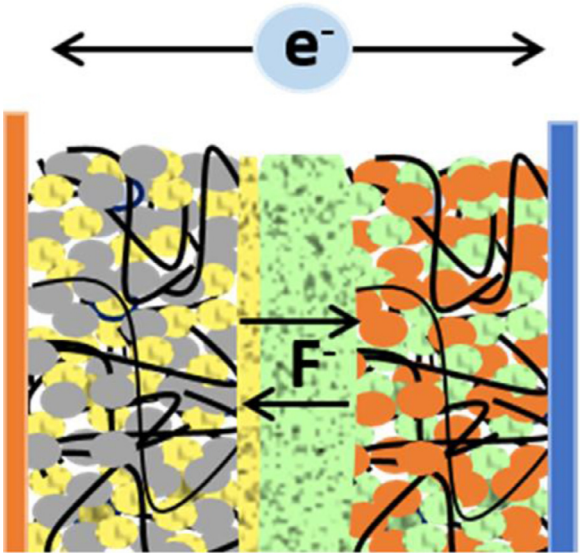

Fig. 16. Schematic illustration of dual-electrolyte solid-state fluoride-ion batteries [124] Copyright 2019 American Chemical Society.

2.2.2. *Facilitating the conductivity of solid-state electrolytes*

Solid-state electrolytes are proposed for lithium metal batteries in the beginning, and penetrate other battery chemistries, benefitting from their potential ionic conductivity and reliable battery safety. However, some remaining challenges, such as favorable manufacturing technology and poor kinetics, are still hamper the practical adoption of solid-state electrolytes. Here, we go over the studies of halogen containing solid-state electrolytes and discussed the recent ongoing technologies and discovers on improved ionic conductivity by halogen chemistries.

2.2.2.1. Lithium-ion conductive solid-state electrolytes. Solid-state electrolytes made by alkali metal halides are a promising strategy for lithium metal batteries in view of the lithium-ion conductivity of alkali metal halides, which has led to research efforts focusing on halogen-containing solid-state electrolytes [127]. Previous reports have discovered that substitution or doping by halogen, particularly fluorine, can further improve the lithium-ion conductivity of conventional solid-state electrolytes by adjusting the sublattices and smoothing the lithium-ion diffusion pathways [128]. However, solid-state electrolytes with promising lithium ionic conductivity and stability have been considered roadblocks for the achievement of all solid-state lithium-ion batteries. A theoretical study of the lithium-ion diffusion mechanism in metal chlorides demonstrates that increased lithium-ion conductivity can be attained from low lithium content and cation concentration together with a sparse

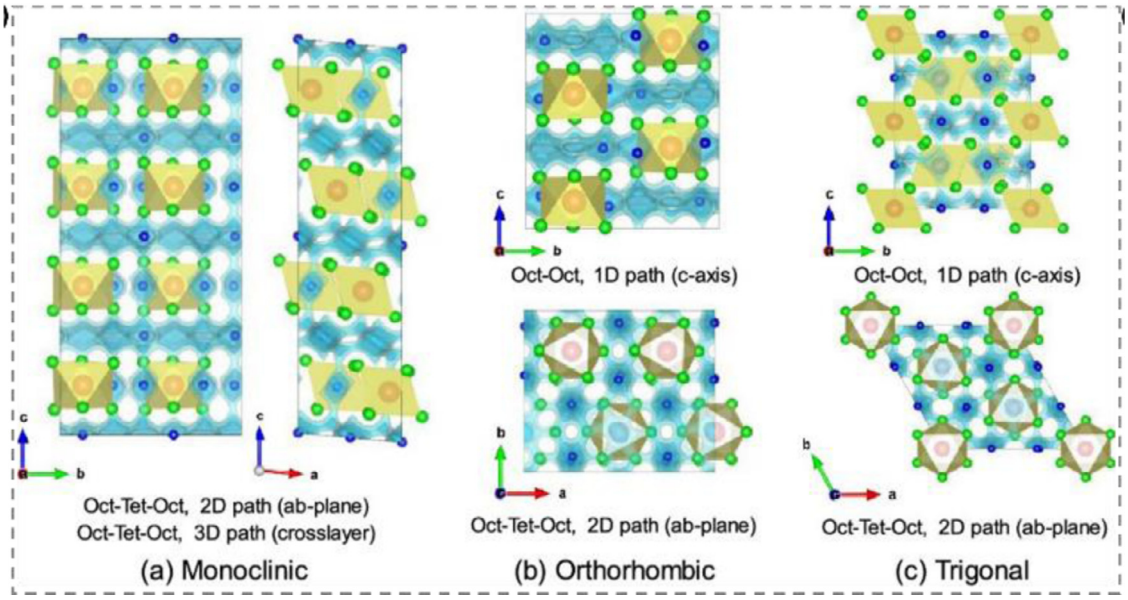

Fig. 17. Simulation of the lithium-ion transport pathway in monoclinic, orthorhombic, and trigonal Li_3MCl_6. Li: Blue atom; MCl_6: yellow polyhedral. The light blue isosurface indicates the Li-ion migration pathways [131] Copyright 2020 American Chemical Society.

cation distribution [129]. Recently, Asano et al. developed a new type of halogen-containing solid-state electrolyte (Li_3YCl_6 and Li_3YBr_6) with a high ionic conductivity of 1 mS cm^{-1} [130]. The halide ions construct framework-type sublattices, in which lithium ions alternatively pass through the tetrahedral and octahedral regions accompanied by matrix cation repulsion. This new type of ion migration mechanism is rather different from the reported sulfides and oxides with anion-aligned *bcc* structures.

Theoretical calculations for such Li_xMCl_y-type solid electrolytes suggest that following research efforts on lithium vacancies are favorable for superior ionic conductivity [131]. Crystalline traits play a significant effect on the ionic conductivity. Lower energy barriers are generated in monoclinic Li_3MCl_6, while higher energy barriers are obtained from orthorhombic and trigonal structures due to sluggish diffusion dynamics. Lithium ions migrated in the monoclinic phase following the two-dimensional intralayer and three-dimensional cross-layer pathways, while lithium ions were transported in trigonal and orthorhombic phases through a one-dimensional path along the *c*-axis and two-dimensional transport along the *ab*-plane, as shown in Fig. 17. In addition to the phase consideration, composition engineering was demonstrated to be effective to the ionic conductivity [132].

2.2.2.2. Sodium-ion conductive solid-state electrolytes. Halogen species are well known as dopants of solid-state electrolytes for improving ionic conductivity by tunning the lattice structures due to the unique size and electronegativity effects. A halogen-doped chalcogenide-type solid-state electrolyte was studied by Jia et al.; in particular, $Na_{3.57}[Sn_{0.67}Si_{0.33}]_{0.67}P_{0.33}S_{3.9}X_{0.1}$ (X=chloride, bromide, and iodide) with a 0.1 atomic stoichiometric ratio was designed and synthesized [133]. The superior ionic conductivity and low activation energy were found for the iodide-doped sample due to the high polarization and large atomic radius of iodide ions, promoting sodium-ion conductivity, as shown in Fig. 18. Additionally, the high electronegativity of chloride ions has also been demonstrated to improve the sodium-ion conductivity in the chloride-doped solid-state electrolyte counterparts [134]. A fluorinated sulfide solid-state electrolyte with an expanded lattice was studied by Fan et al. [135]. After co-doping the large chloride ions and bivalent magnesium into the Na_3SO_4F solid-state electrolyte, the sodium-ion conductivity was improved by three orders of magnitude (up to 10^{-4} S•cm^{-1}, at 60°C), benefitting from the lattice expansion and sodium vacancy generation in the solid-state electrolyte.

In addition, the argyrodite with a general formula of $Li_{12-m\text{-}x}{}^{+}(M^{m+}Y_4{}^{2-})Y_{2\text{-}x}{}^{2-}X_x{}^{-}$, where M is Si, Ge, Sn, P or As; Y is O, S, Se or Te; X is Cl, Br or I; $0 \le x \le 2$, is another type of halogen-containing solid-state electrolytes. The introduction of halogen in the argyrodite plays a crucial effect on the lattice structural disordering due to the size effects and the strong electronegativity of halogen anions, particularly chlorides and bromides, which promotes the delocalization of lithium cations in the solid electrolyte and has a lower diffusion barrier for lithium ions. Therefore, argyrodite solid electrolytes substituted by large-size iodide species generally exhibit lower ionic conductivity relative to the chloride and bromide substituted counterparts. Several review articles have comprehensively summarized and discussed the recent reports on the argyrodite solid electrolytes, in which the effect of halogen on ionic conductivity has been detailed, with the core concept we elaborate above [136–138].

2.2.3. Solid electrolyte interface modification

Halides are also widely utilized as additives of electrolytes in alkali metal-ion batteries, particularly in lithium-ion batteries, for stabilizing the electrode/electrolyte interfaces and obtaining uniform stripping and plotting of anode metals, thus suppressing the dendrite growth. The halogen containing additives are normally utilized in a small amount only to adjust the electrochemical deposition of metal ions upon charging by forming metal halogen compounds in the solid electrolyte interfaces. We provide an overview of the halogen containing solid electrolyte interfaces bellow.

2.2.3.1. Lithium-ion batteries. Lithium-ion batteries were intensively studied after their first commercialization in 1991, with a focus on improving their capacity, safety, and cost-efficiency. Accompanying the increasingly powerful features of electronics and the corresponding penetration into our daily life, conventional lithium-ion batteries are no longer able to meet our demands. Thus, research focus is shifting from conventional lithium-ion batteries to lithium metal batteries (using lithium metal as an anode) to obtain a larger capacity. However, a significant issue in lithium metal batteries is dendrite formation, which is caused by nonuniform lithium-ion deposition on the lithium metal anode surface. During the charging/discharging process, the formed

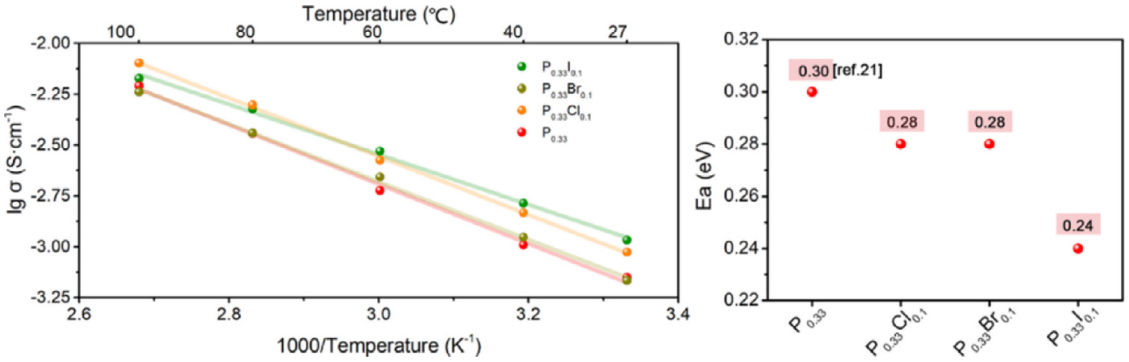

Fig. 18. Arrhenius plot and corresponding activation energies of $Na_{3.67}[Sn_{0.6}Si_{0.33}]_{0.67}P_{0.33}S_4$ and $Na_{3.57}[Sn_{0.6}Si_{0.33}]_{0.67}P_{0.33}S_{3.9}X_{0.1}$ (chloride, bromide, and iodide) [133] Copyright 2020 American Chemical Society.

lithium dendrites pierce the separator and approach the cathode, resulting in battery short circuits. Over the last several years, tremendous efforts to overcome the lithium dendrite issue have been conducted, with favorable progress exhibited. The acknowledged theory regarding addressing lithium dendrites is the generation of a uniform solid electrolyte interface to guide homogenous lithium-ion deposition on the lithium metal surface, meanwhile the robust solid electrolyte interface layer has no cracks or tears upon lithium-ion deposition/stripping. To achieve this target, introducing a halogen species-containing solid electrolyte interface layer is a promising solution that simultaneously promotes lithium-ion diffusion and suppresses lithium dendrite growth. Given the attractive properties of the halogen-containing solid electrolyte interface, enormous research efforts focused on halogen-containing solid-state electrolytes have been carried out. Herein, we refer the readers to a previous (2018) review article for more detailed information about how halogen species improve the electrochemical performance of lithium metal batteries from the perspectives of solid electrolyte interface formation and solid-state electrolytes [139]. In the last two years, studies on the suppression of lithium dendrites have further demonstrated that the LiX (X=fluoride, chloride, bromide, etc.) layer on a lithium metal surface is highly efficient for homogeneous plating/stripping [140,141]. In particular, the lithium fluoride layer on the lithium metal surface exhibited extremely stable lithium-ion plating/stripping [142,143]. Regarding the formation of the solid-state lithium fluoride protective layer, in addition to conventional electrolyte additives [144–146], the fluoride-containing solvents utilized in battery construction can also facilitate lithium fluoride formation, especially when the solvent has a trans-fluoride structure, suggesting that wise selection of the electrolyte solvent is necessary [147,148]. Furthermore, some innovative strategies for lithium fluoride generation have also been reported, such as thermal evaporation [149], slurry coating [150], and solution processing [151]. Although lithium fluoride has been well demonstrated experimentally, the underlying mechanism of how lithium fluoride yields uniform lithium-ion deposition and suppresses lithium dendrites is still poorly understood. According to some operando characterizations, lithium fluoride can yield a dense lithium-deposition layer, which is beneficial for uniform stripping/platting [152]. On the other hand, lithium fluoride alone was demonstrated to compromise the mechanical integrity; thus, an additional outer layer is required to generate a composite solid-state electrolyte [153]. Other fluorides and bromides have also demonstrated to be efficient for dendrite-free lithium metal batteries [154,155].

Alkali metal halides have also demonstrated to have a wide potential window, which is beneficial for high-voltage batteries [156]. In particular, alkali metal fluorides that have the capability to withstand extremely high voltages are also favorable for utilization as the protective layer of electrode materials in high-voltage batteries [157], for which lithium fluoride has already been demonstrated to be an efficient protective layer of composite cathodes and silicon-based anodes, as well as some other composite anodes [158].

Silicon is a potential anode material of lithium-ion batteries that has an extremely high specific capacity. However, its large volume expansion during charging imposes a barrier for its practical utilization. To address the volume-change issue, lithium fluoride has been demonstrated to protect silicon particles from cracking, thereby stabilizing the solid electrolyte interface and, thus, improving the coulombic efficiencies and reducing pulverization by enlarging the lithium diffusion coefficient [159–161].

2.2.3.2. Sodium-ion batteries. Sodium ion batteries have received extensive attention for their cost efficiency and competitive electrochemical performances; however, one of the main issues for sodium ion batteries is the unstable plating/stripping of sodium ions over charging/discharging cycles due to the high diffusion barrier of sodium ions, resulting in detrimental dendrite growth [162]. Studies on sodium halides have demonstrated improved kinetics for sodium ion transport. Choudhury et al. found that the sodium bromide interphase has a lower energy barrier for sodium ion diffusion, displaying more stable sodium-ion deposition [163]. Furthermore, the sodium bromide interphase exhibited an approximate threefold reduction in activation energy for ion transport. Furthermore, the surface energy barriers of metal halides are much lower than that of the usual solid electrolyte interface components consisting of metal hydroxides and metal carbonates, which facilitates the diffusion of adatoms to hamper dendrite growth. On the other hand, the sodium bromide solid-state layer on the sodium anode surface also inhibits the interfacial side reactions. Among the sodium halide layers, Tian et al. demonstrated the lowered diffusion barrier (0.02 eV) of the sodium iodide layer relative to the fluoride counterpart (0.25 eV) for sodium ion diffusion (Fig. 19) [164]. The battery, thus, delivered a high capacity of approximate 110 mAh g^{-1} at 2 C without obvious capacity decay even for 2,200 cycles. Density functional theory theoretical calculations showed that the sodium ions were directly bonded on top of fluoride ions in the sodium fluoride, diffusing through a pathway in the middle of two neighboring layers of fluoride anions; the adsorption and diffusion paths of sodium ions in sodium iodide were similar to those in sodium fluorides, as shown in Fig. 19.

2.2.3.3. . Multivalent metal-ion batteries. Halide ions are extensively adopted as coordination ions in the electrolytes of multivalent-ion batteries, such as magnesium- and aluminum-ion batteries, to render electrode/electrolyte interfaces, which facilitate the stripping and deposition of metal ions and promote electrochemical kinetics. The use of a lithium chloride additive in the electrolyte of magnesium-sulfur batteries has been reported by Fan et al. [165]. A long lifespan of 500 cycles and high coulombic efficiency approaching 100% were attained due to the solubilization of magnesium chloride benefitting from the assistance of lithium chloride, which enabled reduced overpotential of 140 mV during magnesium plating/stripping at 500 μA cm^{-2}. Li et al. demonstrated an effective magnesium iodide solid-electrolyte interface

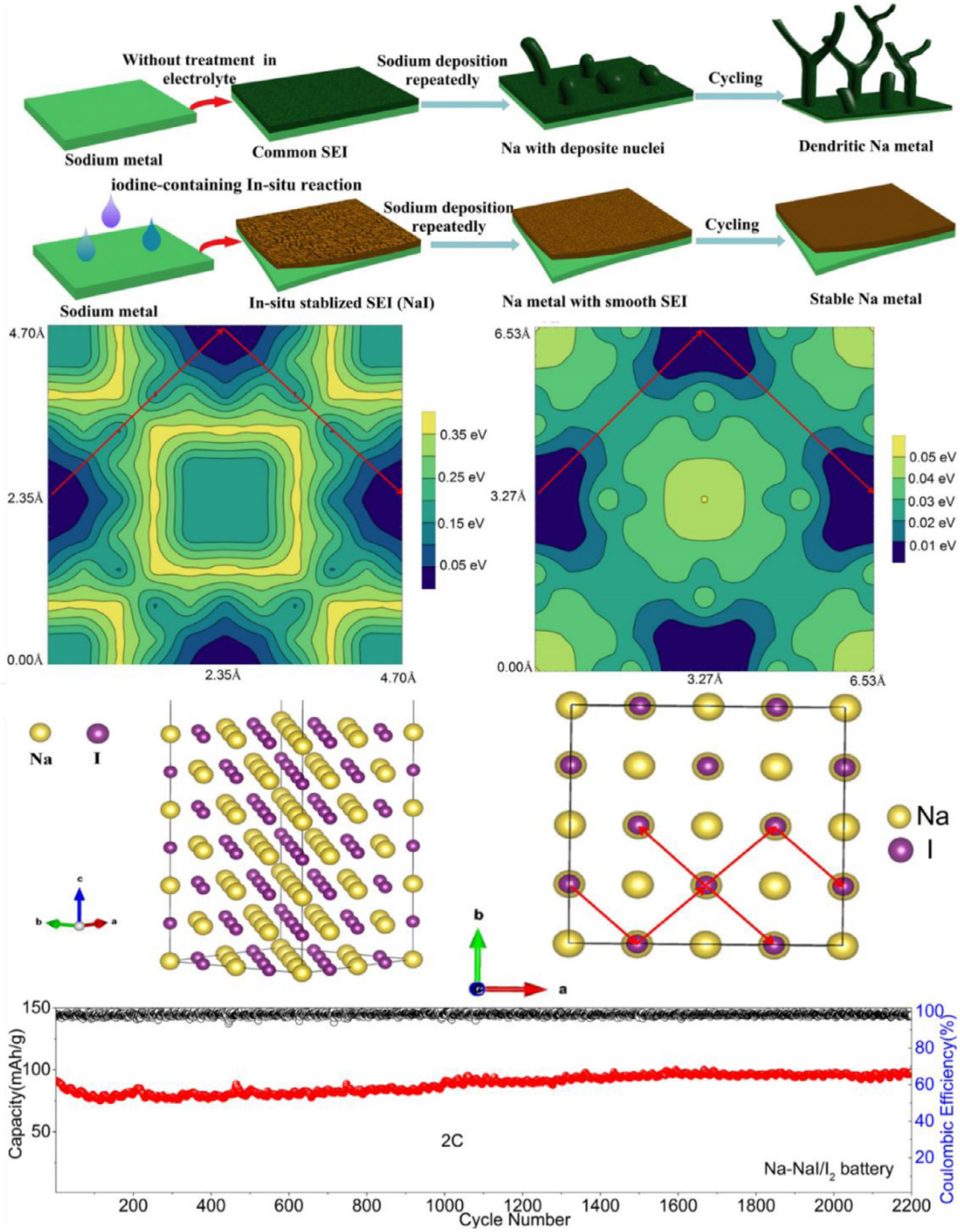

Fig. 19. Schematic illustration of the sodium metal anode with a stable and dendritic solid electrolyte interface layer. Surface diffusion barriers obtained by theoretical calculations: sodium adatoms on sodium fluoride and sodium iodide surfaces and a schematic illustration of the sodium iodide atomic configuration and the transport paths of sodium ions on the sodium iodide surface. Long-term stability of a sodium-iodine battery [164] Copyright 2019 Elsevier.

layer that was formed by introducing an iodine additive into the electrolyte of magnesium-ion batteries; the solid-electrolyte interface was magnesium-ion conductive and thus offering a small voltage hysteresis [166]. A more detailed discussion of the halogen, particularly chlorine and bromine, used in electrolytes is provided in the excellent review of [167]. The introduction of halide ions as coordination ions into electrolytes improves the dissolution and deposition capability, although the halides cause battery corrosion, which is, thus, a double-edged sword. Future efforts need to pay more attention to avoid the corrosion.

3. Halogen conversion-based battery chemistries

Halogen elements, particularly bromine and iodine, have been extensively studied as conversion-type electrodes in rechargeable batteries, including alkali metal-ion batteries, zinc ion batteries, and redox flow batteries, as well as other battery families, such as zinc-bromine, metal-iodine, due to their high reduction potentials and large abondance on earth [168]. In this chapter, we focus on halogen conversion-based battery chemistries and discuss the current research progress correlat-

ing with the corresponding electrochemical performances. This chapter is provided based on different battery systems. The remaining issues in halogen conversion-based battery chemistries and possible solutions are discussed to guide future research efforts.

3.1. Bromine redox for energy storage

3.1.1. Redox flow batteries

Redox flow batteries are among the promising energy storage technologies for integrating renewable energy sources into electric grids [169]. Redox flow batteries are designed and fabricated by decoupling the energy and power densities to separately store the anolyte and catholyte in two individual tanks and circulating them independently through pumping, which enables both high energy and power densities [170]. In this case, the amount of energy storage lies in the volume and concentration of the redox-active electrolytes; the power density relies on the rate of circulation. In this chapter, we mainly discuss redox flow batteries designed based on bromide/bromine conversion reactions.

Zinc-bromine redox flow batteries enable an aqueous battery system with good safety and attractive cost efficiency; issues such as electrolyte crossover contaminations and dendrite growth due to the ununiform zinc ion flux distribution, however, need to be addressed [171–174]. Electrolyte additives demonstrated to be effective approach for stable zinc stripping/deposition [175]. A study on the inhibition of zinc dendrite growth by Kim et al. demonstrated that the utilization of bromine-complexing agents, such as 1-ethyl-1-methyl-pyrrolidinium bromide, led to a uniform deposition of zinc ions by forming an electrostatic shield, as shown in Fig. 20 [176]. A study on electrolyte additives by Wu et al. demonstrated the efficiency of introducing ammonium chloride into the electrolyte for a high energy efficiency of 81.8% [177]. In addition, Wang et al. demonstrated an integrated Br//$NaTi_2(PO_4)_3$ redox flow battery concept (Fig. 21a), which simultaneously conquered the zinc dendrite by utilizing (de)intercalation-type cathode materials [178]. Zeng et al. designed and synthesized tin-bromine hybrid redox flow batteries by using tin as the anode, which delivered a high coulombic efficiency of 97.6% at a high current density of 200 mA cm^{-2}, as well as power densities of 673 (15°C) and 824 (35°C) mW cm^{-2} at a half-charged state (Fig. 21b) [179].

The design of cathode structures and morphologies plays a critical role in suppressing bromine diffusion and transfer [180–183]. Wang et al. designed and fabricated a hollow carbon cage with a proper pore size, which trapped bromine complexing inside via molecular size exclusion [184]. Wang et al. designed and synthesized a titanium nitride nanorod array current collector for high-rate bromine-based redox flow batteries [185]; the highly porous three-dimensional structure and excellent catalytic activity toward the bromine/bromide redox enabled the cell to operate at a high current density of 160 mA cm^{-2}. For such a catalytic effect, many studies have demonstrated the promotion in the redox kinetics, in particular carbon-based materials [186–189]. A study by Wu et al. demonstrated that the electrocatalytically active carbon-paper current collector showed an improved rate capability and 83.5% energy efficiency at 40 mA cm^{-2} compared with their common carbon felt counterparts [190]. Biomass-derived carbon materials further promise wonderful cost efficiency. In a study by Naresh et al. [191], the activated carbon derived from phyllanthus emblica leaves acted as an excellent electrocatalyst for the redox reactions in zinc bromine redox flow batteries; the cell delivered efficiencies of 99% (coulombic), 83% (voltage), and 82% (energy) at 30 mA cm^{-2} and a lifespan of 100 cycles. A nitrogen-doped carbon cathode derived from a glucose precursor by Xiang et al. demonstrated an excellent energy efficiency of 82.5% at 80 mA cm^{-2} and a stability of 200 cycles [192].

Complexing agent study is also beneficial for fixing the intermediates formed during charging/discharging should be conquered, too [193]. A novel complexing agent, 3-chloro-2-hydroxypropyltrimethyl ammonium chloride, reported by Li et al. for preventing polybromides from diffusion and corrosion in a titanium-bromine flow battery demonstrated high coulombic (95%) and energy (83%) efficiencies at 40 mA cm^{-2}, as well as a long lifespan of 1,000 cycles [194]. Li et al. demonstrated a complexing agent, 1-ethyl-2-methyl-pyridinium bromide, for polybromides, which complexed with polybromides stably even at high temperatures (60 °C); as a result, the bromine-based redox flow batteries ran stably for more than 400 cycles [195].

In bromine conversion-related redox flow batteries, bromine unbalancing or crossover between anolytes and catholytes is one key issue. A systematic comparison of the electrochemical performances was provided in Table 3. The undesirable bromine crossover causes accelerating capacity decay, resulting in the requirement of a better membrane with less bromine permeability [196]. To date, enormous research efforts on carbon-based current collectors or cathodes have demonstrated the high efficiency of well-designed and fabricated carbon electrodes for suppressing (poly)bromide diffusion and crossover contaminations, thus preserving the capacities and prolonging the battery lifetime. Generating defect sites by doping heteroatoms, such as nitrogen and phosphorus, improves the active and/or redox sites within the carbon cathodes, thus benefiting the kinetics of redox reactions by catalytic effects and the capacities of active materials by absorption effects. The in-situ monitoring of the charging/discharging process and the study of circulation rates are also significant for improving the performances of redox flow batteries [197,198].

3.1.2. Nonflowing batteries

Metal-bromine batteries, as a type of battery that works based on bromide anion redox conversion, are obtaining increasing attention due to their easy-to-fabrication and cost efficiency. To improve the energy density and cycling stability, enormous efforts have been conducted. The high reduction potential of bromide ions in electrolytes usually causes redox reactions on the electrode surface, through which the battery or capacitor capacity values can be enhanced significantly, enabling a higher energy density. Han et al. demonstrated a hydrogel electrolyte where the bromide ions introduced in the electrolyte served as both charge-shuttling carriers and active species, in which only bare active carbon was employed at the cathode side forming a zinc-ion hybrid supercapacitor [199]. A high energy density of 605 Wh kg^{-1} and a power density of 1,848 W kg^{-1} were attained together with a 5,000-cycle long lifespan, benefitting from the bromide-based redox couple of $3Br^- \leftrightarrow Br_3^- + 2e^-$ and $Zn \leftrightarrow Zn^{2+} + 2e^-$. In a hybrid capacitor reported by Tang et al., the redox reaction of bromide/tribromide on the positive electrode surface renders a gravimetric energy density four times higher than the conventional double layer capacitor [200]. Later, Li et al. developed a bromide-ion battery using copper bromide as the solute of electrolyte, which exhibited a high capacity of 200 mAh g^{-1} and a long lifespan of 8,000 cycles with a capacity retention of 142 mAh g^{-1} [201]. The redox reaction of bromide ions in the electrolyte suggests more insights into the recently popular anion conversion-based battery chemistry. Li et al. reported a bromide ion adsorption/desorption-based charging/discharging principle [202], in which the charging/discharging mechanism was bromide ion adsorption/desorption at carbon black (Fig. 23b). Such simple adsorption/desorption-based charging/discharging concept effectively improved the energy density. To further improve the energy and power densities, Yu et al. proposed a “super-capattery” by combining triple battery-, capacitive-, and pseudocapacitive-type charge storage mechanisms in a signal zinc-bromine battery, as shown in Fig. 23c [203]. High energy (270 Wh kg^{-1}) and power (9,300 W kg^{-1}) densities were attained simultaneously, benefitting from battery-type charge storage for high energy and capacitive- and pseudocapacitive-charge storage for high power.

Electrolyte studies are significant for the improvement of rate performances. Dongmo et al. demonstrated liquid electrolyte system by using alternative bromine species rather than chlorine in hexamethyldisilazide (HMDS)Cl-based electrolyte [204]. As a sequence, it exhibits a stable potential window of approaching 2.4 V, a 1,000-cycle long-term lifetime,

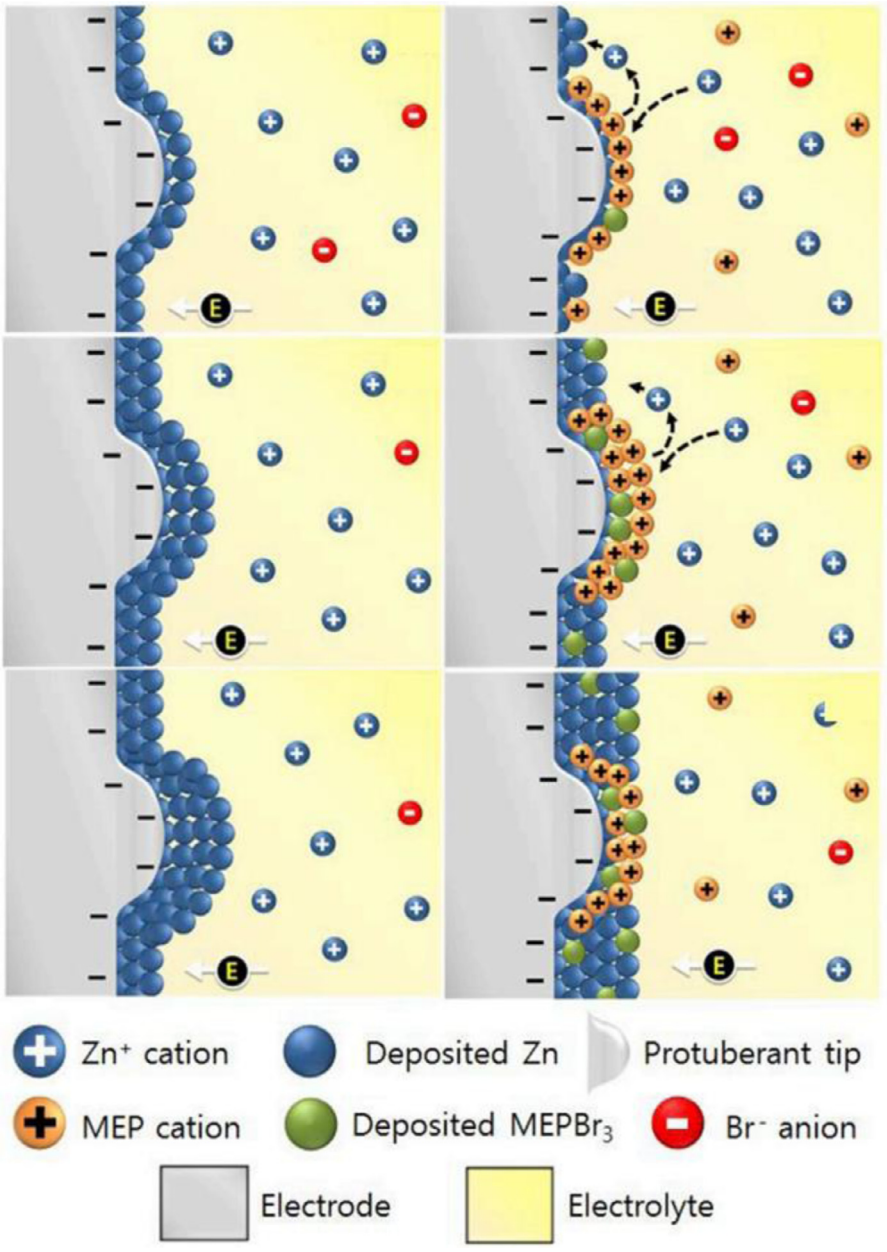

Fig. 20. Schematic illustration of the zinc dendrite growth process and the electrostatic shielding process by use of 1-ethyl-1-methyl pyrrolidinium cations [176] Copyright 2019 Elsevier.

Table 3
Systematic comparison of the electrochemical performances.

Material	Lifetime (cycles)	Energy efficiency (%)	Current density (mA cm^{-2})	Ref.
KCl and NH_4Cl supporting electrolyte	50	82	80	[177]
TiN nanorods array@C felt	100	80	160	[185]
Sn anode	250	83	200	[179]
Cage-like porous C	300	81	80	[184]
C paper electrode	50	84	40	[190]
Phyllanthus emblica leave-derived active C	100	82	30	[191]
N-doped active C derived from glucose	200	83	80	[192]
3-Cl-2-hydroxypropyltrimethyl ammonium Cl complexing agent	500	83	40	[194]
1-Ethyl-2-methyl-pyridinium Br complexing agent	400	84	40	[195]

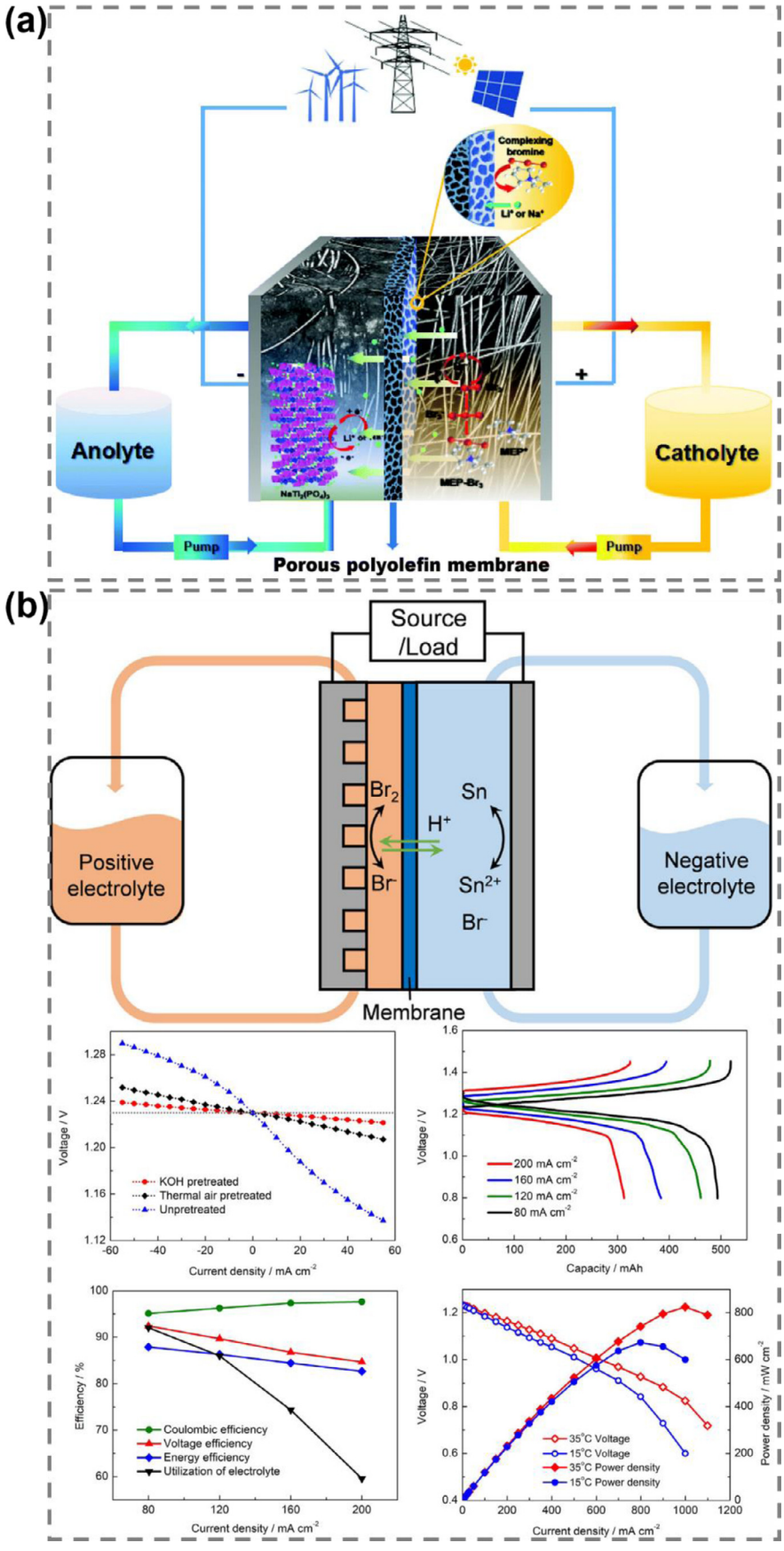

Fig. 21. (a) Structural illustration of the hybrid titanium-bromine redox flow battery system [178] Copyright 2019 The Royal Society of Chemistry. (b) Schematic of tin-bromine redox flow batteries. Polarization curves, charge-discharge curves, battery efficiencies, and full discharge polarization curves of the tin/bromine redox flow batteries with different pretreated electrodes under various conditions [179] Copyright 2019 Elsevier.

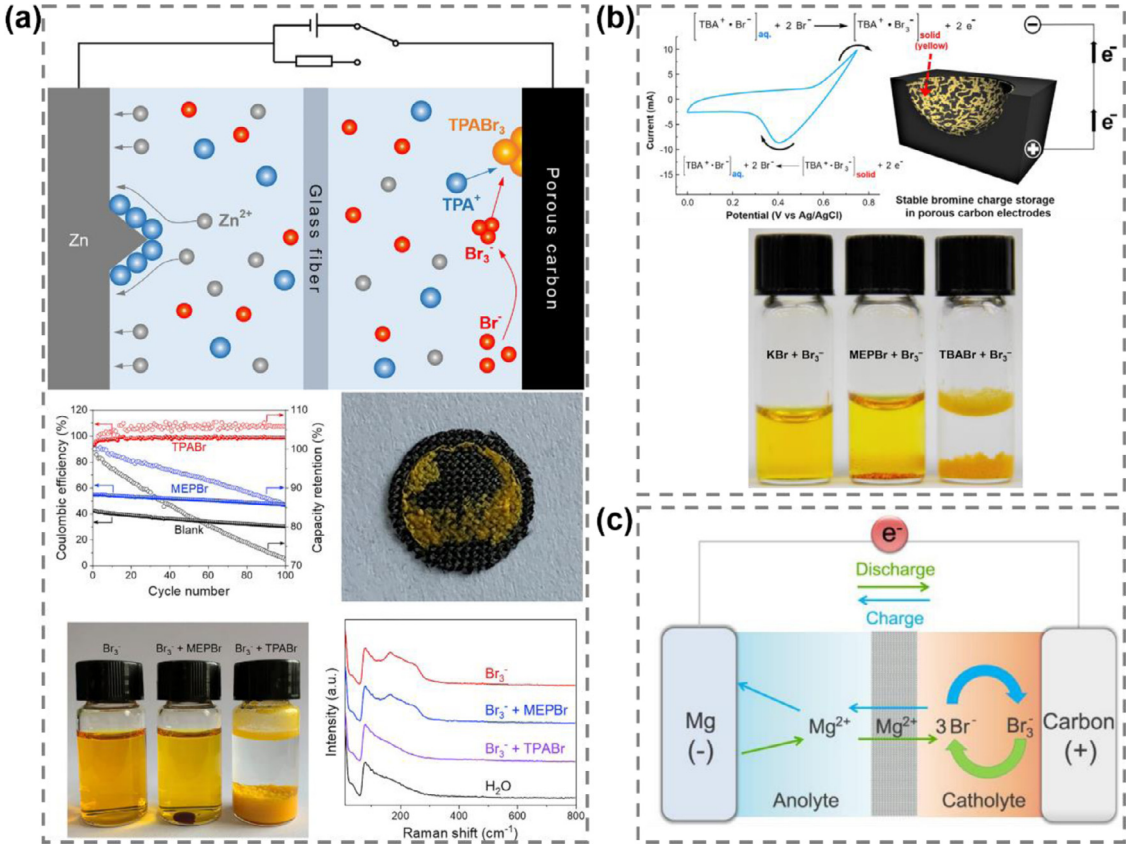

Fig. 22. (a) Schematic illustration of bromide ion fixation by using TPABr. Electrochemical performances for blank (zinc bromide), methyl ethyl pyrrolidinium bromide (MEPBr), and TPABr electrolytes. Carbon cloth electrodes taken out from the TPABr electrolyte. Br_3^- solution, Br_3^-/MEPBr, and Br_3^-/TPABr. Raman spectra of the supernatants [207] Copyright 2020 Elsevier. (b) Schematic illustration of the solidification process of the bromide redox couples. Visualized images of solid-state $TBABr_3$ precipitation [208] Copyright 2017 American Chemical Society. (c) Schematic illustration of the magnesium-bromine battery design [210] Copyright 2016 Elsevier.

and anodic stability, as well as a high ionic conductivity, reaching 1.16 mS cm^{-1}. A rational balance between the nucleation and crystal growth of metallic magnesium is attained, generating a homogenous deposition layer under a low overpotential of less than 188 mV. Park et al. further studied bromide ion migration in a droplet of bromide-based ionic liquid, in which the diffusion coefficient of bromide ions was surprisingly higher than proton conduction through Grotthuss-like hopping, providing a better understanding of the bromide ion transfer in electrolytes [205].

In the studies on bromine conversion-based chemistries, bromide ion diffusion and loss when bromine is used as an active material is a significant issue that needs to be addressed to mitigate capacity decay. The poor electrolyte stability results in severe self-discharge after bromide is oxidized into tribromides. Innovative battery designs are significant for suppressing the shuttling of bromine species. Wang et al. designed a dual-stimuli-responsive battery by using bromine as the cathode material, where the bromide/bromine redox couple serves as the efficient reaction for charge storage [206]. In this work, a dual-electrolyte system was designed by using a thermal-sensitive gel-polymer electrolyte, which solidified when the operating temperature was abnormally high and refined the uncontrolled migration of bromide ions. In addition, Gao et al. found that the introduction of tetrapropylammonium (TPA) bromide into the electrolyte can bond the charging product, tribromides, by forming solid-state $TPABr_3$ (Fig. 22a) [207]. The cell with the TPA bromide exhibits both extremely high coulombic efficiency and capacity retention relative to that of the blank cell. The formed solidified bromide compound is visualized at the carbon fiber current collector after introducing TPA bromide into tribromides, as the further confirmation with Raman spectroscopy (Fig. 22a). Regarding the solidification of bromide redox couples, Yoo et al. demonstrated another solidification media, tetrabutylammonium cation (TBA bromide), which forms solid-state TBA tribromides at the current collector in catholyte after being charged (Fig. 22b) [208]. This study further demonstrated the feasibility of the solidifying bromide-redox-couple concept. Furthermore, Takemoto et al. demonstrated the use of tetraethylammonium (TEA) bromide for the solidification of bromide redox couples [209].

A dual-electrolyte system was demonstrated for overcoming this issue, in which larger tribromide anions were fixed only on the cathode side to mitigate their diffusion to the anode side (Fig. 22c), thereby improving the coulombic efficiency [210]. Yu et al. developed a dual-electrolyte system for an aqueous zinc-bromine battery by employing an acid catholyte and alkaline anolyte (Fig. 23a) [211]. This work suggests important insights into the study of aqueous electrolytes in terms of the suppression of self-discharge owing to soluble redox couples.

Unique electrode designs are efficient approaches for suppressing the bromide shuttling. A dual-halogen (chlorine and bromine) conversion-based battery was designed and constructed by Yang et al. [212]; in particular, lithium chloride and lithium bromide were inserted as redox active materials into the graphite forming a composite hosting material, and the whole product served as a cathode. By adopting a specially designed water-in-salt electrolyte, the battery delivered a high energy density of 460 Wh kg^{-1}. When chlorides were oxidized to chlorine after the whole bromides were oxidized into bromine, a beneficial interhalogen, chloride-bromide, was formed, which helps to stabilize the oxidized chlorine. A graphite felt-supported microporous carbon doped with protonated pyridinic nitrogen electrode was

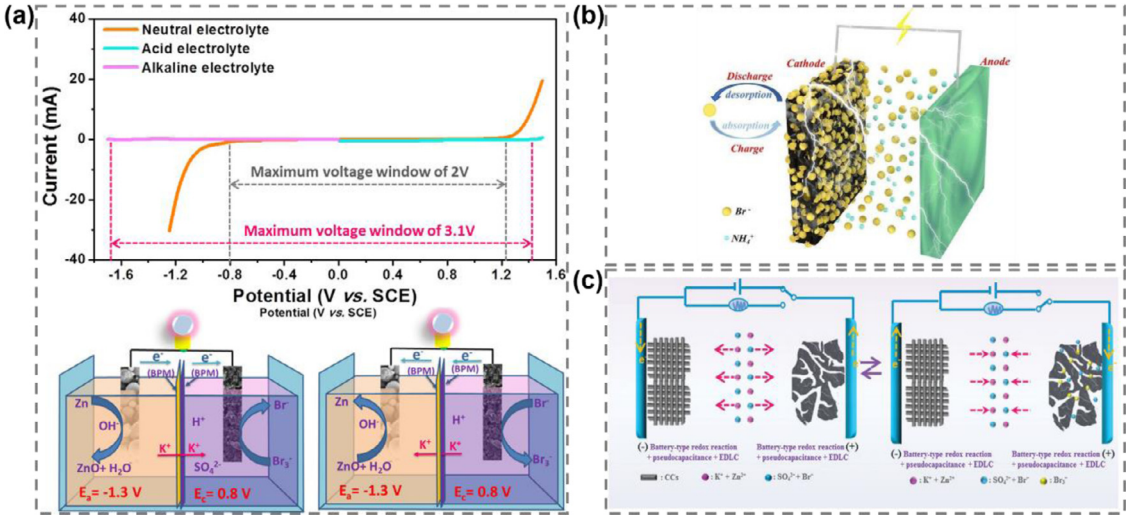

Fig. 23. (a) The electrochemical stability window of the alkaline and acid electrolytes. Schematic illustration of the discharge and charge process in a zinc-bromine battery [211] Copyright 2019 Elsevier. (b) Schematic of the bromide-ion battery [202] Copyright 2020 The Royal Society of Chemistry. (c) Schematic illustration of the triple charge storage and release mechanisms [203] Copyright 2020 The Royal Society of Chemistry.

Table 4
Systematic comparison of the electrochemical performances.

Material	Lifetime (cycles)	Capacity (mAh g^{-1})	Current density (mA g^{-1})	Ref.
Ethylene glycol cyclic sulfate electrolyte solvent	8,000	142	2,000	[201]
Br ion absorption/desorption	3,000	141	2,000	[202]
S/P co-doped C based cathode	5,000	200	1,000	[203]
Tetrapropylammonium Br complexing agent	10,000	200	5,000	[207]
Tetrabutylammonium Br complexing agent	7,000	67	1,000	[208]
Alkaline-acid hybrid electrolyte	2,000	~250	1,000	[211]

designed and fabricated by Lee et al. to capture the bromine and polybromides formed during battery operation [213]. The innovative membrane- and flow-less zinc-bromine battery delivered a long lifespan of 1,000 cycles with an energy efficiency greater than 80% benefitting from the protonated pyridinic nitrogen-doped micro-carbon. A systematic comparison of the electrochemical performances was provided in Table 4.

3.2. Iodine redox for energy storage

Iodine has been extensively studied as a conversion-type cathode, which differs from intercalation cathodes and delivers high theoretical capacities (211 mAh g^{-1}) due to its multivalent features, such as -1, 0, and +1. Mostly, the charge storage of iodine relies on the redox between iodine and anionic iodides given the ease of hydrolysis for cationic iodides. Fabrication of interhalogens, such as iodide-chloride, is an efficient pathway to stabilize the halogen species [214]. Pioneering effort has pursued the possible solution toward such an issue, retarding the effect of aqueous solvents by introducing complexing agents such as acetonitrile and/or chloride/bromide anions [215]. Iodine has been widely studied in redox flow batteries and nonflowing batteries, such as lithium-iodine, iron-iodine, and magnesium-iodine, due to its good solubility, environmental efficiency, and low cost (Fig. 24) [216]. In this chapter, we mainly summarized the utilization of iodine in various battery chemistries, with a focus on the current issues and research efforts. A short outline is provided to emphasize the advances in iodine conversion-based batteries and the underlying concepts.

3.2.1. Lithium-iodine batteries

Rechargeable lithium-iodine chemistry has gained extensive attention because of its advantages, such as high energy densities, large reserves of iodine on earth, low cost, and multielectron chemistry. Iodine undergoes a multistep redox reaction during iodide oxidation to iodine, as shown in Fig. 25a [217]. However, issues such as the high instability of cationic iodides due to hydrolysis and the dissolution and diffusion of iodides into electrolytes result in subsequent side reactions with lithium anodes, restricting the practical applications.

Enormous studies of electrode designs and fabrications have been carried out to overcome the diffusion effect of iodides. Carbon-based electrodes currently exhibit great potentials. Li et al. conducted a study of carbon hosting materials in terms of hindering polyiodide shuttling and electrochemical dynamics [218]. Three different types of carbon hosting materials, nitrogen-doped hollow spheres (N-S), nitrogen-doped hollow hemispheres (N-HS), and nitrogen-doped fold hemispheres (N-FHS), are synthesized (Fig. 25b) and decorated with iodine for lithium-iodine batteries. In particular, N-FHS exhibits the best electrochemical dynamics among the three as-prepared hosting materials. The electrochemical impedance spectra showed the smallest values for N-FHS relative to N-S and N-HS. The good kinetics of N-FHS were further confirmed with the rate performances of the assembled cells (Fig. 25b), in which N-FHS exhibits the greatest capacity value at an enhanced specific current of 20 C. Good electrochemical dynamics has higher charge migrate rates, enabling the battery great capacity utilization at enlarged current densities. Li et al. synthesized a nitrogen and phosphorus co-doped highly porous carbon cloth supporting material for hosting the lithium iodide discharge product [219]. The doping of nitrogen and phospho-

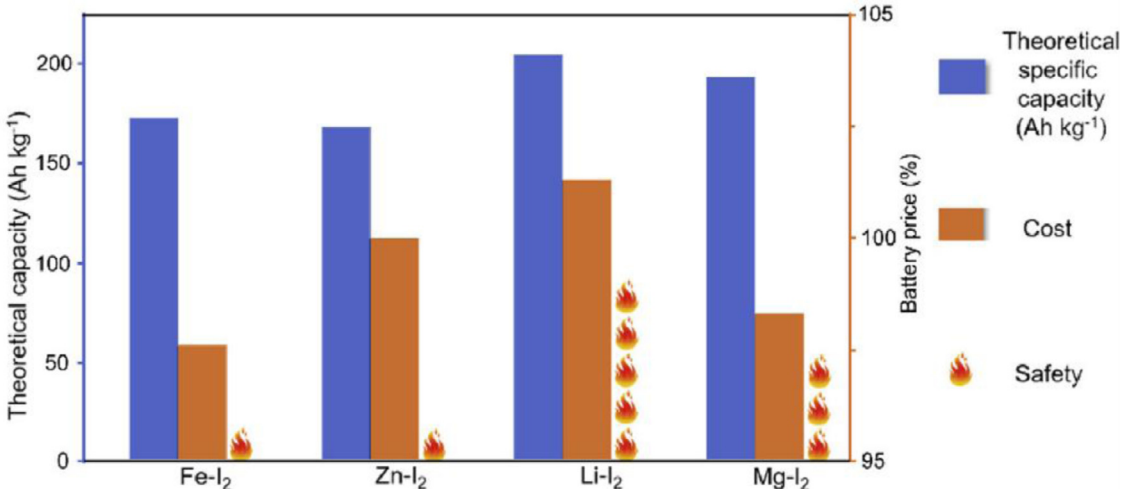

Fig. 24. Crucial parameters for iodine conversion-based battery chemistries [216] Copyright 2020 Elsevier.

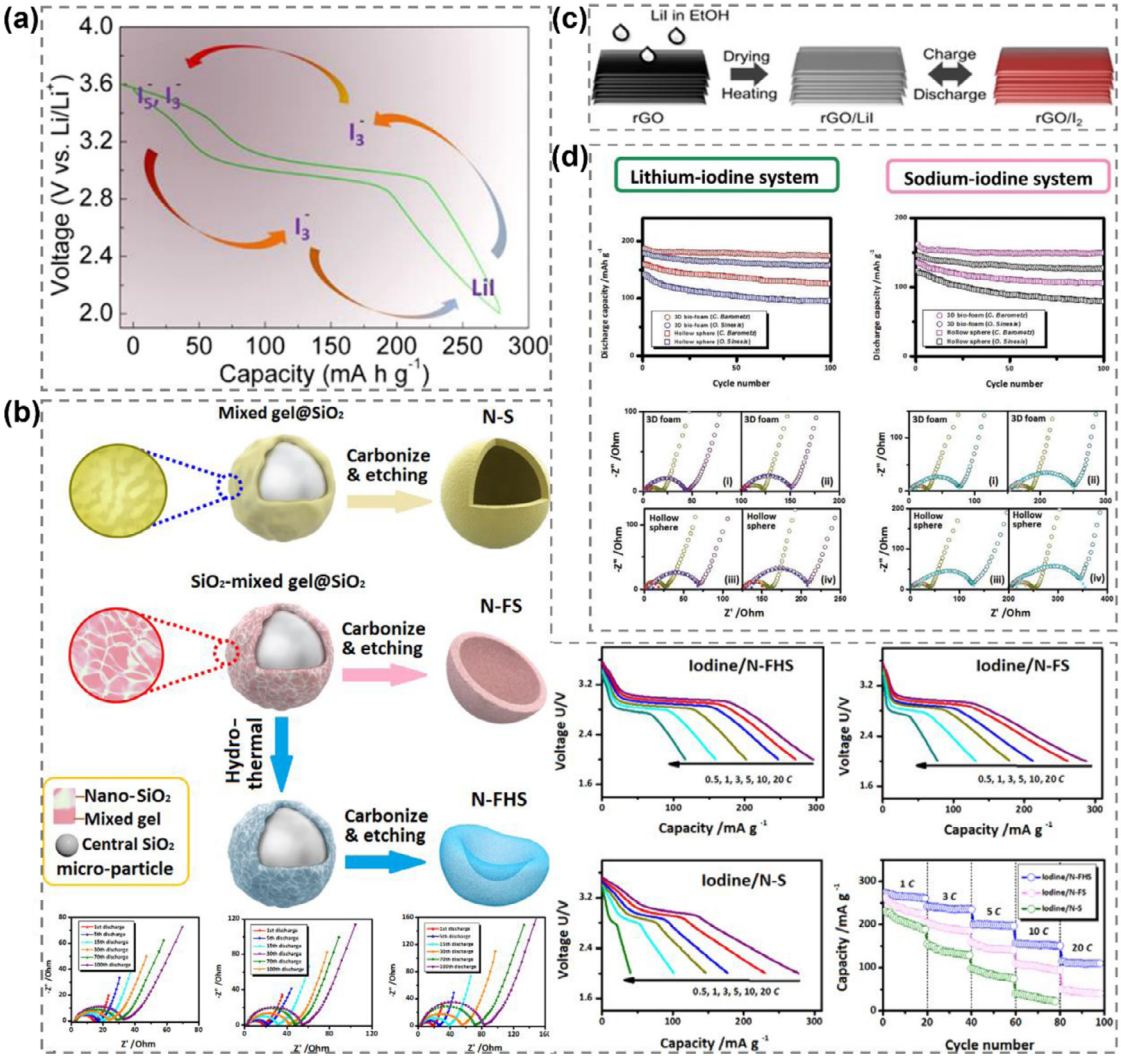

Fig. 25. (a) The evolution of iodine in a lithium-iodine battery [217] Copyright 2018 American Chemical Society. (b) Schematic illustration of the synthesis process: N-S (up); N-HS (middle); N-FHS (bottom). Nyquist plots of N-FHS-, N-HS-, and N-S-based lithium-iodine batteries. Charge/discharge curves and rate performance of the N-FHS-, N-HS-, and N-S-based lihtium-iodine batteries [218] Copyright 2017 American Chemical Society. (c) Schematic illustration of the pre-introduced composite cathode [222] Copyright 2017 American Chemical Society. (d) The cycling properties and Nyquist plots of the iodine/carbon composites [221] Copyright 2017 The Royal Society of Chemistry.

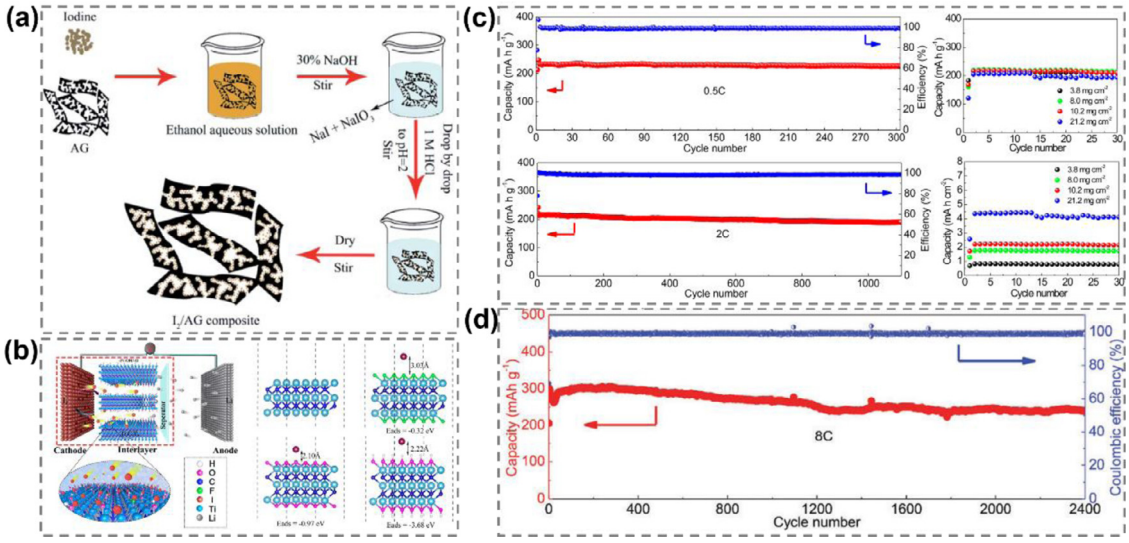

Fig. 26. (a) Schematic illustration of iodine in situ loading on active graphene [223] Copyright 2017 The Royal Society of Chemistry. (b) Schematic illustration of the binding effect of the MXene interface layer toward iodine. Molecular model of Ti_3C_2. Theoretical calculations of the binding energy between MXene and iodine: $Ti_3C_2F_x$, $Ti_3C_2O_x$, $Ti_3C_2(OH)_x$ [225] Copyright 2020 American Chemical Society. (c) Long-term cycle stability of lithium-iodine cells at different rates. Repeated charging/discharging cycling with various iodine loads [217] Copyright 2018 American Chemical Society. (d) Repeated charging/discharging cycling test for the lithium-iodine cell [226] Copyright 2018 The Royal Society of Chemistry.

rus strikingly assists in generating more active sites for redox reactions, which together with the high porosity of the hosting material delivers excellent electrochemical performances, such as a capacity of 221 mAh g^{-1} at 200 mA g^{-1}, an excellent rate capability (95.8% capacity retention at 1 A g^{-1}), and a superior long lifespan of 2,000 cycles with a 96% capacity retention.

Natural biomass-derived carbon materials are promising for the encapsulation of polyiodides from the perspective of sustainable development. Su et al. demonstrated the encapsulation effect of B_2O_3 nanocrystal-decorated carbon microtubes on polyiodide for lithium-iodine batteries, in which the carbon nanotubes were derived from green and renewable poplar catkin [220]. As a result, the B_2O_3/carbon microtube-enabled lithium-iodine battery exhibited a capacity of 177 mAh g^{-1} after 500 cycles at 20 C and a long lifetime of 5,000 cycles at 100 C with a capacity retention of 140 mAh g^{-1}. This study shows a pioneering example of introducing metal-oxide nanoparticles into a carbon hosting material, suggesting a new avenue toward the study on encapsulation of polyiodide shuttling. A further study of the encapsulation effect of a three-dimensional carbon host on iodine and polyiodides was further demonstrated in lithium-iodine batteries [221]. Both three-dimensional bio-foam and hollow spheres are synthesized by using natural precursors and are characterized in electrochemical applications. The three-dimensional bio-foam-based iodine cathode exhibits improved rate performance (Fig. 25d) by virtue of thin slices. The cell constructed with three-dimensional bio-foam provides capacity retentions of 94% in lithium-iodine batteries after 500 cycles of consecutive charging/discharging.

The reported three-dimensional carbon spheres demonstrated decent improvement in the battery performance benefitting from their high surface areas and porosity. Two-dimensional graphene, which was known for good ionic conductivity, high porosity and robust mechanical properties, is a potential candidate for use in batteries. Kim et al. unprecedently introduced iodide ions into a reduced graphene oxide hosting material and used it as a cathode for lithium-iodine battery chemistry [222]. Relative to the encapsulation of polyiodides during redox, the direct loading of iodides on cathode material suggested a new concept for future electrode designs and fabrications (Fig. 25c). An in-situ deposition route (Fig. 26a) through $I_2 + 6OH^- \rightarrow IO_3^- + 5I^- + 3H_2O$ and $IO_3^- + 5I^- + 6H^+ \rightarrow 3I_2$ (deposition) + $3H_2O$ studied the confinement of graphene for iodine and polyiodides in lithium-iodine batteries [223]. The as-prepared graphene/iodine electrode with 56 wt.% iodine loading provides a high capacity of 218 mAh g^{-1} at a current density of 211 mA g^{-1} as well as a long lifetime of 500 cycles with 161 mAh g^{-1} capacity retention.

In addition to in-carbon (a composite electrode) confinement, a membrane confinement method was developed by Wu et al. by inserting a carbon nanotube membrane between the cathode and separator [224]. The proof-of-concept battery delivered a capacity of 100 mAh g^{-1} with a 5,000-cycle lifetime and an approximate 100% columbic efficiency at 21.1 A g^{-1}. MXene ($Ti_3C_2T_x$)-type inserting layer between the separator and iodine cathode by Sun et al. demonstrated hampered polyiodides and iodine shuttling by forming strong chemical bonds with them [225]. Furthermore, the introduction of MXene boosted the redox, enabling a 5.2 mg cm^{-2} ultrahigh iodine loading mass. Bonding features between MXene sheets and iodine were theoretically studied with the assistance of density functional theory calculations (Fig. 26b). Functional groups, such as -F, -O, and -OH, on MXene sheets promoted the binding toward polyiodides, thereby inhibiting the shuttling.

Polymers are another candidate for trapping polyiodides, some polymers, such as polyvinylpyrrolidone, can interact with polyiodides and prevent it from shuttling [217]. Benefitting from the interaction between polyvinylpyrrolidone and polyiodides, the lithium-iodine cell exhibited good stability during repeated charging/discharging, even with high iodine load amounts (21.2 mg cm^{-2}, 200 mAh g^{-1}, 4.5 mAh cm^{-2}, Fig. 26c). An active carbon cloth-supported polyvinylpyrrolidone/iodine composite electrode (Fig. 26d) by Meng et al. further demonstrated a high-rate performance (approximate 1.5 A g^{-1}, 2,400 cycles) in lithium-iodine batteries [226]. In addition, Cai et al. demonstrated the encapsulation effect of β-cyclodextrin toward polyiodide, attaining an initial capacity of 175 mAh g^{-1} at 20 mA g^{-1} with a 300-cycle lifetime [227]. Water-soluble polymers, methyl-beta-cyclodextrin, polyvinylpyrrolidone, and amylose corn starch, by Zhang et al. demonstrated capacity performances of 228 mAh g^{-1} for methyl-beta-cyclodextrin, 222 mAh g^{-1} for polyvinylpyrrolidone, and 224 mAh g^{-1} for amylose corn starch after complexing with iodine/porous carbon (Fig. 27a), with capacity retentions, 87.3, 90.1, and 79.7%, and coulombic efficiencies, 97, 98 and 96%, which were higher than those without polymer coating, 74.2% capacity retention and 94% coulom-

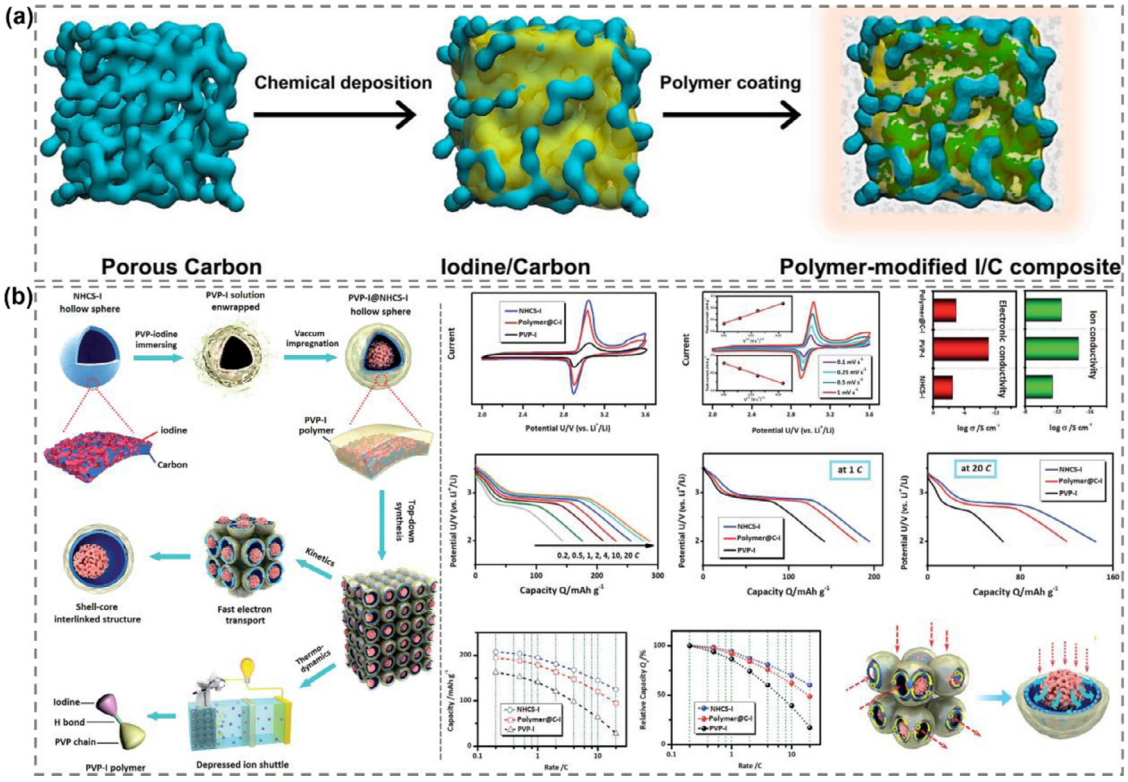

Fig. 27. (a) Schematic illustration of a polymer-modified composite [228] Copyright 2020 Elsevier. (b) Schematic illustration of the synthesis process and analysis of the structure and encapsulation effect. Nitrogen-doped hollow carbon sphere (NHCS)-iodine: an NHCS with encapsulated iodine. Electrochemical dynamic study using cyclic voltammograms, calculated electronic and ion conductivities, and discharge curves. Electron pathways and electrolyte penetration in the polymer@carbon-iodine spheres [229] Copyright 2018 The Royal Society of Chemistry.

bic efficiency [228]. Conductive polymers were further considered by Zhang et al. by designing and fabricating a composite electrode of polyvinylpyrrolidone/interconnected hollow carbon spheres given the general poor conductivity of polymers [229]. The interconnected hollow carbon spheres generated a high-way electron transfer, which together with the good diffusion of electrolyte promotes good rate performances (Fig. 27b). Sequentially, the cell assembled with the as-synthesized cathode exhibits a capacity of approximately 240 mAh g^{-1} with a lifetime of 400 cycles.

In addition to the routine carbon/organic composite hosting materials, ceramics are interesting candidates. Anju et al. demonstrated that titanium carbonitride with a certain composition, $TiC_{0.7}N_{0.3}$, possesses favorable adsorption capability toward polyiodides [230]. The titanium carbonitride catalyzed the iodide/triiodide redox, facilitating the electrochemical reaction based on the density functional theory calculations. The titanium carbonitride enables a new type of cathode material to suppress the polyiodide shuttling in lithium-iodine batteries. The lithium-iodine battery assembled with the such $TiC_{0.7}N_{0.3}$ nanowire delivers an excellent capacity of approaching 700 mAh g^{-1} and great cycling stability with coulombic efficiency approaching 100%.

In addition to the studies of suppressing polyiodide shuttling, an unstable anode/electrolyte interface is another issue for practical applications. Some efficient pathways have been reported. An aprotic lithium-sodium alloy melted onto a carbon cloth was studied by Yu et al. By coupling with an iodine cathode to form a lithium-iodine battery, it delivered great cycling stability with 84.8% after a 2,000-cycle repeated test [231]. In addition, a molten lithium anode supported by N,P-co-doped carbon cloth by Li et al. was introduced into a lithium-iodine battery, demonstrating excellent electrochemical performances of approximately 100% capacity retention over 4,000 cycles and improved high-rate capability [232].

The suppression of the polyiodide shuttling has seen substantial progress after the enormous research efforts. To date, carbon-based composite materials exhibited great potential in lithium iodine batteries. A systematic comparison of the electrochemical performances was provided in Table 5. Further attention should be put on the explorations of innovative electrode designs and materials fabrications with considerations of affordable cost and environmental sustainability. Apart from the conventional polyiodide shuttling issue in lithium-iodine batteries, other remaining issues, such as electrolyte explorations and a stable anode/electrolyte interface, impose roadblocks toward practical applications [233]. The further research efforts, in fact, can refer to the strategies and concepts in highly advanced lithium metal batteries.

3.2.2. *Sodium-iodine batteries*

Considering the limited lithium resources on earth, metal alternatives, such as sodium, promise cost efficiency and a sufficient potential window for high energy densities. Gong et al. synthesized an iodine quantum dot-decorated graphene cathode for sodium-iodine batteries [234]. The formed sodium-iodine battery delivers a reversible capacity of 141 mAh g^{-1} after 500 cycles at a current density of 100 mA g^{-1} with a 500-cycle lifetime, as well as a good rate capability and 56% capacity retention when the drain current density is enhanced from 100 mA g^{-1} to 1,000 mA g^{-1}. During the discharge process, sodium ions intercalate into the iodine unit and form a sodium iodide discharge product, which enables outstanding electrochemical performances. Two-dimensional iodine, iodinene, sheets with enlarged size relative to the quantum dot by Qian et al. further demonstrated the improved rate capability, 109.5 mAh g^{-1} at 10 A g^{-1}, in sodium-iodine batteries [235]. The innovative two-dimensional iodinene was prepared through a liquid-phase exfoliation method, generating iodinene with a thickness of approximate 1 nm and a lateral size approaching hundreds of nanometers. Additionally, first-principles calculations confirmed that sodium ions migrate in the

Table 5
Systematic comparison of the electrochemical performances.

Material	Lifetime (cycles)	Capacity (mAh g^{-1})	Current density (mA g^{-1})	Ref.
N-doped hollow C fold-hemisphere	300	200	200	[218]
Dual heteroatom-doped C cloth	2,000	200	2,000	[219]
B_2O_3/C microtubes	500	177	4,000	[220]
Iodine@bio-hollow sphere	500	160	800	[221]
Reduced graphene/iodine	200	200	2,000	[222]
Active graphene/iodine	500	218	211	[223]
C nanotube membranes	5,000	100	21,100	[224]
$Ti_3C_2T_x$ membranes	1,000	~100	400	[225]
Polyvinylpyrrolidone-iodine	1,100	~200	400	[217]
Activated C cloth/polyvinylpyrrolidone-iodine	2,400	~200	1,500	[226]
Iodine/β-cyclodextrin	300	175	20	[227]
Core-shell interlinked polyvinylpyrrolidone@C-iodine	400	~90	800	[228]

iodinene through a vertical manner instead of in the horizontal direction that occurred in common bulk iodine, which results in a lowered energy barrier of 0.07 eV for sodium ion transport.

Framework-type materials, such as metal-organic frameworks and covalent-organic frameworks, are potential candidates for hampering the shuttling of polyiodides in sodium-iodine batteries. Wang et al. demonstrated the suppressing effect of metal-organic frameworks on polyiodides shuttling, exemplifying with fully conjugated copper-phthalocyanine-zinc (or nickel or iron) metal-organic frameworks [236]. Surprisingly, the planar iron-bis(dihydroxy) species in copper-phthalocyanine-iron metal-organic frameworks were the key part for bonding polyiodides and restricting its shuttling. The sodium-iodine battery showed a 3,200-cycle lifetime with a capacity of 150 mAh g^{-1}.

Regarding the development of sodium-iodine batteries, more research efforts are suggested to put on the stability improvement of anode/electrolyte interfaces and the design of functional composite cathodes to synergistically enhance the electrochemical performances given the high activeness of sodium anode and high solubility of iodide species.

3.2.3. Potassium-iodine batteries

Potassium-iodine chemistry is an alternative to the lithium-iodine system, given its comparable potential and affordable costs. The current research efforts were highly focus on the fixation of polyiodides at cathode. Qian et al. demonstrated the encapsulation effect of mesoporous carbon on both iodine and polyiodides in potassium-iodine battery chemistry, by which it exhibited improved redox kinetics, exhibiting capacities of 167 mAh g^{-1} at 50 mA g^{-1} and 89.3 mA h g^{-1} at 500 mA g^{-1} as well as a 300-cycle lifespan with a capacity retention of 126 mAh g^{-1} at 170 mA g^{-1} [237]. A reversible solid-liquid-solid phase transitions along iodine, potassium triiodide and potassium iodide in potassium-iodine batteries by Lu et al. enabled a high capacity of 156 mAh g^{-1} with a lifespan of 500 cycles (Fig. 28) [238].

In the potassium-iodine batteries, beside the anode/electrolyte interface and polyiodide shuttling issues that were faced by lithium- and sodium-iodine batteries, too, a special attention on the limited kinetics of large-sized potassium ions is necessary. Furthermore, the poor rate performance due to the poor conductivity of iodine active species highlights the remaining research efforts. More highly conductive composite electrodes may be suitable options for fast redox kinetics. Well integrated composite electrodes over repeated charging/discharging are favorable for high-performance sodium-ion batteries.

3.2.4. Magnesium-iodine batteries

Magnesium-iodine chemistry based on magnesium metal anode, as an emerging star, attained increasing attention. In contrast to conventional monovalent alkali metal anodes, the magnesium anode featuring stripping/platting of magnesium ions has more sluggish kinetics due to the higher charge density compared to the monovalent ions. To boost the performance of magnesium-iodine batteries, pioneering efforts have been carried out. Tian et al. demonstrated a new liquid-to-solid mechanism to release the potential of high gravimetric capacity of iodine in magnesium-iodine batteries [239]. In particular, soluble polyiodides reacted with magnesium ions during discharge, forming a soluble intermediate, which then formed a solid-state final discharge product. This strategy intelligently circumvents the shuttling of polyiodides by forming the intrinsic insoluble magnesium iodide product. More research efforts and engineering on the cathode hosting materials and(or) current collectors would be the next step for further improvement in the electrochemical performances of magnesium-iodine batteries.

3.2.5. Zinc-iodine batteries

As another typical bivalent cation, zinc ions have been widely studied in aqueous batteries due to the steady plating and stripping of zinc ions at the anode/electrolyte interface, enabling a highly safe battery chemistry, which is extremely crucial in practical utilization. Most of the studies of zinc-iodine batteries were conducted in aqueous phases and thus had high potential in terms of battery safety. However, the side reactions induced by electrolyte hydrolysis over charging are harsh issues. To ensure that the aqueous zinc-iodine batteries operate without severe side reactions, electrolyte engineering is an efficient solution. As hydrogen evolution proceeding, the electrolyte pH increases accordingly, which inspires scientists to develop a pH-sensitive electrolyte to shut off the battery when hydrogen evolution occurs. Wang et al. found that poly(2-vinylpyridine) exhibited solidification behavior when the pH was higher than a critical value, 5, accompanied by a decrease of ionic conductivity, which returned to a liquid state when the pH restored to lower than 5 along with the recovery of ionic conductivity [240]. Benefitting from the unique pH responsibility, a self-protective aqueous zinc-iodine battery demonstrated desirable self-protection behavior through solidifying the electrolyte and delivers only 6% of the normal capacity. After the pH returned to less than 6, nearly 100% capacity recovery was achieved.

Regarding the polyiodides shuttling issue, two main concepts, steric confinement and chemical absorption, have been extensive demonstrated. The former highly relies on the design of porous hosting or sieving materials [241]; the latter, however, focuses on composite materials with desirable capabilities, such as catalysis and absorption interaction. We particularly summarized the studies on this issue from these two aspects below.

A solution based on size exclusion can sieve large iodides and triiodides and hamper their shuttling. Therefore, highly porous metal-organic frameworks well-known for use at the cathode side are favorable for use as membranes in aqueous zinc-iodine batteries owing to their intrinsic porosity and adjustable pore size. Yang et al. synthesized a zinc-benzene-1,3,5-tricarboxylic acid (BTC) metal-organic framework membrane and employed it as an ionic sieve in aqueous zinc-iodine batteries [242]. The zinc-BTC sieve membrane not only efficiently suppressed polyiodides shuttling, but also hampered side reac-

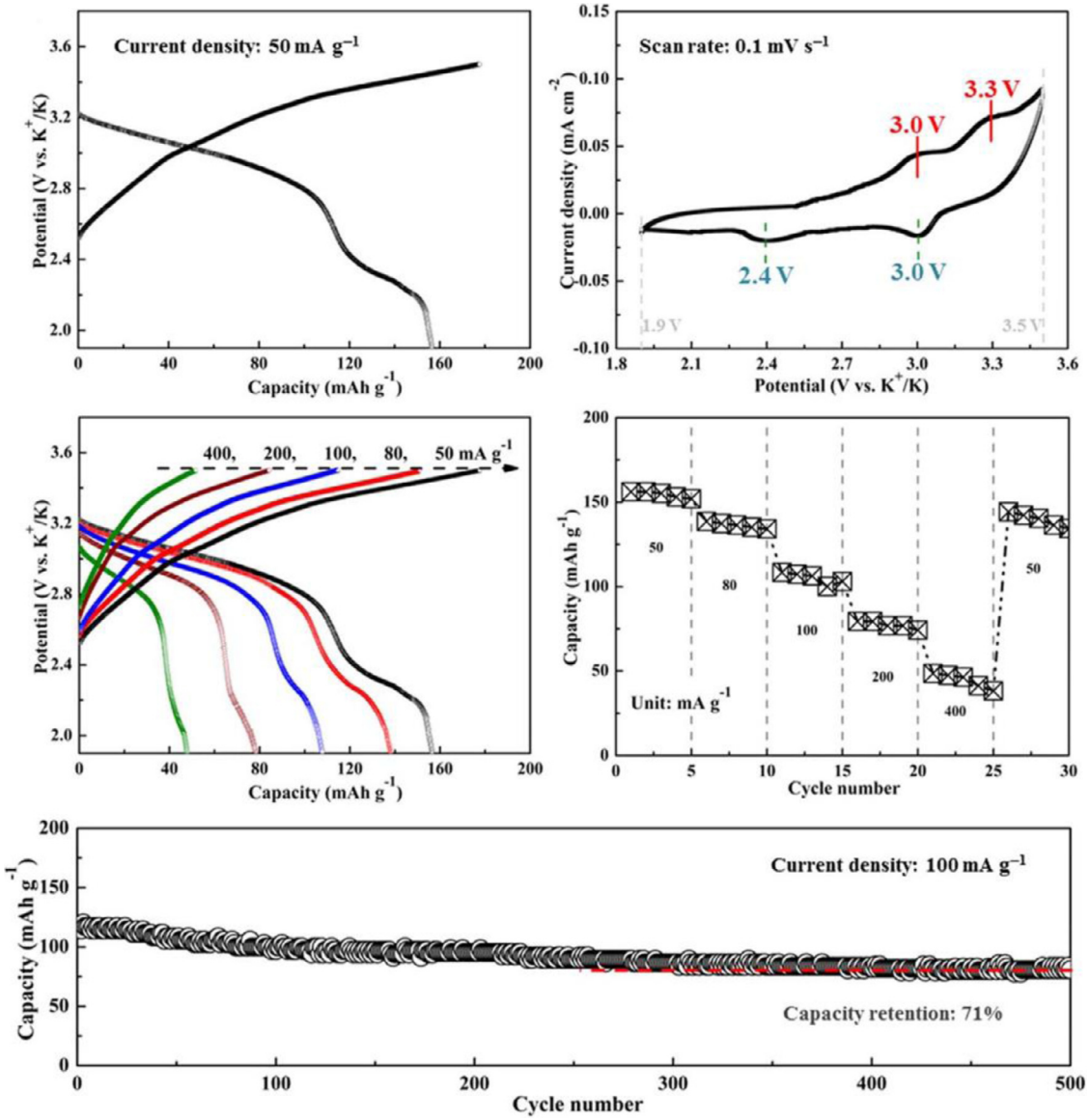

Fig. 28. Electrochemical characterizations of the potassium-iodine battery: charge/discharge profiles, cyclic voltammetry curves, voltage profiles, rate performance, long-term cycling [238] Copyright 2019 Elsevier.

tions on the zinc anode surface by regulating the electrolyte solvation structure and forming the more aggregative ion associations. Sequentially, the aqueous zinc-iodine battery fabricated achieved an ultralong lifetime of over 6,000 cycles with a high-capacity retention of 84.6% and 99.65% coulombic efficiency. This work provides an innovative concept for electrolyte engineering, which is regulating the ion solvation structures and hampering the associated side reactions by framework-type membranes.

Steric confinement of polyiodides is another approach for restraining polyiodides shuttling. Many studies have demonstrated the effectiveness of carbon hosting materials in hampering polyiodides and iodine dissolution and shuttling. Bai et al. synthesized a nanopore carbon cloth cathode for trapping iodine in aqueous zinc-iodine batteries [243]. The battery with well-trapped iodine delivers a capacity of 255 mAh g^{-1} at 100 mA g^{-1} and good rate capability of 160 mAh g^{-1} at 1 A g^{-1}, as well as a long lifetime with a capacity retention of approximate 150 mAh g^{-1} after 1,500 cycles. Similarly, Li et al. employed a carbon cloth with micropores as the cathode of aqueous zinc-iodine batteries [244]. The authors found that zinc iodide only was generated instead of other polyiodides according to the density functional theory calculation (Fig. 30b), verifying the absence of polyiodides shuttling. Regarding the carbon hosting materials, an in-depth explanation and understanding of the process, however, was presented by Pan et al. by deeply analyzing polyiodides shuttling and absorption in an aqueous zinc-iodine battery under the help of experimental, using the microporous carbon as the cathode, and theoretical calculations [245]; the polyiodides dissolving into the electrolyte and being absorbed at the cathode were a competitive process as confirmed by the negative yet different active energy changes (Fig. 30c). The absorption process of polyiodides at microporous carbon requires less energy than the dissolution behavior counterparts, thus restricting the shuttling and reserving the capacity during cyclic measurements. Furthermore, an adsorption mechanism of carbon-related hosting materials was revealed by Yu et al. through theoretical calculations, exemplifying the different absorption efficiencies of carbon hosting materials with diverse doping atom configurations [246]. Graphitic nitrogen exhibited the lowest adsorption energy (-5.3 eV) relative to other configurations, suggesting the best stability in terms of absorbing iodine (Fig. 29a). The doping species and amount of carbon hosting materials, thus, are highly responsible for the final electrochemical performances, particularly the cyclic stability.

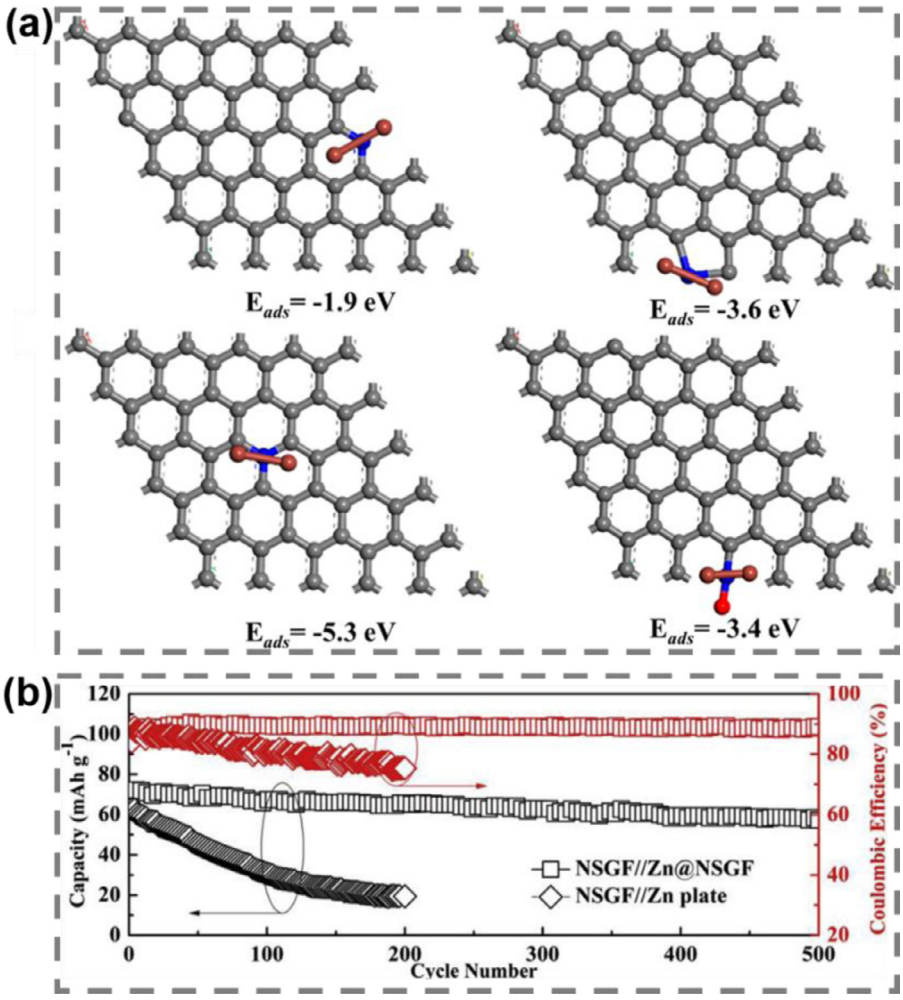

Fig. 29. (a) Simulated adsorption energy of carbon hosting materials with different nitrogen configurations [246] Copyright 2020 American Chemical Society. (b) Cyclic performance of zinc-iodine batteries using zinc plates and zinc nanosheets at 200 mA g^{-1} [249] Copyright 2019 Elsevier.

Solid-state polymers with good ionic conductivity provide a potential solution for trapping polyiodides and hampering the shuttling disadvantage. Sonigara et al. developed a full solid-state zinc-iodine battery utilizing a polymer-gel electrolyte and catholyte [247]. The pluronic F77 polymer was employed for solidifying both the electrolyte and the catholyte; the formed complex generated selective zinc ion transport channels throughout the entire battery for electrochemical redox reactions. Less than 70% capacity retention is attained for the above study when the specific current was enhanced from 20 to 400 mA g^{-1}. The limited ionic conductivity and transport rates appear to be one longstanding issue in solid-state zinc-iodine batteries. Therefore, conductive polymers, such as polyvinylpyrrolidone and polyaniline, that have chemical interactions with polyiodides are potential candidates for suppressing the shuttling effect of polyiodides without highly sacrificing the electrochemical performances. Zeng et al. synthesized an iodine/polyaniline composite for aqueous zinc-iodine batteries [248]. The aggregative interaction between polyiodides and polyanilines was favorable for preventing polyiodides from diffusion and shuttling (Fig. 30a). The battery stability demonstration exhibited a capacity retention of 79% initial capacity after 700 cycles at a high current density of 1.5 A g^{-1}. More explorations on the functional polymers are necessary.

Dendrite growth on zinc foil surfaces is a challenging issue; smooth deposition of zinc ions is crucial for long-term stability. Replacing the bulk zinc foil with zinc nanoparticles to eliminate the surficial defects of zinc foils is an efficient solution given the high specific surface area and smooth particle surface of zinc nanoparticles. Lu et al. found that by replacing zinc foil with zinc nanosheets and loading them on a nitrogen- and sulfur-co-doped graphene foam, the zinc-iodine battery exhibits excellent cyclic stability relative to that using zinc foils (Fig. 29b) [249].

The regulation of zinc deposition through the introduction of electrolyte additives is adoptable, which can not only hamper intrinsic side reactions but also enhance the electrochemical kinetics by improving the ionic conductivity. Jian et al. studied the ammonium bromide additive in an aqueous zinc-iodine batteries [250]; the ionic conductivity was increased from 120 to 180 mS cm^{-1}, meanwhile the ammonium ions regulated the deposition of zinc ions by forming an electrostatic shielding layer.

In the studies of zinc-iodine batteries, many research efforts should focus on the suppression of zinc dendrites in addition to the suppression of polyiodide shuttling. Current reports on overcoming the zinc dendrites are mainly limited to artificial solid-electrolyte interfaces formed by either direct modification on zinc surfaces or introducing electrolyte additives, which provide insights into the stable deposition of zinc ions in zinc iodine batteries. Hydrolysis on the zinc surface in aqueous zinc iodine batteries can be inhibited, too, by the adoption of artificial solid-electrolyte interface. Regarding the polyiodide shuttling, functional composite electrodes with good electronic conductivity and ionic diffusion are favorable candidates, and more innovative electrode designs are suggested. A systematic comparison of the electrochemical performances was provided in Table 6.

3.2.6. *Iron-iodine batteries*

Iron-iodine batteries based on iron anodes have emerged as a low-cost alternative to conventional lithium-ion batteries. The pioneering research efforts have demonstrated the high potential of iron iodine bat-

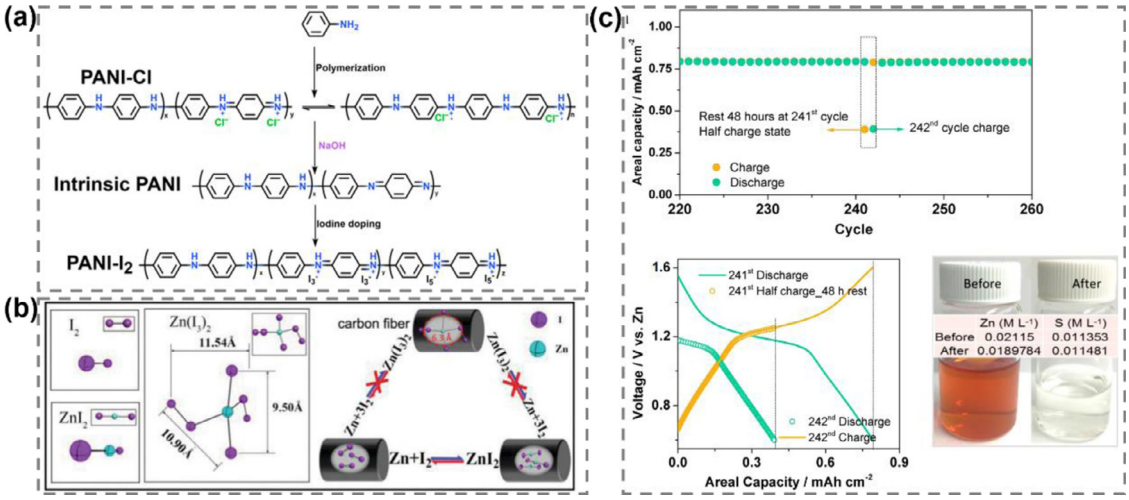

Fig. 30. (a) Schematic illustration of the polyaniline-iodine synthesis process [248] Copyright 2020 American Chemical Society. (b) Density functional theory-calculated configurations of iodine and Zn iodides and the proposed electrode reaction [244] Copyright 2018 The Royal Society of Chemistry. (c) Self-discharge tests of zinc-iodine batteries: a half-charged zinc-iodine battery rests for 48 h at the 241st cycle. Charge and discharge curves of the 241st and 242nd cycles. Visualized comparison of polyiodides adsorption by the cathode material [245] Copyright 2017 American Chemical Society.

Table 6
Systematic comparison of the electrochemical performances.

Material	Lifetime (cycles)	Capacity (mAh g^{-1})	Current density (mA g^{-1})	Ref.
Zn-BTC membrane	6,000	90	1,920	[242]
Activated C cloth/iodine	500	~200	100	[243]
Iodine/C cloth	200	300	227	[244]
Copolymer F77 catholyte	500	198	200	[247]
Polyaniline/iodine	700	160	1,500	[248]
S and N co-doped graphene foam electrode current collector	500	70	200	[249]

teries. Bai et al. developed an iron-iodine battery by using ascorbic acid-modified metallic iron as an anode for suppressing iron dendrite formation and by using nitrogen-doped iodine/porous carbon as a cathode for hindering polyiodide shuttling [216]. The designed iron-iodine battery provides a high capacity of ~190 mAh g^{-1} at 5,000 mA g^{-1} and 550 cycles of cycling stability with near 100% capacity retention (Fig. 31). The cycling stability implies that co-modification of both the anode and cathode is a necessary process for achieving highly revisable redox. Visualized evidence of the absorption behavior of nitrogen-doped highly porous carbon toward iodine and polyiodides was obtained by mixing iodine and polyiodides with the carbon host (Fig. 31) and the hindering effect on polyiodides shuttling was observed. Carbon nanotubes have also been demonstrated to be effective in iodine and polyiodides encapsulation applications [251].

More research efforts on the iron-iodine batteries are needed before the future practical applications given the cost efficiency and decent electrochemical performances. The research efforts should focus on the iron anode to expand the fundamental understanding of iron redox chemistry in addition to the studies of the iodine cathode.

3.2.7. Aluminum-iodine batteries

Aluminum-iodine battery chemistry is a typical type of conversion-based aluminum-ion batteries differing from the conventional intercalation-based charge storage mechanism. In this conversion chemistry, shuttling of the polyiodide compounds formed after being discharged is one of the remaining issues. To address the polyiodide shuttling, several advanced technologies have been reported. A chemical method of hydrogen-bonding interaction by Tian et al. demonstrated effectiveness on suppressing polyiodides shuttling [252]. The developed aluminum-iodine cell exhibited a high capacity of more than 200 mAh g^{-1} at a current density of 42.2 mA g^{-1} and a 150-cycle lifetime at 211 mA g^{-1} benefitting from the iodide/triiodide redox couple. The authors found that a hydrogen bond is formed inside the polyvinylpyrrolidone-iodine composite, which effectively hinders the polyiodide shuttling. Later, the hydrogen bond was demonstrated by density functional theory calculations by Zhang et al. [253]. The cathode was fabricated by using iodine supported with active carbon cloth and dispersed with polyvinylpyrrolidone to suppress the shuttling of polyiodide compounds during operation (Fig. 32). The constructed aluminum-iodine battery achieves a capacity of 180 mAh g^{-1} at a current density of 42.2 mA g^{-1} and a long lifespan of 1,050 cycles at 211 mA g^{-1}. The electron transfer (accumulation, yellow color and depletion, cyan color, Fig. 32) suggests a strong electrostatic reaction between polyiodides and the hosting material of polyvinylpyrrolidone. The formation energy (0.98 eV) of polyvinyl pyrrolidone-triiodide from polyvinyl pyrrolidone-iodide is almost 2 times higher than that of polyvinyl pyrrolidone-pentaiodide from polyvinyl pyrrolidone-triiodide (0.54 eV, Fig. 32). The high formation of polyvinyl pyrrolidone-iodides with aluminum enabled a favorable battery stability.

Differing from the other mono or bivalent metal ions, the trivalent aluminum ions show sluggish electrochemical kinetics although it has the smallest ionic radius among metal ions. Intensive research efforts on the aluminum anode/electrode interfaces are urgently needed. More feasible electrolytes are waiting to be explored given the high costs of ionic liquid electrolytes. Regarding the cathode side, intense electrostatic interaction between the charge-rich aluminum ions and the iodine lattices is one potential issue that limits the repeated charging/discharging.

3.2.8. Carbon-iodine batteries

Given the disadvantages, such as dendrite growth, unstable electrode/electrolyte interfaces, and side reactions, faced by the metal

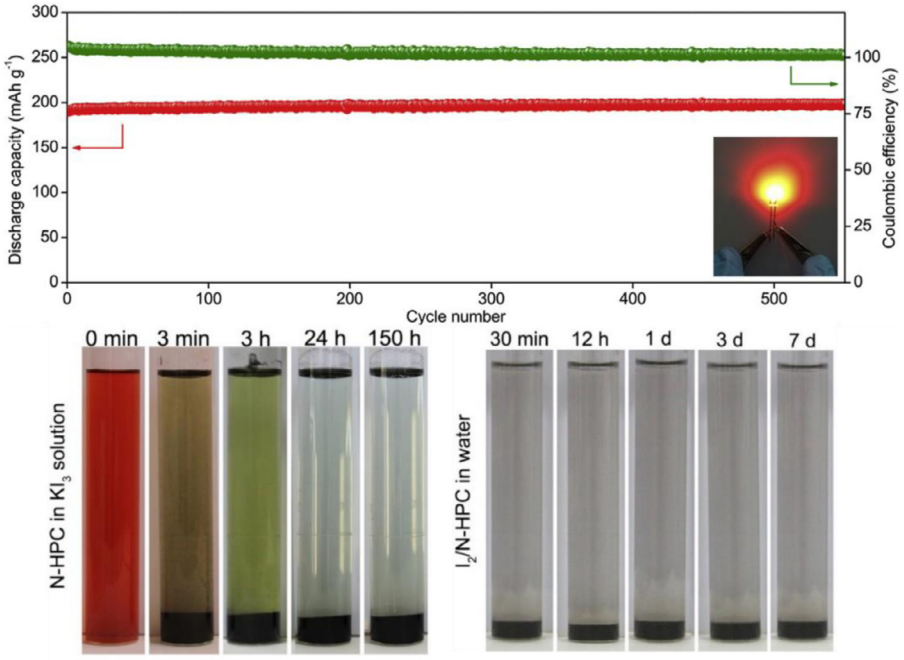

Fig. 31. Long-term cycling performance at a specific current of 2,000 mA g^{-1}. The iron-iodine battery can power a light emitting diode. Photographs of adsorption behavior of nitrogen-doped hierarchically porous carbon (N-HPC) [216] Copyright 2020 Elsevier.

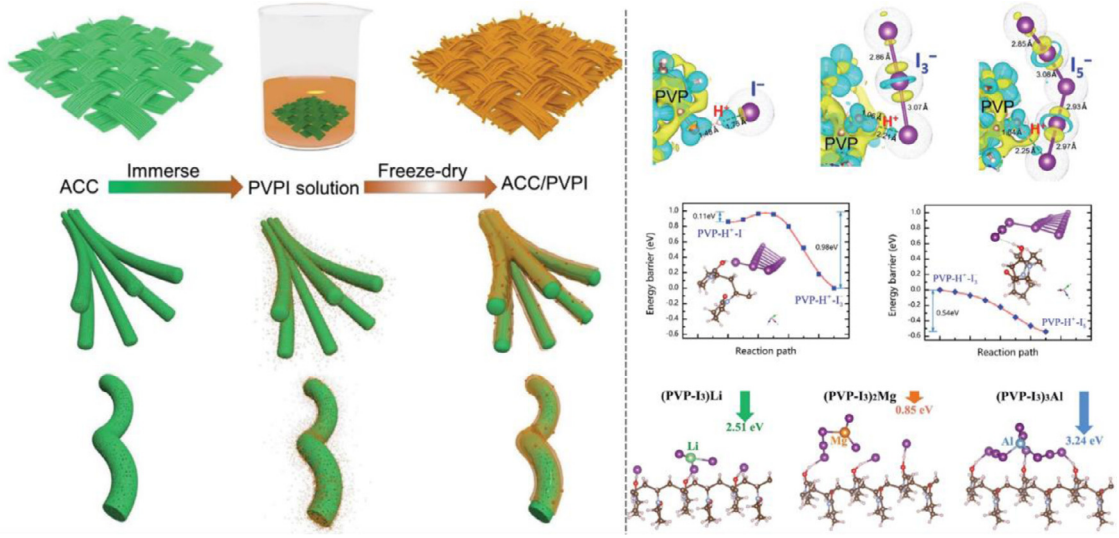

Fig. 32. Preparation process of the active carbon cloth-supported polyvinylpyrrolidone iodine composite electrode. Optimized iso-surface of the charge density for polyvinyl pyrrolidone-iodide, polyvinyl pyrrolidone-triiodide, and polyvinyl pyrrolidone-pentaiodide. Reaction energy barrier for iodine adsorption on polyvinyl pyrrolidone-iodide and polyvinyl pyrrolidone-triiodide. Simulated structures of (polyvinyl pyrrolidone-I_3)Li, (polyvinyl pyrrolidone-I_3)$_2$Mg, and (polyvinyl pyrrolidone-I_3)$_3$Al with negative formation energy [253] Copyright 2018 The Royal Society of Chemistry.

anodes in metal-iodine chemistries above, replacing metal anodes with nonmetallic carbon anodes promises reliable safety and potential stability of the anode/electrolyte interfaces. The carbon anodes store charges through multiple processes, such as surface adsorption, pseudocapacitive-type charge storage, and intercalation, which enables the capacity balance of the anode and iodine cathode. An innovative carbon-iodine battery by Lu et al. was fabricated by using nitrogen and phosphorous co-doped hierarchically porous carbon matrix nanoparticles (HPCM-NPs) as the hosting material for both anodes and cathodes [254]. Iodine was absorbed by HPCM-NPs, forming iodine-HPCM-NPs, which exhibited excellent electrochemical performances in both lithium-iodine and sodium-iodine battery systems. A battery constructed by pairing HPCM-NPs and iodine-HPCM-NPs realized the first example of coupling intercalation and extrinsic conversion charge storage mechanisms. This study verified the good encapsulation effect of a well-designed carbon matrix on both iodine and polyiodides. The porous carbon hampers the dissolution of polyiodides by slowing down the formation of triiodides and pentaiodides, which are responsible for self-discharge by shuttling, persisting to form favorable solid-state iodine deposition [255].

Carbon-iodine batteries were built up by replacing the conventional metal anodes with the carbon anodes to have a stable anode/electrolyte interface, which opened up a new avenue toward the studies of advanced secondary iodine-based batteries. The electrolytes used in the carbon-iodine battery is customized based on the need of practical devices. The carbon anodes assembled for alkali metal-ion batteries have currently seen great progress; the carbon anodes for multivalent-ion batteries, however, are still in fancy. More studies of carbon-iodine batteries with various electrolyte systems are beneficial for the fundamental understanding of the carbon-iodine batteries.

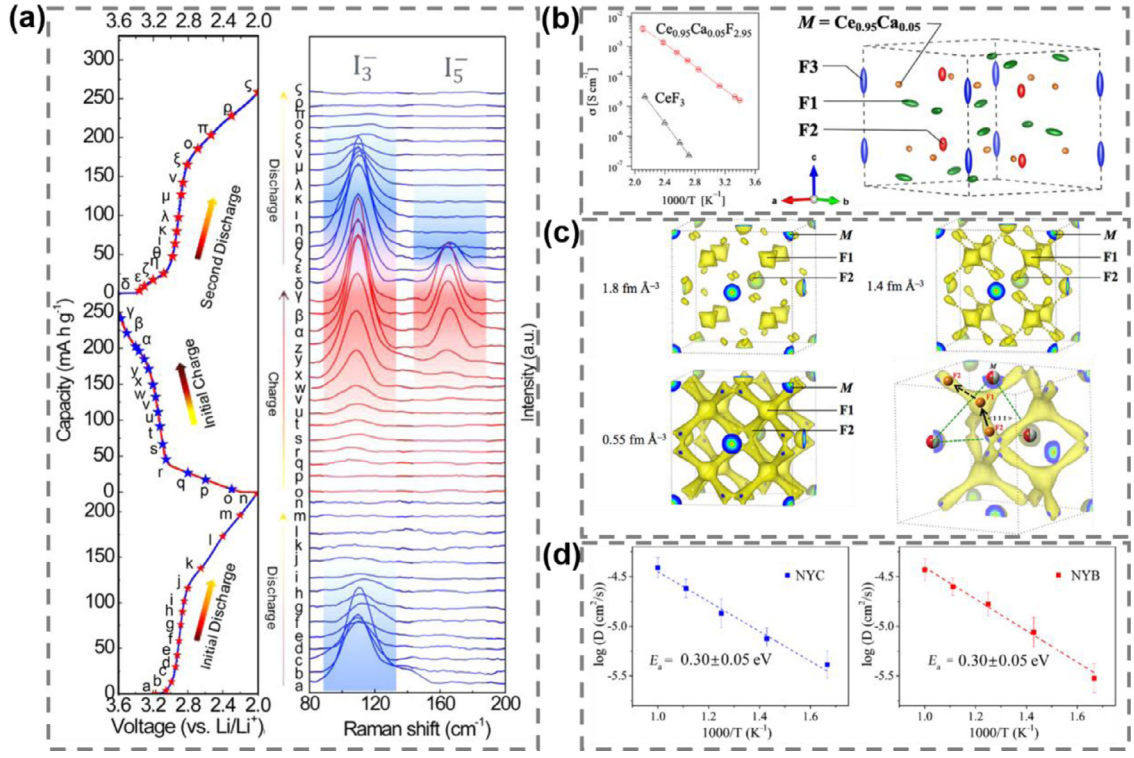

Fig. 33. (a) In situ Raman analysis of the charge/discharge process of lithium-iodine batteries [217] Copyright 2018 American Chemical Society. (b) Schematic illustration of fluoride migration pathways [258] Copyright 2020 American Chemical Society. (c) Nuclear density distribution calculated by the maximum entropy method for $Ba_{0.6}La_{0.4}F_{2.4}$ at 239°C. Interstitial diffusion-based model for the $Ba_{0.6}La_{0.4}F_{2.4}$ solid electrolyte [259] Copyright 2020 American Chemical Society. (d) Arrhenius plots of the sodium ion diffusion coefficient in Na_3YCl_6 (NYC) and Na_3YBr_6 (NYB) [261] Copyright 2020 American Chemical Society.

4. Advanced characterization techniques

To reveal the in-depth charge/discharge mechanisms and underlying (electro)chemical reactions, in-situ and ex-situ characterizations, such as X-ray diffraction, scanning electron microscopy, transition electron microscopy, Raman spectroscopy, and Fourier transform infrared spectroscopy, are commonly utilized and play a significant role in such an objective. Furthermore, mathematical induction, such as the power law equation, Tafel's law, Nernst-Planck formulation, and Butler-Volmer formulation, helps to quantitatively and qualitatively analyze the experimental results, assisting the evaluation of electrochemical process, such as ion transport and charge transfer [256]. In-situ characterizations directly reveal the inside electrochemical process during the redox reactions, offering direct evidence for the redox reactions inside batteries, as shown in Fig. 33a. Compared with the ex-situ process, the in-situ analysis circumvents unfavorable side reactions occurred when the battery components meet the ambient environment.

Simulation and computation are efficient methods for analyzing the ionic conductivities, migration pathways, and shuttling mechanisms within solid-state electrodes and electrolytes, providing beneficial insights into facilitating the development of solid-state batteries [257]. Mori et al. studied the ionic conductivities through simulation using the typical solid-state tysonite $Ce_{0.95}A_{0.05}F_{2.95}$, where A could be a Ca, Sr, and Ba electrolyte [258]. As a result, $Ce_{0.95}Ca_{0.05}F_{2.95}$ showed the highest conductivity. An important finding of this report was that the F1-F1 and F1-F3 sublattices play a key role in highly fluoride-ion conductive solid-state electrolytes (Fig. 33b).

Mori et al. conducted Rietveld refinements to further understand the fluoride-ion diffusion mechanism in the superior solid-state electrolyte $Ba_{0.6}La_{0.4}F_{2.4}$. The authors employed neutrons to trace small nuclei accurately rather than X-rays [259]. Fig. 33c exhibits the nuclear density distribution at different contour surfaces at high temperature by changing the atomic motion from vibration to diffusion. The F1 and F2 (fluoride ion position inside crystal structure) sites anisotropically spread until connecting with each other, forming an F1-[F2-F2]-F1 ionic pathway inside the $Ba_{0.6}La_{0.4}F_{2.4}$. Beyond the diffusion pathways, the authors further pursued a fluoride-ion diffusion model, as shown in Fig. 33c, where the fluoride ions migrate from F2 to F1 along the <111> axis; the original fluoride ions at the F1 sites were transferred to the F2 sites, as marked with a dashed arrow. However, this transfer process was restrained by triangular metal ions.

Regarding the F1 and F2 sites associated with fluoride-ion conductivity in solid-state electrolytes, Dieudonné et al. synthesized $Sm_{1-x}Ca_xF_{3-x}$ solid-state electrolytes and found that the local environment of F1 is greatly responsible for the entire ionic conductivity, which changes with the calcium content [260]. Briefly, the author concluded that the higher buckling effect into the F2/F3 sheets resulted in higher distortion at the F1 local sites, thereby obtaining higher ionic conductivity. A theoretical study conducted by Qie et al. demonstrated that yttrium-sodium halides (Na_3YX_6, X=chloride or bromide) exhibited a sodium-ion conductivity of 0.77 mS cm^{-1} and an electrochemical window of 0.51-3.75 V when X=chloride and 0.44 mS cm^{-1} and 0.57-3.36 V when X=bromide at 300 K (Fig. 33d), as well as excellent interfacial stability with the sodium metal anode and high-voltage cathode materials, achieving a balance between the sodium-ion conductivity and electrochemical stability [261].

5. Conclusion and perspectives

Halogen have been extensively studied in battery chemistries. In this review, we summarized the advances achieved in recent years in halogen-related rechargeable battery applications. The whole review article is rationally organized in terms of two types of application concepts, which are halogen-based battery chemistries featuring no redox and halogen conversion-based battery chemistries featuring the redox of halogen species.

The discussion of redox-free halogen-based battery chemistries were conducted from the perspectives of electrodes and electrolytes. In the electrode parts, we further classified the reported studies based on different types of materials, including metal halide compounds, metal-oxy-halogen compounds, fluoride-containing metal-based polyanions, and halogen-doped composite electrodes. In each chapter, the applications of halogen-containing electrodes were comprehensively discussed in various battery chemistries. In the electrolyte portion, we further organized the review from the effects of halogen species in electrolytes. Various effects of halogen species in electrolytes were discussed by associating with various battery chemistries.

Halogen-containing compounds are considered as promising electrodes in battery chemistries given the advantages such as high abundance and a variety of functions. However, the remaining obstacles of using halogen-containing compound electrodes are their inferior structural stability, poor electronic conductivity, and limited ionic migration, which highly restrict the battery exploration. Rational designs and fabrications of such halogen-containing compounds promise improved electrochemical performances. Current studies have demonstrated that lattice modulation, morphology design, and heterogeneous electrodes are efficient solutions for addressing above issues. Further studies on composite electrodes, particularly electrodes with protective layers, such as carbon coating and polymer coating, are of great potential to improve the performances of halogen-containing electrodes.

Halogen-containing components have also demonstrated to be potential candidates for utilizations in electrolytes from the perspectives of being as charge carriers, facilitating ionic conductivity of solid-state electrolytes, and stabilizing the solid electrolyte interfaces. Halogen-ion batteries mainly rely on the halogen ion shuttling in electrolytes to form a circulated current loop. Fluoride- and chloride-ion batteries are extensively studied, accompanied with the common issue of lack more feasible, cost-efficient, and high-performance electrolyte systems. In addition, halogen have demonstrated to be good dopants for solid electrolytes to improve the ionic conductivity. Typically, several halogen-containing solid-state electrolytes for lithium- and sodium-ion batteries demonstrated the lattice modulating effects of halogen species. Studies on the mechanisms of ionic migration within such halogen-modified solid-state electrolytes demonstrated inner three-dimensional tunnels for ion migration. However, the current halogen-containing solid-state electrolytes still face the challenge of lacking in-depth fundamental understanding. Further research efforts on the understanding of the effects of halogen doping are suggested. More studies on the fundamental understanding of ion migration within such halogen containing solid-state electrolytes and how to manipulate the conductive channels are beneficial for exploring novel types of solid-state electrolytes. Moreover, the study on halogen-containing compounds for stable solid electrolyte interfaces in alkali metal batteries have seen great progress, particularly lithium metal batteries. Further efforts of halogen-containing solid electrolyte interfaces in other battery chemistries, such as zinc-ion batteries, are favorable to stabilize the plating/stripping of metal ions and thus circumvent the formation of notorious dendrites, promising battery safety. Accordingly, more fabrication and engineering strategies are beneficial for demonstrating further applications of halogen species for the artificial solid electrolyte interfaces.

Regarding halogen-conversion electrochemistries, we discussed the bromine and iodine redox separately. Redox flow and flowless batteries based on bromine conversion-based battery chemistries were reviewed. For the iodine conversion-based batteries, we organized the reports from a perspective of various battery chemistries, including lithium-iodine, sodium-iodine, potassium-iodine, magnesium-iodine, zinc-iodine, iron-iodine, aluminum-iodine, and carbon-iodine batteries. Current issues and promising solutions are reviewed in the halogen conversion-based battery chemistries. Some suggestions and possible strategies were also provided as a guideline.

For halogen conversion-based battery chemistries, a majority of studies on bromine and iodine conversion-based battery chemistries have been conducted, due to the proper electronegativity and physical conditions (solid or liquid) relative to gaseous fluorine and chlorine. Bromine has been extensively investigated in redox flow batteries due to the liquid form and good solubility of bromine, which circumvents the difficulty of design and fabrication of complex electrodes. However, crossover contamination is still a challenge faced by such redox flow batteries, which leads to the need of costly membranes. To this end, innovative membrane-free and flowless bromine conversion-based batteries are designed and fabricated by capturing bromides or bromine with specially designed hosting materials; however, this battery technology is still in its infancy and needs more intensive attention. Iodine is widely utilized in metal-iodine batteries. The diffusion and shuttling of polyiodides lead to rapid capacity decay and battery failure, due to the loss of active materials and side reactions between polyiodides and metallic anodes. Current studies demonstrated the efficiency of rationally designed carbon-based host materials for preventing polyiodides from dissolution and shuttling. More designs based on other concepts, such as membrane and electrolyte engineering, are needed to widen the fundamental understanding of iodine conversion-based rechargeable batteries. In addition, more attempts and efforts on chlorine conversion-based battery chemistries are encouraged for high energy density batteries.

Another challenge for using halogen in battery applications is the corrosion issue, which should be carefully considered throughout the entire battery study process, starting from protocol design to battery packaging, as well as the analysis of battery results. The corrosion by halogen speies should be fully circumvented to avoid the decay of battery performances, such as lifespan and safety.

On the other hand, we emphasized the significance of in-situ and ex-situ characterizations for the illustration of underlying charging/discharging mechanisms. More characterizations based on in-situ methods are suggested given the contamination usually occurs when the ex-situ samples are removed from the battery to analysis instruments, especially the oxidation of samples by oxygen in the ambient environment.

Declaration of Competing Interest

The authors declare no conflict of interest.

Acknowledgements

This work is supported by the National Key R&D Program of China (2017YFA0208200), the Fundamental Research Funds for the Central Universities (0205-14380266), the NSFC Projects of China (22022505, 21872069, 22109069), the Natural Science Foundation of Jiangsu Province (BK20180008), the Shenzhen Fundamental Research Program of Science, Technology and Innovation Commission of Shenzhen Municipality (JCYJ20180307155007589), and the Doctoral Innovation and Entrepreneurship Program of Jiangsu Province (JSSCBS20210045).

References

[1] C. Zhang, Y.-L. Wei, P.-F. Cao, M.-C. Lin, Energy storage system: current studies on batteries and power condition system, Renew. Sust. Energy Rev. 82 (2018) 3091–3106.
[2] F. Baskoro, H.Q. Wong, H.J. Yen, Strategic structural design of a gel polymer electrolyte toward a high efficiency lithium-ion battery, ACS Appl. Energy Mater. 2 (2019) 3937–3971.
[3] X. Tian, J. Jin, S. Yuan, C.K. Chua, S.B. Tor, K. Zhou, Emerging 3D-printed electrochemical energy storage devices: a critical review, Adv. Energy Mater. 7 (2017) 1700127.
[4] X. Wang, M. Salari, D. Jiang, J.C. Varela, B. Anasori, D.J. Wesolowski, S. Dai, M.W. Grinstaff, Y. Gogotsi, Electrode material-ionic liquid coupling for electrochemical energy storage, Nat. Rev. Mater. 5 (2020) 787–808.
[5] M. Yang, R. Chen, Y. Shen, X. Zhao, X. Shen, A high-energy aqueous manganese-metal hydride hybrid battery, Adv. Mater. 32 (2020) 2001106.
[6] Y. Shen, Y. Wang, Y. Miao, M. Yang, X. Zhao, X. Shen, High-energy interlayer-expanded copper sulfide cathode material in non-corrosive electrolyte for rechargeable magnesium batteries, Adv. Mater. 32 (2020) 1905524.

[7] J. Hwang, K. Matsumoto, R. Hagiwara, $Na_3V_2(PO_4)_3$/C Positive electrodes with high energy and power densities for sodium secondary batteries with ionic liquid electrolytes that operate across wide temperature ranges, Adv. Sustain. Syst. 2 (2018) 1700171.
[8] J.-T. Li, Z.-Y. Wu, Y.-Q. Lu, Y. Zhou, Q.-S. Huang, L. Huang, S.-G. Sun, Water soluble binder, an electrochemical performance booster for electrode materials with high energy density, Adv. Energy Mater. 7 (2017) 1701185.
[9] N. Kosar, M. Asgar, K. Ayub, T. Mahmood, Halides encapsulation in aluminum/boron phosphide nanoclusters: an effective strategy for high cell voltage in Na-ion battery, Mat. Sci. Semicon. Proc. 97 (2019) 71–79.
[10] R. Rahimi, M. Solimannejad, The potential application of borazine (B_3N_3)-doped nanographene decorated with halides as anode materials for Li-ion batteries: a first-principles study, J. Mol. Model. 26 (2020) 1–8.
[11] A.D. Bui, S.-H. Choi, H. Choi, Y.-J. Lee, C.-H. Doh, J.-W. Park, B.G. Kim, W.-J. Lee, S.-M. Lee, Y.-C. Ha, Origin of the outstanding performance of dual halide doped $Li_7P_2S_8X$ (X= I, Br) solid electrolytes for all-solid-state lithium batteries, ACS Appl. Energy Mater. 4 (2021) 1–8.
[12] X. Zhao, Z. Zhao-Karger, M. Fichtner, X. Shen, Halide-based materials and chemistry for rechargeable batteries, Angew. Chem. Int. Edit. 59 (2020) 5902–5949.
[13] G. Wang, X. Xiong, D. Xie, X. Fu, X. Ma, Y. Li, Y. Liu, Z. Lin, C. Yang, M. Liu, Suppressing dendrite growth by a functional electrolyte additive for robust Li metal anodes, Energy Storage Mater. 23 (2019) 701–706.
[14] C. Wang, J. Liang, M. Jiang, X. Li, S. Mukherjee, K. Adair, M. Zheng, Y. Zhao, F. Zhao, S. Zhang, R. Li, H. Huang, S. Zhao, L. Zhang, S. Lu, C.V. Singh, X. Sun, Interface-assisted in-situ growth of halide electrolytes eliminating interfacial challenges of all-inorganic solid-state batteries, Nano Energy 76 (2020) 105015.
[15] P.K. Dutta, Y. Myung, R.K. Venkiteswaran, L. Mehdi, N. Browning, P. Banerjee, S. Mitra, Mechanism of Na-ion storage in BiOCl anode and the sodium-ion battery formation, J. Phys. Chem. C 123 (2019) 11500–11507.
[16] M. Salama, I. Shterenberg, L.J.W. Shimon, K. Keinan-Adamsky, M. Afri, Y. Gofer, D. Aurbach, Structural analysis of magnesium chloride complexes in dimethoxyethane solutions in the context of Mg batteries research, J. Phys. Chem. C 121 (2017) 24909–24918.
[17] F. Wu, G. Yushin, Conversion cathodes for rechargeable lithium and lithium-ion batteries, Energy Environ. Sci. 10 (2017) 435–459.
[18] F. Wu, O. Borodin, G. Yushin, In situ surface protection for enhancing stability and performance of conversion-type cathodes, MRS Energy Sustain. 9 (2017) 4.
[19] X. Fan, Y. Zhu, C. Luo, L. Suo, Y. Lin, T. Gao, K. Xu, C. Wang, Pomegranate-structured conversion-reaction cathode with a built-in Li source for high-energy Li-ion batteries, ACS Nano 10 (2016) 5567–5577.
[20] G.G. Amatucci, N. Pereira, Fluoride based electrode materials for advanced energy storage devices, J. Fluorine Chem. 128 (2007) 243–262.
[21] F. Badway, F. Cosandey, N. Pereira, G.G. Amatucci, Carbon metal fluoride nanocomposites: high-capacity reversible metal fluoride conversion materials as rechargeable positive electrodes for Li batteries, J. Electrochem. Soc. 150 (2003) A1318.
[22] F. Cosandey, J.F. Al-Sharab, F. Badway, G.G. Amatucci, P. Stadelmann, EELS spectroscopy of iron fluorides and FeF_x/C nanocomposite electrodes used in Li-ion batteries, Microsc. Microanal. 13 (2007) 87.
[23] Y. Makimura, A. Rougier, L. Laffont, M. Womes, J.C. Jumas, J.B. Leriche, J.M. Tarascon, Electrochemical behaviour of low temperature grown iron fluoride thin films, Electrochem. Commun. 8 (2006) 1769–1774.
[24] Q. Cheng, Y. Chen, X. Lin, J. Liu, Z. Yuan, Y. Cai, Hybrid cobalt (II) fluoride derived from a bimetallic zeolitic imidazolate framework as a high-performance cathode for lithium-ion batteries, J. Phys. Chem. C 124 (2020) 8624–8632.
[25] Y. Zhang, J. Meng, K. Chen, H. Wu, J. Hu, C. Li, Garnet-based solid-state lithium fluoride conversion batteries benefiting from eutectic interlayer of superior wettability, ACS Energy Lett. 5 (2020) 1167–1176.
[26] G. Ali, G. Rahman, K.Y. Chung, Cobalt-doped pyrochlore-structured iron fluoride as a highly stable cathode material for lithium-ion batteries, Electrochim. Acta 238 (2017) 49–55.
[27] J. Zhai, Z. Lei, D. Rooney, K. Sun, Top-down synthesis of iron fluoride/reduced graphene nanocomposite for high performance lithium-ion battery, Electrochim. Acta 313 (2019) 497–504.
[28] Y. Bai, X. Zhou, C. Zhan, L. Ma, Y. Yuan, C. Wu, M. Chen, G. Chen, Q. Ni, F. Wu, R. Shahbazian-Yassar, T. Wu, J. Lu, K. Amine, 3D hierarchical nano-flake/micro-flower iron fluoride with hydration water induced tunnels for secondary lithium battery cathodes, Nano Energy 32 (2017) 10–18.
[29] F. Wu, V. Srot, S. Chen, S. Lorger, P.A. Aken, J. Maier, Y. Yu, 3D honeycomb architecture enables a high-rate and long-life iron (III) fluoride-lithium battery, Adv. Mater. 31 (2019) 1905146.
[30] N. Bensalah, D. Turki, F.Z. Kamand, K. Saoud, Hierarchical nanostructured MWCNT-MnF_2 composites with stable electrochemical properties as cathode material for lithium ion batteries, Phys. Status Solidi-a 215 (2018) 1800151.
[31] Q. Zhang, C. Sun, L. Fan, N. Zhang, K. Sun, Iron fluoride vertical nanosheets array modified with graphene quantum dots as long-life cathode for lithium ion batteries, Chem. Eng. J. 371 (2019) 245–251.
[32] J. Zhai, Z. Lei, D. Rooney, K. Sun, Top-down synthesis of iron fluoride/reduced graphene nanocomposite for high performance lithium-ion battery, Electrochim. Acta 313 (2019) 497–504.
[33] Q. Huang, K. Turcheniuk, X. Ren, A. Magasinski, A.-Y. Song, Y. Xiao, D. Kim, G. Yushin, Cycle stability of conversion-type iron fluoride lithium battery cathode at elevated temperatures in polymer electrolyte composites, Nat. Mater. 18 (2019) 1343–1349.
[34] F. Wu, V. Srot, S. Chen, M. Zhang, P.A. Aken, Y. Wang, J. Maier, Y. Yu, Metal-organic framework-derived nanoconfinements of CoF_2 and mixed-conducting wiring for high-performance metal fluoride-lithium battery, ACS Nano 15 (2021) 1509–1518.
[35] E. Zhao, O. Borodin, X. Gao, D. Lei, Y. Xiao, X. Ren, W. Fu, A. Magasinski, K. Turcheniuk, G. Yushin, Lithium-iron (III) fluoride battery with double surface protection, Adv. Energy Mater. 8 (2018) 1800721.
[36] Q. Cheng, Y. Pan, Y. Chen, A. Zeb, X. Lin, Z. Yuan, J. Liu, Nanostructured iron fluoride derived from Fe-based metal-organic framework for lithium ion battery cathodes, Inorg. Chem. 59 (2020) 12700–12710.
[37] N. Tanibata, M. Kato, S. Takimoto, H. Takeda, M. Nakayama, H. Sumi, High formability and fast lithium diffusivity in metastable spinel chloride for rechargeable all-solid-state lithium-ion batteries, Adv. Energy Sustain. Res. 1 (2020) 2000025.
[38] X. Qi, B.-T. Li, S.-K. Peng, N. Wang, X. Chen, S.-J. Yan, Cobalt chloride-ferric chloride-graphite Bi-intercalation compounds as anode materials for high-performance lithium-ion batteries, J. Alloy Compd. 854 (2021) 157178.
[39] S.H. Lim, G.D. Park, D.S. Jung, J.-H. Lee, Y.C. Kang, Towards an efficient anode material for Li-ion batteries: understanding the conversion mechanism of nickel hydroxy chloride with Li-ions, J. Mater. Chem. A 8 (2020) 1939–1946.
[40] J. Wang, B. Ding, X. Hao, Y. Xu, Y. Wang, L. Shen, H. Dou, X. Zhang, A modified molten-salt method to prepare graphene electrode with high capacitance and low self-discharge rate, Carbon 102 (2016) 255–261.
[41] M. Holzapfel, D. Wilde, C. Hupbauer, K. Ahlbrecht, T. Berger, Medium-temperature molten sodium batteries with aqueous bromine and iodine cathodes, Electrochim. Acta 237 (2017) 12–21.
[42] G. Li, X. Lu, J. Kim, K. Meinhardt, H. Chang, N. Canfield, V. Sprenkle, Advanced intermediate temperature sodium-nickel chloride batteries with ultra-high energy density, Nat. Commun. 7 (2016) 1–6.
[43] X. Lu, G. Xia, J.P. Lemmon, Z. Yang, Advanced materials for sodium-beta alumina batteries: status, challenges and perspectives, J. Power Sources 195 (2010) 2431–2442.
[44] K.B. Hueso, M. Armand, T. Rojo, High temperature sodium batteries: status, challenges and future trends, Energy Environ. Sci. 6 (2013) 734–749.
[45] J. Xu, K. Liu, Y. Jin, B. Sun, Z. Zhang, Y. Chen, D. Su, G. Wang, H. Wu, Y. Cui, A garnet-type solid-electrolyte-based molten lithium-molybdenum-iron (II) chloride battery with advanced reaction mechanism, Adv. Mater. 32 (2020) 2000960.
[46] K. Liu, J. Lang, M. Yang, J. Xu, B. Sun, Y. Wu, K. Wang, Z. Zheng, Z. Huang, C. Wang, H. Wu, Y. Jin, Y. Cui, Molten lithium-brass/zinc chloride system as high--performance and low-cost battery, Matter 3 (2020) 1714–1724.
[47] B.-M. Ahn, C.-W. Ahn, B.-D. Hahn, J.-J. Choi, Y.-D. Kim, S.-K. Lim, K. Jung, Y.-C. Park, J.-H. Choi, Easy approach to realize low cost and high cell capacity in sodium nickel-iron chloride battery, Compos. Part B-Eng. 168 (2019) 442–447.
[48] S. Bracco, F. Delfino, A. Trucco, S. Zin, Electrical storage systems based on sodium/nickel chloride batteries: a mathematical model for the cell electrical parameter evaluation validated on a real smart microgrid application, J. Power Sources 399 (2018) 372–382.
[49] M. Li, J. Lu, Z. Chen, K. Amine, 30 Years of lithium-ion batteries, Adv. Mater. 30 (2018) 1800561.
[50] C. Rongeat, M.A. Reddy, T. Diemant, R.J. Behm, M. Fichtner, Development of new anode composite materials for fluoride ion batteries, J. Mater. Chem. A 2 (2014) 20861–20872.
[51] C. Rongeat, M.A. Reddy, R. Witter, M. Fichtner, Solid electrolytes for fluoride ion batteries: ionic conductivity in polycrystalline tysonite-type fluorides, ACS Appl. Mater. Inter. 6 (2014) 2103–2110.
[52] A. Grenier, A.G. Porras-Gutierrez, M. Body, C. Legein, F. Chrétien, E. Raymundo-Piñero, M. Dollé, H. Groult, D. Dambournet, Solid fluoride electrolytes and their composite with carbon: issues and challenges for rechargeable solid state fluoride-ion batteries, J. Phys. Chem. C 121 (2017) 24962–24970.
[53] L. Zhang, M.A. Reddy, M. Fichtner, Electrochemical performance of all solid-state fluoride-ion batteries based on thin-film electrolyte using alternative conductive additives and anodes, J. Solid State Electr. 22 (2018) 997–1006.
[54] H. Konishi, T. Minato, T. Abe, Z. Ogumi, Electrochemical performance of a lead fluoride electrode mixed with carbon in an electrolyte containing triphenylboroxine as an anion acceptor for fluoride shuttle batteries, Mater. Chem. Phys. 226 (2019) 1–5.
[55] D.T. Thieu, M.H. Fawey, H. Bhatia, T. Diemant, V.S.K. Chakravadhanula, R.J. Behm, C. Kübel, M. Fichtner, CuF_2 as reversible cathode for fluoride ion batteries, Adv. Funct. Mater. 27 (2017) 1701051.
[56] H. Konishi, T. Minato, T. Abe, Z. Ogumi, Improvement of cycling performance in bismuth fluoride electrodes by controlling electrolyte composition in fluoride shuttle batteries, J. Appl. Electrochem. 48 (2018) 1205–1211.
[57] M.A. Nowroozi, K. Wissel, J. Rohrer, A.R. Munnangi, O. Clemens, $LaSrMnO_4$: reversible electrochemical intercalation of fluoride ions in the context of fluoride ion batteries, Chem. Mater. 29 (2017) 3441–3453.
[58] M.A. Nowroozi, S. Ivlev, J. Rohrer, O. Clemens, La_2CoO_4: a new intercalation based cathode material for fluoride ion batteries with improved cycling stability, J. Mater. Chem. A 6 (2018) 4658–4669.
[59] S. Kobayashi, H. Nakamoto, D. Yokoe, A. Kuwabara, T. Abe, Y. Ikuhara, Nanoscale defluorination mechanism and solid electrolyte interphase of a MgF_2 anode in fluoride-shuttle batteries, ACS Appl. Energy Mater. 4 (2021) 996–1003.
[60] T. Yamanaka, A.C. Kucuk, Z. Ogumi, T. Abe, Evolution of fluoride shuttle battery reactions of BiF_3 microparticles in a CsF/LiBOB/tetraglyme electrolyte: dependence on structure, size, and shape, ACS Appl. Energy Mater. 3 (2020) 9390–9400.
[61] J. Haruyama, K. Okazaki, Y. Morita, H. Nakamoto, E. Matsubara, T. Ikeshoji, M. Otani, Two-phase reaction mechanism for fluorination and defluorination in fluoride-shuttle batteries: a first-principles study, ACS Appl. Mater. Inter. 12 (2019) 428–435.

[62] H. Nakano, T. Matsunaga, T. Mori, K. Nakanishi, Y. Morita, K. Ide, K. Okazaki, Y. Orikasa, T. Minato, K. Yamamoto, Z. Ogumi, Y. Uchimoto, Fluoride-ion shuttle battery with high volumetric energy density, Chem. Mater. 33 (2021) 459–466.
[63] Q. Zhang, R. Karthick, X. Zhao, L. Zhang, Y. Shi, L. Sun, C.-Y. Su, F. Chen, Sb nanoparticle decorated rGO as a new anode material in aqueous chloride ion batteries, Nanoscale 12 (2020) 12268–12274.
[64] Z. Zhang, K. Shen, Y. Zhou, X. Hou, Q. Ru, Q. He, C. Su, L. Sun, S.H. Aung, F. Chen, The composite electrode of Bi@carbon-texture derived from metal-organic frameworks for aqueous chloride ion battery, Ionics 26 (2020) 2395–2403.
[65] T. Xia, Y. Li, L. Huang, W. Ji, M. Yang, X. Zhao, Room-temperature stable inorganic halide perovskite as potential solid electrolyte for chloride ion batteries, ACS Appl. Mater. Inter. 12 (2020) 18634–18641.
[66] Q. Yin, J. Luo, J. Zhang, S. Zhang, J. Han, Y. Lin, J. Zhou, L. Zheng, M. Wei, Ultra-long-life chloride ion batteries achieved by the synergistic contribution of intralayer metals in layered double hydroxides, Adv. Funct. Mater. 30 (2020) 1907448.
[67] X. Li, X. Ou, Y. Tang, 6.0 V High-voltage and concentrated electrolyte toward high energy density K-based dual-graphite battery, Adv. Energy Mater. 10 (2020) 2002567.
[68] Y. Qiao, K. Jiang, X. Li, H. Deng, Y. He, Z. Chang, S. Wu, S. Guo, H. Zhou, A hybrid electrolytes design for capacity-equivalent dual-graphite battery with superior long-term cycle life, Adv. Energy Mater. 8 (2018) 1801120.
[69] L. Xiang, X. Ou, X. Wang, Z. Zhou, X. Li, Y. Tang, Highly concentrated electrolyte towards enhanced energy density and cycling life of dual-ion battery, Angew. Chem. Int. Edit. 59 (2020) 17924–17930.
[70] T. Yu, X. Zhao, L. Ma, X. Shen, Intercalation and electrochemical behaviors of layered FeOCl cathode material in chloride ion battery, Mater. Res. Bull. 96 (2017) 485–490.
[71] B.-M. Jun, S. Kim, J. Heo, C.M. Park, N. Her, M. Jang, Y. Huang, J. Han, Y. Yoon, Review of MXenes as new nanomaterials for energy storage/delivery and selected environmental applications, Nano Res. 12 (2019) 471–487.
[72] F. Chen, Z.Y. Leong, H.Y. Yang, An aqueous rechargeable chloride ion battery, Energy Storage Mater. 7 (2017) 189–194.
[73] X. Zhao, Q. Li, T. Yu, M. Yang, K. Fink, X. Shen, Carbon incorporation effects and reaction mechanism of FeOCl cathode materials for chloride ion batteries, Sci. Rep. 6 (2016) 1–8.
[74] K.P. Lakshmi, K.J. Janas, M.M. Shaijumon, Antimony oxychloride embedded graphene nanocomposite as efficient cathode material for chloride ion batteries, J. Power Sources 433 (2019) 126685.
[75] X. Hu, F. Chen, S. Wang, Q. Ru, B. Chu, C. Wei, Y. Shi, Z. Ye, Y. Chu, X. Hou, L. Sun, Electrochemical performance of $Sb_4O_5Cl_2$ as a new anode material in aqueous chloride-ion battery, ACS Appl. Mater. Inter. 11 (2019) 9144–9148.
[76] P. Gao, M.A. Reddy, X. Mu, T. Diemant, L. Zhang, Z. Zhao-Karger, V.S.K. Chakravadhanula, O. Clemens, R.J. Behm, M. Fichtner, VOCl as a cathode for rechargeable chloride ion batteries, Angew. Chem. Int. Edit. 128 (2016) 4357–4362.
[77] T. Yu, R. Yang, X. Zhao, X. Shen, Polyaniline-intercalated FeOCl cathode material for chloride-ion batteries, ChemElectroChem 6 (2019) 1761–1767.
[78] T. Yu, Q. Li, X. Zhao, H. Xia, L. Ma, J. Wang, Y.S. Meng, X. Shen, Nanoconfined iron oxychloride material as a high-performance cathode for rechargeable chloride ion batteries, ACS Energy Lett. 2 (2017) 2341–2348.
[79] Q. Yin, D. Rao, G. Zhang, Y. Zhao, J. Han, K. Lin, L. Zheng, J. Zhang, J. Zhou, M. Wei, CoFe-Cl layered double hydroxide: a new cathode material for high-performance chloride ion batteries, Adv. Funct. Mater. 29 (2019) 1900983.
[80] Q. Yin, J. Luo, J. Zhang, L. Zheng, G. Cui, J. Han, D. OHare, High-performance, long lifetime chloride ion battery using a NiFe-Cl layered double hydroxide cathode, J. Mater. Chem. A 8 (2020) 12548–12555.
[81] J. Luo, Q. Yin, J. Zhang, S. Zhang, L. Zheng, J. Han, NiMn-Cl layered double hydroxide/carbon nanotube networks for high-performance chloride ion batteries, ACS Appl. Energy Mater. 3 (2020) 4559–4568.
[82] R. Yang, T. Yu, X. Zhao, Polypyrrole-coated iron oxychloride cathode material with improved cycling stability for chloride ion batteries, J. Alloy Compd. 788 (2019) 407–412.
[83] W.-J. Shi, Y.-W. Yan, C. Chi, X.-T. Ma, D. Zhang, S.-D. Xu, L. Chen, X.-M. Wang, S.-B. Liu, Fluorine anion doped $Na_{0.44}MnO_2$ with layer-tunnel hybrid structure as advanced cathode for sodium ion batteries, J. Power Sources 427 (2019) 129–137.
[84] D. Deng, Transition metal oxyfluorides for next-generation rechargeable batteries, ChemNanoMat 3 (2017) 146–159.
[85] K.P. Lakshmi, K.J. Janas, M.M. Shaijumon, Antimony oxychloride/graphene aerogel composite as anode material for sodium and lithium ion batteries, Carbon 131 (2018) 86–93.
[86] M. Park, J.-H. Shim, H. Kim, H. Park, N. Kim, J. Kim, FeOF ellipsoidal nanoparticles anchored on reduced graphene oxides as a cathode material for sodium-ion batteries, J. Power Sources 396 (2018) 551–558.
[87] J. Sun, W. Tu, C. Chen, A. Plewa, H. Ye, J.A.S. Oh, L. He, T. Wu, K. Zeng, L. Lu, Chemical bonding construction of reduced graphene oxide-anchored few-layer bismuth oxychloride for synergistically improving sodium-ion storage, Chem. Mater. 31 (2019) 7311–7319.
[88] L. Ju, G. Wang, K. Liang, M. Wang, G.E. Sterbinsky, Z. Feng, Y. Yang, Significantly improved cyclability of conversion-type transition metal oxyfluoride cathodes by homologous passivation layer reconstruction, Adv. Energy Mater. 10 (2020) 1903333.
[89] D. Cui, Z. Zheng, X. Peng, T. Li, T. Sun, L. Yuan, Fluorine-doped SnO_2 nanoparticles anchored on reduced graphene oxide as a high-performance lithium ion battery anode, J. Power Sources 362 (2017) 20–26.
[90] D. Wang, J. Zhou, J. Li, Y. Wang, L. Hou, F. Gao, Iodine and nitrogen-codoped carbon microspheres for ultrahigh volumetric capacity of Li-ion batteries, ACS Sustain. Chem. Eng. 6 (2018) 7339–7345.
[91] T. Lu, J. He, R. Li, K. Wang, Z. Yang, X. Shen, Y. Li, J. Xiao, C. Huang, Adjusting the interface structure of graphdiyne by H and F Co-doping for enhanced capacity and stability in Li-ion battery, Energy Storage Mater. 29 (2020) 131–139.
[92] N. Wang, J. He, Z. Tu, Z. Yang, F. Zhao, X. Li, C. Huang, K. Wang, T. Jiu, Y. Yi, Y. Li, Synthesis of chlorine-substituted graphdiyne and applications for lithium-ion storage, Angew. Chem. Int. Edit. 129 (2017) 10880–10885.
[93] X. Zhao, Z. Zhao, Y. Miao, Chloride ion-doped polypyrrole nanocomposite as cathode material for rechargeable magnesium battery, Mater. Res. Bull. 101 (2018) 1–5.
[94] Z. Zhao, T. Yu, Y. Miao, X. Zhao, Chloride ion-doped polyaniline/carbon nanotube nanocomposite materials as new cathodes for chloride ion battery, Electrochim. Acta 270 (2018) 30–36.
[95] X. Zhao, Z. Zhao, M. Yang, H. Xia, T. Yu, X. Shen, Developing polymer cathode material for the chloride ion battery, ACS Appl. Mater. Inter. 9 (2017) 2535–2540.
[96] H. Konishi, T. Minato, T. Abe, Z. Ogumi, Improvement of cycling performance in bismuth fluoride electrodes by controlling electrolyte composition in fluoride shuttle batteries, J. Appl. Electrochem. 48 (2018) 1205–1211.
[97] V.K. Davis, C.M. Bates, K. Omichi, B.M. Savoie, N. Momčilović, Q. Xu, W.J. Wolf, M.A. Webb, K.J. Billings, N.H. Chou, S. Alayoglu, R.K. McKenney, I.M. Darolles, N.G. Nair, A. Hightower, D. Rosenberg, M. Ahmed, C.J. Brooks, T.F. Miller, R.H. Grubbs, S.C. Jones, Room-temperature cycling of metal fluoride electrodes: liquid electrolytes for high-energy fluoride ion cells, Science 362 (2018) 1144–1148.
[98] X. Hou, Z. Zhang, K. Shen, S. Cheng, Q. He, Y. Shi, D.Y.W. Yu, C. Su, L.-J. Li, F. Chen, An aqueous rechargeable fluoride ion battery with dual fluoride electrodes, J. Electrochem. Soc. 166 (2019) A2419.
[99] P. Srimuk, S. Husmann, V. Presser, Low voltage operation of a silver/silver chloride battery with high desalination capacity in seawater, RSC Adv. 9 (2019) 14849–14858.
[100] K. Kim, S.M. Hwang, J.-S. Park, J. Han, J. Kim, Y. Kim, Highly improved voltage efficiency of seawater battery by use of chloride ion capturing electrode, J. Power Sources 313 (2016) 46–50.
[101] G. Tan, H. Li, H. Zhu, S. Lu, J. Fan, G. Li, X. Zhu, Concentration flow cells based on chloride-ion extraction and insertion with metal chloride electrodes for efficient salinity gradient energy harvest, ACS Sustain. Chem. Eng. 6 (2018) 15212–15218.
[102] G. Tan, S. Lu, J. Fan, G. Li, X. Zhu, Chloride-ion concentration flow cells for efficient salinity gradient energy recovery with bismuth oxychloride electrodes, Electrochim. Acta 322 (2019) 134724.
[103] H. Konishi, T. Minato, T. Abe, Z. Ogumi, Electrochemical performance of a lead fluoride electrode mixed with carbon in an electrolyte containing triphenylboroxine as an anion acceptor for fluoride shuttle batteries, Mater. Chem. Phys. 226 (2019) 1–5.
[104] K. Okazaki, Y. Uchimoto, T. Abe, Z. Ogumi, Charge-discharge behavior of bismuth in a liquid electrolyte for rechargeable batteries based on a fluoride shuttle, ACS Energy Lett. 2 (2017) 1460–1464.
[105] M.-C. Lin, M. Gong, B. Lu, Y. Wu, D.-Y. Wang, M. Guan, M. Angell, C. Chen, J. Yang, B.-J. Hwang, H. Dai1, An ultrafast rechargeable aluminum-ion battery, Nature 520 (2015) 324–328.
[106] X. Zhang, Y. Tang, F. Zhang, C.-S. Lee, A novel aluminum-graphite dual-ion battery, Adv. Energy Mater. 6 (2016) 1502588.
[107] S. Wang, S. Jiao, W.-L. Song, H.-S. Chen, J. Tu, D. Tian, H. Jiao, C. Fu, D.-N. Fang, A novel dual-graphite aluminum-ion battery, Energy Storage Mater. 12 (2018) 119–127.
[108] E. Zhang, W. Cao, B. Wang, X. Yu, L. Wang, Z. Xu, B. Lu, A novel aluminum dual-ion battery, Energy Storage Mater. 11 (2018) 91–99.
[109] M. Angell, C.-J. Pan, Y. Rong, C. Yuan, M.-C. Lin, B.-J. Hwang, H. Dai, High coulombic efficiency aluminum-ion battery using an $AlCl_3$-urea ionic liquid analog electrolyte, P. Natl. Acad. Sci. USA 114 (2017) 834–839.
[110] H. Xu, T. Bai, H. Chen, F. Guo, J. Xi, T. Huang, S. Cai, X. Chu, J. Ling, W. Gao, Z. Xu, C. Gao, Low-cost $AlCl_3/Et_3NHCl$ electrolyte for high-performance aluminum-ion battery, Energy Storage Mater. 17 (2019) 38–45.
[111] Q. Gong, W. Ding, A. Bonk, H. Li, K. Wang, A. Jianu, A. Weisenburger, A. Bund, T. Bauer, Molten iodide salt electrolyte for low-temperature low-cost sodium-based liquid metal battery, J. Power Sources 475 (2020) 228674.
[112] H. Bhatia, D.T. Thieu, A.H. Pohl, V.S.K. Chakravadhanula, M.H. Fawey, C. Kü, M. Fichtner, Conductivity optimization of tysonite-type $La_{1-x}Ba_xF_{3-x}$ solid electrolytes for advanced fluoride ion battery, ACS Appl. Mater. Inter. 9 (2017) 23707–23715.
[113] L. Zhang, M.A. Reddy, P. Gao, M. Fichtner, Development of dense solid state thin–film electrolyte for fluoride ion batteries, J. Alloy Compd. 684 (2016) 733–738.
[114] C. Rongeat, M.A. Reddy, R. Witter, M. Fichtner, Solid electrolytes for fluoride ion batteries: ionic conductivity in polycrystalline tysonite-type fluorides, ACS Appl. Mater. Inter. 6 (2014) 2103–2110.
[115] D. Pan, Y. Fu, J. Chen, K.J. Czech, J.C. Wright, S. Jin, Visualization and studies of ion-diffusion kinetics in cesium lead bromide perovskite nanowires, Nano Lett. 18 (2018) 1807–1813.
[116] M.A. Nowroozi, K. Wissel, M. Donzelli, N. Hosseinpourkahvaz, S. Plana-Ruiz, U. Kolb, R. Schoch, M. Bauer, A.M. Malik, J. Rohrer, S. Ivlev, F. Kraus, O. Clemens, High cycle life all-solid-state fluoride ion battery with La_2NiO_{4+d} high voltage cathode, Comms. Mat. 1 (2020) 1–16.
[117] S. Breuer, S. Lunghammer, A. Kiesl, M. Wilkening, F anion dynamics in cation-mixed nanocrystalline LaF_3:SrF_2, J. Mater. Sci. 53 (2018) 13669–13681.

[118] C. Rongeat, M.A. Reddy, R. Witter, M. Fichtner, Nanostructured fluorite-type fluorides as electrolytes for fluoride ion batteries, J. Phys. Chem. C 117 (2013) 4943–4950.
[119] L.N. Patro, K. Hariharan, Influence of synthesis methodology on the ionic transport properties of $BaSnF_4$, Mater. Res. Bull. 46 (2011) 732–737.
[120] L.N. Patro, K. Hariharan, Ionic transport studies in $Sn_{(1-x)}K_xF_{(2-x)}$ type solid electrolytes, Mater. Res. Bull. 47 (2012) 2492–2497.
[121] I. Mohammad, R. Witter, M. Fichtner, M.A. Reddy, Room-temperature, rechargeable solid-state fluoride-ion batteries, ACS Appl. Energy Mater. 1 (2018) 4766–4775.
[122] T. Vergentev, A. Banshchikov, A. Filimonov, E. Koroleva, N. Sokolov, M.C. Wurz, Longitudinal conductivity of LaF_3/SrF_2 multilayer heterostructures, Sci. Technol. Adv. Mat. 17 (2016) 799–806.
[123] F. Fujisaki, K. Mori, M. Yonemura, Y. Ishikawa, T. Kamiyama, T. Otomo, E. Matsubara, T. Fukunaga, Mechanical synthesis and structural properties of the fast fluoride-ion conductor $PbSnF_4$, J. Solid State Chem. 253 (2017) 287–293.
[124] I. Mohammad, R. Witter, M. Fichtner, M.A. Reddy, Introducing interlayer electrolytes: toward room-temperature high-potential solid-state rechargeable fluoride ion batteries, ACS Appl. Energy Mater. 2 (2019) 1553–1562.
[125] C. Chen, T. Yu, M. Yang, X. Zhao, X. Shen, An all-solid-state rechargeable chloride ion battery, Adv. Sci. 6 (2019) 1802130.
[126] M.A. Nowroozi, I. Mohammad, P. Molaiyan, K. Wissel, A.R. Munnangi, O. Clemens, Fluoride ion batteries-past, present, and future, J. Mater. Chem. A 9 (2021) 5980–6012.
[127] L. Li, X. Yang, J. Li, Y. Xu, A novel and shortcut method to prepare ionic liquid gel polymer electrolyte membranes for lithium-ion battery, Ionics 24 (2018) 735–741.
[128] Y. Lu, X. Meng, J.A. Alonso, M.T. Fernandez-Diaz, C. Sun, Effects of fluorine doping on structural and electrochemical properties of $Li_{6.25}Ga_{0.25}La_3Zr_2O_{12}$ as electrolytes for solid-state lithium batteries, ACS Appl. Mater. Inter. 11 (2018) 2042–2049.
[129] Y. Liu, S. Wang, A.M. Nolan, C. Ling, Y. Mo, Tailoring the cation lattice for chloride lithium-ion conductors, Adv. Energy Mater. 10 (2020) 2002356.
[130] T. Asano, A. Sakai, S. Ouchi, M. Sakaida, A. Miyazaki, S. Hasegawa, Solid halide electrolytes with high lithium-ion conductivity for application in 4 V class bulk-type all-solid-state batteries, Adv. Mater. 30 (2018) 1803075.
[131] D. Park, H. Park, Y. Lee, S.-O. Kim, H.-G. Jung, K.Y. Chung, J.H. Shim, S. Yu, Theoretical design of lithium chloride superionic conductors for all-solid-state high–voltage lithium-ion batteries, ACS Appl. Mater. Inter. 12 (2020) 34806–34814.
[132] M. Feinauer, H. Euchner, M. Fichtner, M.A. Reddy, Unlocking the potential of fluoride-based solid electrolytes for solid-state lithium batteries, ACS Appl. Energy Mater. 2 (2019) 7196–7203.
[133] H. Jia, X. Liang, T. An, L. Peng, J. Feng, J. Xie, Effect of halogen doping in sodium solid electrolytes based on the Na-Sn-Si-P-S quinary system, Chem. Mater. 32 (2020) 4065–4071.
[134] H. Jia, Y. Sun, Z. Zhang, L. Peng, T. An, J. Xie, Group 14 element based sodium chalcogenide $Na_4Sn_{0.67}Si_{0.33}S_4$ as structure template for exploring sodium superionic conductors, Energy Storage Mater. 23 (2019) 508–513.
[135] S. Fan, M. Lei, H. Wu, J. Hu, C. Yin, T. Liang, C. Li, A Na-rich fluorinated sulfate anti-perovskite with dual doping as solid electrolyte for Na metal solid state batteries, Energy Storage Mater. 31 (2020) 87–94.
[136] L. Zhou, N. Minafra, W.G. Zeier, L.F. Nazar, Innovative approaches to Li-argyrodite solid electrolytes for all solid-state lithium batteries, Acc. Chem. Res. 54 (2021) 2717–2728.
[137] C. Yu, F. Zhao, J. Luo, L. Zhang, X. Sun, Recent development of lithium argyrodite solid-state electrolytes for solid-state batteries: synthesis, structure, stability and dynamics, Nano Energy 83 (2021) 105858.
[138] X. Bai, Y. Duan, W. Zhuang, R. Yang, J. Wang, Research progress in Li-argyrodite-based solid-state electrolytes, J. Mater. Chem. A 8 (2020) 25663–25686.
[139] Q. Yang, C. Li, Li metal batteries and solid state batteries benefiting from halogen-based strategies, Energy Storage Mater. 14 (2018) 100–117.
[140] Y. Chen, Y. Mao, X. Hao, Y. Cao, W. Wang, A stable fluorine-containing solid electrolyte interface toward dendrite-free lithium-metal anode for lithium-sulfur batteries, ChemElectroChem 8 (2021) 1500–1506.
[141] P. Li, W. Feng, X. Dong, Y. Wang, Y. Xia, A new strategy of constructing a highly fluorinated solid-electrolyte interface towards high-performance lithium anode, Adv. Mater. Inter. 7 (2020) 2000154.
[142] C. Cui, C. Yang, N. Eidson, J. Chen, F. Han, L. Chen, C. Luo, P.-F. Wang, X. Fan, C. Wang, A highly reversible, dendrite-free lithium metal anode enabled by a lithium-fluoride-enriched interphase, Adv. Mater. 32 (2020) 1906427.
[143] H. Yuan, J. Nai, H. Tian, Z. Ju, W. Zhang, Y. Liu, X. Tao, X.W. Lou, An ultrastable lithium metal anode enabled by designed metal fluoride spansules, Sci. Adv. 6 (2020) eaaz3112.
[144] X. Han, J. Sun, Design of A LiF-rich solid electrolyte interface layer through salt-additive chemistry for boosting fast-charging phosphorus-based lithium ion battery performance, Chem. Commun. 56 (2020) 6047–6049.
[145] T. Gao, B. Wang, J. Gao, D. Wang, Lithium fluoride additive for inorganic $LiAlCl_4{\cdot}3SO_2$ electrolyte toward stable lithium metal anode, Electrochim. Acta 345 (2020) 136193.
[146] X. Fu, G. Wang, D. Dang, Q. Liu, X. Xiong, C. Wu, Sulfuryl chloride as a functional additive towards dendrite-free and long-life Li metal anodes, J. Mater. Chem. A 7 (2019) 25003–25009.
[147] A. Bhandari, J. Bhattacharya, R.G.S. Pala, Adsorption preference of HF over ethylene carbonate leads to dominant presence of fluoride products in $LiFePO_4$ cathode–electrolyte interface in Li-ion batteries, J. Phys. Chem. C 124 (2020) 9170–9177.
[148] Y. Zhang, V. Viswanathan, Not all fluorination is the same: unique effects of fluorine functionalization of ethylene carbonate for tuning solid-electrolyte interphase in Li metal batteries, Langmuir 36 (2020) 11450–11466.
[149] J. Ko, Y.S. Yoon, Lithium fluoride layer formed by thermal evaporation for stable lithium metal anode in rechargeable batteries, Thin Solid Films 673 (2019) 119–125.
[150] R. Li, X. Sun, J. Zou, Q. He, Lithium fluoride as an efficient additive for improved electrochemical performance of Li-S batteries, Colloid Surf. A 598 (2020) 124737.
[151] Y.-C. Yin, Q. Wang, J.-T. Yang, F. Li, G. Zhang, C.-H. Jiang, H.-S. Mo, J.-S. Yao, K.-H. Wang, F. Zhou, H.-X. Ju, H.-B. Yao, Metal chloride perovskite thin film based interfacial layer for shielding lithium metal from liquid electrolyte, Nat. Commun. 11 (2020) 1–9.
[152] C. Gong, S.D. Pu, X. Gao, S. Yang, J. Liu, Z. Ning, G.J. Rees, I. Capone, L. Pi, B. Liu, G.O. Hartley, J. Fawdon, J. Luo, M. Pasta, C.R.M. Grovenor, P.G. Bruce, A.W. Robertson, Revealing the role of fluoride-rich battery electrode interphases by operando transmission electron microscopy, Adv. Energy Mater. 11 (2021) 2003118.
[153] M. He, R. Guo, G.M. Hobold, H. Gao, B.M. Gallant, The intrinsic behavior of lithium fluoride in solid electrolyte interphases on lithium, P. Natl. A. Sci. 117 (2020) 73–79.
[154] Z. Wang, Z. Xu, X. Jin, J. Li, Q. Xu, Y. Chong, C. Ye, W. Li, D. Ye, Y. Lu, Y. Qiu, Dendrite-free and air-stable lithium metal batteries enabled by electroless plating with aluminum fluoride, J. Mater. Chem. A 8 (2020) 9218–9227.
[155] S. Qi, J. He, J. Liu, H. Wang, M. Wu, F. Li, D. Wu, X. Li, J. Ma, Phosphonium bromides regulating solid electrolyte interphase components and optimizing solvation sheath structure for suppressing lithium dendrite growth, Adv. Funct. Mater. 31 (2021) 2009013.
[156] S. Yu, H. Park, D.J. Siegel, Thermodynamic assessment of coating materials for solid-state Li, Na, and K batteries, ACS Appl. Mater. Inter. 11 (2019) 36607–36615.
[157] G. Liang, X. Sun, J. Lai, C. Wei, Y. Huang, H. Hu, Adding lithium fluoride to improve the electrochemical properties SnO_2@C/MWCNTs composite anode for lithium-ion batteries, J. Electroanal. Chem. 853 (2019) 113401.
[158] O. Tiurin, N. Solomatin, M. Auinat, Y. Ein-Eli, Atomic layer deposition (ALD) of lithium fluoride (LiF) protective film on Li-ion battery $LiMn_{1.5}Ni_{0.5}O_4$ cathode powder material, J. Power Sources 448 (2020) 227373.
[159] Q. Li, X. Liu, X. Han, Y. Xiang, G. Zhong, J. Wang, B. Zheng, J. Zhou, Y. Yang, Identification of the solid electrolyte interface on the Si/C composite anode with FEC as the additive, ACS Appl. Mater. Inter. 11 (2019) 14066–14075.
[160] M. Xia, Y. Li, Y. Wu, H. Zhang, J. Yang, N. Zhou, Z. Zhou, X. Xiong, Improving the electrochemical properties of a SiO@C/graphite composite anode for high-energy lithium-ion batteries by adding lithium fluoride, Appl. Surf. Sci. 480 (2019) 410–418.
[161] J. Lin, H. Peng, J.-H. Kim, B.R. Wygant, M.L. Meyerson, R. Rodriguez, Y. Liu, K. Kawashima, D. Gu, D.-L. Peng, H. Guo, A. Heller, C.B. Mullins, Lithium fluoride coated silicon nanocolumns as anodes for lithium ion batteries, ACS Appl. Mater. Inter. 12 (2020) 18465–18472.
[162] X. Zheng, C. Bommier, W. Luo, L. Jiang, Y. Hao, Y. Huang, Sodium metal anodes for room-temperature sodium-ion batteries: applications, challenges and solutions, Energy Storage Mater. 16 (2019) 6–23.
[163] S. Choudhury, S. Wei, Y. Ozhabes, D. Gunceler, M.J. Zachman, Z. Tu, J.H. Shin, P. Nath, A. Agrawal, L.F. Kourkoutis, T.A. Arias, L.A. Archer, Designing solid-liquid interphases for sodium batteries, Nat. Commun. 8 (2017) 1–10.
[164] H. Tian, H. Shao, Y. Chen, X. Fang, P. Xiong, B. Sun, P.H.L. Notten, G. Wang, Ultra-stable sodium metal-iodine batteries enabled by an in-situ solid electrolyte interphase, Nano Energy 57 (2019) 692–702.
[165] H. Fan, Z. Zheng, L. Zhao, W. Li, J. Wang, M. Dai, Y. Zhao, J. Xiao, G. Wang, X. Ding, H. Xiao, J. Li, Y. Wu, Y. Zhang, Extending cycle life of Mg/S battery by activation of Mg anode/electrolyte interface through an LiCl-assisted $MgCl_2$ solubilization mechanism, Adv. Funct. Mater. 30 (2020) 1909370.
[166] X. Li, T. Gao, F. Han, Z. Ma, X. Fan, S. Hou, N. Eidson, W. Li, C. Wang, Reducing Mg anode overpotential via ion conductive surface layer formation by iodine additive, Adv. Energy Mater. 8 (2018) 1701728.
[167] Y. Li, S. Guan, H. Huo, Y. Ma, Y. Gao, P. Zuo, G. Yin, A review of magnesium aluminum chloride complex electrolytes for Mg batteries, Adv. Funct. Mater. 31 (2021) 2100650.
[168] R. Lin, A.P. Amrute, J. Pérez-Ramírez, Halogen-mediated conversion of hydrocarbons to commodities, Chem. Rev. 117 (2017) 4182–4247.
[169] D. Kim, Y. Kim, Y. Lee, J. Jeon, 1, 2-Dimethylimidazole based bromine complexing agents for vanadium bromine redox flow batteries, Int. J. Hydrogen Energy 44 (2019) 12024–12032.
[170] R. Kim, H.G. Kim, G. Doo, C. Choi, S. Kim, J.-H. Lee, J. Heo, H.-Y. Jung, H.-T. Kim, Ultrathin nafion-filled porous membrane for zinc/bromine redox flow batteries, Sci. Rep. 7 (2017) 1–8.
[171] S. Bae, J. Lee, D.S. Kim, The effect of Cr^{3+}-functionalized additive in zinc-bromine flow battery, J. Power Sources 413 (2019) 167–173.
[172] H.R. Jiang, M.C. Wu, Y.X. Ren, W. Shyy, T.S. Zhao, Towards a uniform distribution of zinc in the negative electrode for zinc bromine flow batteries, Appl. Energy 213 (2018) 366–374.
[173] M. Schneider, G.P. Rajarathnam, M.E. Easton, A.F. Masters, T. Maschmeyer, A.M. Vassallo, The influence of novel bromine sequestration agents on zinc/bromine flow battery performance, RSC Adv. 6 (2016) 110548–110556.
[174] G.P. Rajarathnam, M.E. Easton, M. Schneider, A.F. Masters, T. Maschmeyer, A.M. Vassallo, The influence of ionic liquid additives on zinc half-cell electrochemical performance in zinc/bromine flow batteries, RSC Adv. 6 (2016) 27788–27797.
[175] M.C. Wu, T.S. Zhao, L. Wei, H.R. Jiang, R.H. Zhang, Improved electrolyte for zinc-bromine flow batteries, J. Power Sources 384 (2018) 232–239.

[176] M. Kim, D. Yun, J. Jeon, Effect of a bromine complex agent on electrochemical performances of zinc electrodeposition and electrodissolution in zinc-bromide flow battery, J. Power Sources 438 (2019) 227020.
[177] M.C. Wu, T.S. Zhao, H.R. Jiang, Y.K. Zeng, Y.X. Ren, High-performance zinc bromine flow battery via improved design of electrolyte and electrode, J. Power Sources 355 (2017) 62–68.
[178] H. Wang, R. Wang, Z. Song, H. Zhang, H. Zhang, Y. Wang, X. Li, A novel aqueous Li^+(or Na^+)/Br^- hybrid-ion battery with super high areal capacity and energy density, J. Mater. Chem. A 7 (2019) 13050–13059.
[179] Y. Zeng, Z. Yang, F. Lu, Y. Xie, A novel tin-bromine redox flow battery for large-scale energy storage, Appl. Energy 255 (2019) 113756.
[180] B.P. Williams, G.L. Shebert, Y.L. Joo, Metal oxide coatings on carbon electrodes with large mesopores for deeply charged zinc bromine redox flow batteries, J. Electrochem. Soc. 166 (2019) A2245.
[181] C. Wang, X. Li, X. Xi, W. Zhou, Q. Lai, H. Zhang, Bimodal highly ordered mesostructure carbon with high activity for Br_2/Br^- redox couple in bromine based batteries, Nano Energy 21 (2016) 217–227.
[182] K.S. Archana, R. Naresh, H. Enale, V. Rajendran, A.M.V. Mohan, A. Bhaskar, P. Ragupathy, D. Dixon, Effect of positive electrode modification on the performance of zinc-bromine redox flow batteries, J. Energy Storage 29 (2020) 101462.
[183] J.-N. Lee, E. Do, Y. Kim, J.-S. Yu, K.J. Kim, Development of titanium 3D mesh interlayer for enhancing the electrochemical performance of zinc-bromine flow battery, Sci. Rep. 11 (2021) 1–9.
[184] C. Wang, Q. Lai, P. Xu, D. Zheng, X. Li, H. Zhang, Cage-like porous carbon with superhigh activity and Br_2-complex-entrapping capability for bromine-based flow batteries, Adv. Mater. 29 (2017) 1605815.
[185] C. Wang, W. Lu, Q. Lai, P. Xu, H. Zhang, X. Li, A TiN nanorod array 3D hierarchical composite electrode for ultrahigh-power-density bromine-based flow batteries, Adv. Mater. 31 (2019) 1904690.
[186] X. Yuan, J. Mo, J. Huang, J. Liu, C. Liu, X. Zeng, W. Zhou, J. Yue, X. Wu, Y. Wu, An aqueous hybrid zinc-bromine battery with high voltage and energy density, ChemElectroChem 7 (2020) 1531–1536.
[187] M.C. Wu, T.S. Zhao, R.H. Zhang, L. Wei, H.R. Jiang, Carbonized tubular polypyrrole with a high activity for the Br_2/Br^- redox reaction in zinc-bromine flow batteries, Electrochimica Acta 284 (2018) 569–576.
[188] S. Suresh, M. Ulaganathan, R. Aswathy, P. Ragupathy, Enhancement of bromine reversibility using chemically modified electrodes and their applications in zinc bromine hybrid redox flow batteries, ChemElectroChem 5 (2018) 3411–3418.
[189] S. Suresh, M. Ulaganathan, N. Venkatesan, P. Periasamy, P. Ragupathy, High performance zinc-bromine redox flow batteries: role of various carbon felts and cell configurations, J. Energy Storage 20 (2018) 134–139.
[190] M. Wu, T. Zhao, R. Zhang, H. Jiang, L. Wei, A zinc-bromine flow battery with improved design of cell structure and electrodes, Energy Technol. 6 (2018) 333–339.
[191] R. Naresh, K. Mariyappan, K.S. Archana, S. Suresh, D. Ditty, M. Ulaganathan, P. Ragupathy, Activated carbon-anchored 3D carbon network for bromine activity and its enhanced electrochemical performance in Zn-Br_2 hybrid redox flow battery, ChemElectroChem 6 (2019) 5688–5697.
[192] H.-X. Xiang, A.-D. Tan, J.-H. Piao, Z.-Y. Fu, Z.-X. Liang, Efficient nitrogen-doped carbon for zinc-bromine flow battery, Small 15 (2019) 1901848.
[193] D. Bryans, B.G. McMillan, M. Spicer, A. Wark, L. Berlouis, Complexing additives to reduce the immiscible phase formed in the hybrid $ZnBr_2$ flow battery, J. Electrochem. Soc. 164 (2017) A3342.
[194] X. Li, C. Xie, T. Li, Y. Zhang, X. Li, Low-cost titanium-bromine flow battery with ultrahigh cycle stability for grid-scale energy storage, Adv. Mater. 32 (2020) 2005036.
[195] X. Li, T. Li, P. Xu, C. Xie, Y. Zhang, X. Li, A complexing agent to enable a wide-temperature range bromine-based flow battery for stationary energy storage, Adv. Funct. Mater. 31 (2021) 2100133.
[196] M.R. Gerhardt, E.S. Beh, L. Tong, R.G. Gordon, M.J. Aziz, Comparison of capacity retention rates during cycling of quinone-bromide flow batteries, MRS Adv. 2 (2017) 431–438.
[197] H.J. Lee, D.W. Kim, J.H. Yang, Estimation of state-of-charge for zinc-bromine flow batteries by in situ Raman spectroscopy, J. Electrochem. Soc. 164 (2017) A754.
[198] H.S. Yang, J.H. Park, H.W. Ra, C.-S. Jin, J.H. Yang, Critical rate of electrolyte circulation for preventing zinc dendrite formation in a zinc-bromine redox flow battery, J. Power Sources 325 (2016) 446–452.
[199] L. Han, H. Huang, J. Li, X. Zhang, Z. Yang, M. Xu, L. Pan, A novel redox bromide-ion additive hydrogel electrolyte for flexible Zn-ion hybrid supercapacitors with boosted energy density and controllable zinc deposition, J. Mater. Chem. A 8 (2020) 15042–15050.
[200] X. Tang, Y.H. Lui, B. Chen, S. Hu, Functionalized carbon nanotube based hybrid electrochemical capacitors using neutral bromide redox-active electrolyte for enhancing energy density, J. Power Sources 352 (2017) 118–126.
[201] H. Li, M. Li, T. Li, A novel rechargeable metal halides battery with ethylene glycol cyclic sulfate electrolyte system, Mater. Lett. 282 (2021) 128826.
[202] H. Li, M. Li, X. Zhou, T. Li, H. Zhao, A novel rechargeable bromine-ion battery and the induction of bromine ions on metal electrodes, Sustain. Energy Fuels 4 (2020) 3871–3878.
[203] F. Yu, C. Zhang, F. Wang, Y. Gu, P. Zhang, E.R. Waclawik, A. Du, K. Ostrikov, H. Wang, A zinc bromine “supercapattery” system combining triple functions of capacitive, pseudocapacitive and battery-type charge storage, Mater. Horiz. 7 (2020) 495–503.
[204] S. Dongmo, S. Zaubitzer, P. Scheler, S. Krieck, L. Jçrissen, M. Wohlfahrt-Mehrens, M. Westerhausen, M. Marinaro, Stripping and plating a magnesium metal anode in bromide-based non-nucleophilic electrolytes, ChemSusChem 13 (2020) 3530–3538.
[205] S. Park, D.H. Han, J.G. Lee, T.D. Chung, Current amplification and ultrafast charge transport in a single microdroplet of bromide/polybromide-based ionic liquid, ACS Appl. Energy Mater. 3 (2020) 5285–5292.
[206] F. Wang, H. Yang, J. Zhang, P. Zhang, G. Wang, X. Zhuang, G. Cuniberti, X. Feng, A dual-stimuli-responsive sodium-bromine battery with ultrahigh energy density, Adv. Mater. 30 (2018) 1800028.
[207] L. Gao, Z. Li, Y. Zou, S. Yin, P. Peng, Y. Shao, X. Liang, A high-performance aqueous zinc-bromine static battery, Iscience 23 (2020) 101348.
[208] S.J. Yoo, B. Evanko, X. Wang, M. Romelczyk, A. Taylor, X. Ji, S.W. Boettcher, G.D. Stucky, Fundamentally addressing bromine storage through reversible solid-state confinement in porous carbon electrodes: design of a high-performance dual-redox electrochemical capacitor, J. Am. Chem. Soc. 139 (2017) 9985–9993.
[209] K. Takemoto, H. Yamada, Development of rechargeable lithium-bromine batteries with lithium ion conducting solid electrolyte, J. Power Sources 281 (2015) 334–340.
[210] X. Yao, J. Luo, Q. Dong, D. Wang, A rechargeable non-aqueous Mg-Br_2 battery, Nano Energy 28 (2016) 440–446.
[211] F. Yu, L. Pang, X. Wang, E.R. Waclawik, F. Wang, K. Ostrikov, H. Wang, Aqueous alkaline-acid hybrid electrolyte for zinc-bromine battery with 3V voltage window, Energy Storage Mater 19 (2019) 56–61.
[212] C. Yang, J. Chen, X. Ji, P. Pollard, X. Lü, C.-J. Sun, S. Hou, Q. Liu, C. Liu, T. Qing, Y. Wang, O. Borodin, Y. Ren, K. Xu, C. Wang, Aqueous Li-ion battery enabled by halogen conversion-intercalation chemistry in graphite, Nature 569 (2019) 245–250.
[213] J.-H. Lee, Y. Byun, G.H. Jeong, C. Choi, J. Kwen, R. Kim, I.H. Kim, S.O. Kim, H.-T. Kim, High-energy efficiency membraneless flowless Zn-Br battery: utilizing the electrochemical-chemical growth of polybromides, Adv. Mater. 31 (2019) 1904524.
[214] Q. Guo, K.-I. Kim, S. Li, A.M. Scida, P. Yu, S.K. Sandstrom, L. Zhang, S. Sun, H. Jiang, Q. Ni, D. Yu, M.M. Lerner, H. Xia, X. Ji, Reversible insertion of I-Cl interhalogen in a graphite cathode for aqueous dual-ion batteries, ACS Energy Lett 6 (2021) 459–467.
[215] Y. Zou, T. Liu, Q. Du, Y. Li, H. Yi, X. Zhou, Z. Li, L. Gao, L. Zhang, X. Liang, A four-electron Zn-I_2 aqueous battery enabled by reversible $I^-/I_2/I^+$ conversion, Nature Commun 12 (2021) 1–11.
[216] C. Bai, H. Jin, Z. Gong, X. Liu, Z. Yuan, A high-power aqueous rechargeable Fe-I_2 battery, Energy Storage Mater 28 (2020) 247–254.
[217] Z. Meng, H. Tian, S. Zhang, X. Yan, H. Ying, W. He, C. Liang, W. Zhang, X. Hou, W.-Q. Han, Polyiodide-shuttle restricting polymer cathode for rechargeable lithium/iodine battery with ultralong cycle life, ACS Appl. Mater. Inter. 10 (2018) 17933–17941.
[218] K. Li, B. Lin, Q. Li, H. Wang, S. Zhang, C. Deng, Anchoring iodine to N-doped hollow carbon fold-hemisphere: toward a fast and stable cathode for rechargeable lithium-iodine batteries, ACS Appl. Mater. Inter. 9 (2017) 20508–20518.
[219] K. Li, S. Chen, S. Chen, X. Liu, W. Pan, J. Zhang, Nitrogen, phosphorus Co-doped carbon cloth as self-standing electrode for lithium-iodine batteries, Nano Res 12 (2019) 549–555.
[220] Z. Su, C.-J. Tong, D.-Q. He, C. Lai, L.-M. Liu, C. Wang, K. Xi, Ultra-small B_2O_3 nanocrystals grown in situ on highly porous carbon microtubes for lithium-iodine and lithium-sulfur batteries, J. Mater. Chem. A 4 (2016) 8541–8547.
[221] H. Wang, G. Zhang, L. Ke, B. Liu, S. Zhang, C. Deng, Understanding the effects of 3D porous architectures on promoting lithium or sodium intercalation in iodine/C cathodes synthesized via a biochemistry-enabled strategy, Nanoscale 9 (2017) 9365–9375.
[222] S. Kim, S.-K. Kim, P. Sun, N. Oh, P.V. Braun, Reduced graphene oxide/LiI composite lithium ion battery cathodes, Nano Lett. 17 (2017) 6893–6899.
[223] Q. Zhang, Z. Wu, F. Liu, S. Liu, J. Liu, Y. Wang, T. Yan, Encapsulating a high content of iodine into an active graphene substrate as a cathode material for high-rate lithium-iodine batteries, J. Mater. Chem. A 5 (2017) 15235–15242.
[224] Z.Z. Wu, S.Y. Wang, R.Y. Wang, J. Liu, S.H. Ye, Carbon nanotubes as effective interlayer for high performance Li-I_2 batteries: long cycle life and superior rate performance, J. Electrochem. Soc. 165 (2018) A1156.
[225] C. Sun, X. Shi, Y. Zhang, J. Liang, J. Qu, C. Lai, $Ti_3C_2T_x$ MXene interface layer driving ultra-stable lithium-iodine batteries with both high iodine content and mass loading, ACS Nano 14 (2020) 1176–1184.
[226] Z. Meng, X. Tan, S. Zhang, H. Ying, X. Yan, H. Tian, G. Wang, W.-Q. Han, Ultra-stable binder-free rechargeable Li/I_2 batteries enabled by “betadine” chemical interaction, Chem. Commun. 54 (2018) 12337–12340.
[227] F. Cai, Y. Duan, Z. Yuan, Iodine/β-cyclodextrin composite cathode for rechargeable lithium-iodine batteries, J. Mater. Sci.-Mater. El. 29 (2018) 11540–11545.
[228] Q. Zhang, Y.-H. Zeng, S.-H. Ye, S. Liu, Inclusion complexation enhanced cycling performance of iodine/carbon composites for lithium-iodine battery, J. Power Sources 463 (2020) 228212.
[229] G. Zhang, H. Wang, S. Zhang, C. Deng, Using core-shell interlinked polymer@C-iodine hollow spheres to synergistically depress polyiodide shuttle and boost kinetics for iodine-based batteries, J. Mater. Chem. A 6 (2018) 9019–9031.
[230] V.G. Anju, M.P. Austeria, S. Sampath, Work function tunable titanium carbonitride nanostructures for high-efficiency, rechargeable Li-iodine batteries, Adv. Mater. Interfaces 4 (2017) 1700151.
[231] D. Yu, D. Liu, L. Shi, J. Qiu, L. Dai, High-performance metal-iodine batteries enabled by a bifunctional dendrite-free Li-Na alloy anode, J. Mater. Chem. A 9 (2021) 538–545.
[232] K. Li, Z. Hu, J. Ma, S. Chen, D. Mu, J. Zhang, A 3D and stable lithium anode for high-performance lithium-iodine batteries, Adv. Mater. 31 (2019) 1902399.

[233] T. Shiga, Y. Kato, M. Inoue, Y. Hase, Bifunctional catalytic activity of iodine species for lithium-carbon dioxide battery, ACS Sustain. Chem. Eng. 7 (2019) 14280–14287.
[234] D. Gong, B. Wang, J. Zhu, R. Podila, A.M. Rao, X. Yu, Z. Xu, B. Lu, An iodine quantum dots based rechargeable sodium-iodine battery, Adv. Energy Mater. 7 (2017) 1601885.
[235] M. Qian, Z. Xu, Z. Wang, B. Wei, H. Wang, S. Hu, L.-M. Liu, L. Guo, Realizing few-layer iodinene for high-rate sodium-ion batteries, Adv. Mater. 32 (2020) 2004835.
[236] F. Wang, Z. Liu, C. Yang, H. Zhong, G. Nam, P. Zhang, R. Dong, Y. Wu, J. Cho, J. Zhang, X. Feng, Fully conjugated phthalocyanine copper metal-organic frameworks for sodium-iodine batteries with long-time-cycling durability, Adv. Mater. 32 (2020) 1905361.
[237] M. Qian, M. Tang, J. Yang, W. Wei, M. Chen, J. Chen, J. Xu, Q. Liu, H. Wang, Iodine encapsulated in mesoporous carbon enabling high-efficiency capacitive potassium-ion storage, J. Colloid Interf. Sci. 551 (2019) 177–183.
[238] K. Lu, H. Zhang, F. Ye, W. Luo, H. Ma, Y. Huang, Rechargeable potassium-ion batteries enabled by potassium-iodine conversion chemistry, Energy Storage Mater 16 (2019) 1–5.
[239] H. Tian, T. Gao, X. Li, X. Wang, C. Luo, X. Fan, C. Yang, L. Suo, Z. Ma, W. Han, C. Wang, High power rechargeable magnesium/iodine battery chemistry, Nat. Commun. 8 (2017) 1–8.
[240] F. Wang, J. Tseng, Z. Liu, P. Zhang, G. Wang, G. Chen, W. Wu, M. Yu, Y. Wu, X. Feng, A stimulus-responsive zinc-iodine battery with smart overcharge self-protection function, Adv. Mater. 32 (2020) 2000287.
[241] P. Tangthuam, J. Pimoei, A.A. Mohamad, F. Mahlendorf, A. Somwangthanaroj, S. Kheawhom, Carboxymethyl cellulose-based polyelectrolyte as cationic exchange membrane for zinc-iodine batteries, Heliyon 6 (2020) e05391.
[242] H. Yang, Y. Qiao, Z. Chang, H. Deng, P. He, H. Zhou, A metal-organic framework as a multifunctional ionic sieve membrane for long-life aqueous zinc-iodide batteries, Adv. Mater. 32 (2020) 2004240.
[243] C. Bai, F. Cai, L. Wang, S. Guo, X. Liu, Z. Yuan, A sustainable aqueous Zn-I_2 battery„ Nano Res. 11 (2018) 3548–3554.
[244] Y. Li, L. Liu, H. Li, F. Cheng, J. Chen, Rechargeable aqueous zinc-iodine batteries: pore confining mechanism and flexible device application, Chem. Commun. 54 (2018) 6792–6795.
[245] H. Pan, B. Li, D. Mei, Z. Nie, Y. Shao, G. Li, X.S. Li, K.S. Han, K.T. Mueller, V. Sprenkle, J. Liu, Controlling solid-liquid conversion reactions for a highly reversible aqueous zinc-iodine battery, ACS Energy Lett. 2 (2017) 2674–2680.
[246] D. Yu, A. Kumar, T.A. Nguyen, M.T. Nazir, G. Yasin, High-voltage and ultra-stable aqueous zinc-iodine battery enabled by N-doped carbon materials: revealing the contributions of nitrogen configurations, ACS Sustain. Chem. Eng. 8 (2020) 13769–13776.
[247] K.K. Sonigara, J. Zhao, H.K. Machhi, G. Cui, S.S. Soni, Self-assembled solid-state gel catholyte combating iodide diffusion and self-discharge for a stable flexible aqueous Zn-I_2 battery, Adv. Energy Mater. 10 (2020) 2001997.
[248] X. Zeng, X. Meng, W. Jiang, J. Liu, M. Ling, L. Yan, C. Liang, Anchoring polyiodide to conductive polymers as cathode for high-performance aqueous zinc-iodine batteries, ACS Sustain. Chem. Eng. 8 (2020) 14280–14285.
[249] K. Lu, H. Zhang, B. Song, W. Pan, H. Ma, J. Zhang, Sulfur and nitrogen enriched graphene foam scaffolds for aqueous rechargeable zinc-iodine battery, Electrochim. Acta 296 (2019) 755–761.
[250] Q.P. Jian, M.C. Wu, H.R. Jiang, Y.K. Lin, T.S. Zhao, A trifunctional electrolyte for high-performance zinc-iodine flow batteries, J. Power Sources 484 (2021) 229238.
[251] N. Kato, Y. Ishii, Y. Yoshida, Y. Sakamoto, K. Matsushita, M. Takahashi, R. Date, S. Kawasaki, Electrochemical reactions of iodine molecules encapsulated in single-walled carbon nanotubes, ACS Omega 4 (2019) 2547–2553.
[252] H. Tian, S. Zhang, Z. Meng, W. He, W.-Q. Han, Rechargeable aluminum/iodine battery redox chemistry in ionic liquid electrolyte, ACS Energy Lett. 2 (2017) 1170–1176.
[253] S. Zhang, X. Tan, Z. Meng, H. Tian, F. Xu, W.-Q. Han, Naturally abundant high-performance rechargeable aluminum/iodine batteries based on conversion reaction chemistry, J. Mater. Chem. A 6 (2018) 9984–9996.
[254] K. Lu, Z. Hu, J. Ma, H. Ma, L. Dai, J. Zhang, A rechargeable iodine-carbon battery that exploits ion intercalation and iodine redox chemistry, Nat. Commun. 8 (2017) 1–10.
[255] C. Prehal, H. Fitzek, G. Kothleitner, V. Presser, B. Gollas, S.A. Freunberger, Q. Abbas, Persistent and reversible solid iodine electrodeposition in nanoporous carbons, Nat. Commun. 11 (2020) 1–10.
[256] H. Zhu, R.J. Kee, Computational modeling of sodium-iodine secondary batteries, Electrochim. Acta 219 (2016) 70–81.
[257] S.D. Sessa, F. Palone, A. Necci, R. Benato, Sodium-nickel chloride battery experimental transient modelling for energy stationary storage, J. Energy Storage 9 (2017) 40–46.
[258] K. Mori, Y. Morita, T. Saito, T. Kamiyama, T. Otomo, T. Abe, T. Fukunaga, Structural and electrochemical properties of tysonite $Ce_{0.95}A_{0.05}F_{2.95}$ (A = Mg, Ca, Sr, and Ba): fast-fluoride-ion-conducting solid electrolytes, J. Phys. Chem. C 124 (2020) 18452–18461.
[259] K. Mori, A. Mineshige, T. Saito, M. Sugiura, Y. Ishikawa, F. Fujisaki, K. Namba, T. Kamiyama, T. Otomo, T. Abe, T. Fukunaga, Experimental visualization of interstitialcy diffusion pathways in fast-fluoride-ion-conducting solid electrolyte $Ba_{0.6}La_{0.4}F_{2.4}$, ACS Appl. Energy Mater. 3 (2020) 2873–2880.
[260] B. Dieudonné, J. Chable, F. Mauvy, S. Fourcade, E. Durand, E. Lebraud, M. Leblanc, C. Legein, M. Body, V. Maisonneuve, A. Demourgues, Exploring the $Sm_{1-x}Ca_xF_{3-x}$ tysonite solid solution as a solid-state electrolyte: relationships between structural features and F-ionic conductivity, J. Phys. Chem. C 119 (2015) 25170–25179.
[261] Y. Qie, S. Wang, S. Fu, H. Xie, Q. Sun, P. Jena, Yttrium-sodium halides as promising solid-state electrolytes with high ionic conductivity and stability for Na-ion batteries, J. Phys. Chem. Lett. 11 (2020) 3376–3383.